EXPERIMENTAL STUDIES ON THE DEVELOPMENT OF NANOPARTICLE BASED OPTICAL FIBER HUMIDITY SENSOR WITH LINEAR RESPONSE OVER A LARGE DYNAMIC RANGE

A Thesis Submitted in Partial Fulfillment of the Requirements for the

Award of the Degree

of

DOCTOR OF PHILOSOPHY

by

ANEESH R

DEPARTMENT OF PHYSICS

INDIAN INSTITUTE OF TECHNOLOGY, GUWAHATI

GUWAHATI-781039, INDIA

DECEMBER-2011

The present thesis dedicated to

my parents!

STATEMENT

I hereby declare that the research work presented in this thesis entitled "EXPERIMENTAL STUDIES ON THE DEVELOPMENT OF NANOPARTICLE BASED OPTICAL FIBER HUMIDITY SENSOR WITH LINEAR RESPONSE OVER A LARGE DYNAMIC RANGE", is carried out by me under the supervision of **Dr. Sunil K. Khijwania**, Associate Professor, Department of Physics, Indian Institute of Technology-Guwahati. The contents of this thesis have not been submitted to any other Institute or University for the award of any degree.

Date: 28/12/2011

Aneesh R

Research student
Department of Physics
Indian Institute of Technology-Guwahati
Assam-781039
India

CERTIFICATE

This is to certify that work contained in the thesis entitled "EXPERIMENTAL STUDIES ON THE DEVELOPMENT OF NANOPARTICLE BASED OPTICAL FIBER HUMIDITY SENSOR WITH LINEAR RESPONSE OVER A LARGE DYNAMIC RANGE," by **Mr. Aneesh R** (Roll No. 06612101), a student of Department of Physics, Indian Institute of Technology-Guwahati, for the award of degree of Doctor of Philosophy, has been carried out under my supervision. The contents of this thesis have not been submitted to any other Institute or University for the award of any degree.

Date: 28/12/2011

Dr. Sunil K. Khijwania

Associate Professor, Department of Physics
Indian Institute of Technology-Guwahati
Assam-781039
India

ACKNOWLEDGEMENTS

First and foremost, I would like to express my deepest gratitude to my respected guide **Dr. Sunil K. Khijwania** for providing me the opportunity to work under his supervision. He has supported me throughout my thesis with his knowledge, ideas and patience which gave me right path in all the time of research for and writing of this thesis. His stimulating suggestions, encouragement and training have made him a source of inspiration throughout my life. I am also thankful for the excellent example he has provided as a successful physicist and professor.

I would like to express my sincere thanks to my doctoral committee members, **Dr. P. K. Giri**, **Dr. Ashwini K. Sharma** and **Dr. Utpal Bora** for reviewing my research work regularly and for all valuable suggestions.

I am highly indebted to the members in Fiber Optics lab, Muninder, Debasish, Vipul, Jayakrishnan, Abhinav, Manoj, Utsav, Meeth, Sougata, Debopam, Anshul and Sanjeev for their immense support and help.

My special thanks to the staffs of Department of Physics, Mr. Basab Purkhastya, Dr. Sidananda Sarma, Mr. Atul Chandra Deka, Mr. Lokesh Chakraborty and Mr. Bimal Kumar Sarma for their support and timely assistance.

I always grateful to Dr. Rajan K. John, director, George Sudarshan Centre for Physics and Computer Science, CMS College, Kottayam, Kerala, for his inspiring guidance, constant encouragement and support which motivated me to pursue research in Physics.

I also thankful to my batch mates Arpita, Biswanath Samantaray and Biswanath Dutta for their constant support and help.

I am grateful to my friends, Sangeetha, Suresh, Shyni, Meera, Sunish James Mathews, Sabitha Mohan, Agile Mathew and all others who helped me at various levels during my stay at IIT Guwahati.

Finally, I am forever obliged to my parents and brother for their understanding, endless patience and encouragement when it was most required.

Guwahati

December-2011 Aneesh R

ABSTRACT

The present thesis work is focused on the development of optical fiber relative humidity sensor with linear response over a widest possible dynamic range with an optimum sensitivity through a simple optical fiber sensor configuration. A comprehensive experimental study is carried out employing three schemes, namely, evanescent-wave (EW) absorption employing Zinc oxide (ZnO) as well as Titanium dioxide (TiO_2) nanoparticle immobilized nanostructured sensing fiber cladding, direct guided mode exhaustive attenuation employing ZnO nanoparticle immobilized microstructured sensing fiber core, and Localized Surface Plasmon Resonance (LSPR) employing in-house scaled metal (gold) as well as metal-dielectric (silver-TiO_2) nanoparticles film in order to fulfill the objective. Response of all the proposed sensors was optimized against all possible influential compositional parameters such as chemical composition, reaction parameters, thickness etc. A wide linear dynamic range of 4-96%RH is observed with a sensitivity of 0.0012/%RH for the sensor employing evanescent wave absorption scheme with ZnO nanoparticles immobilized sol-gel sensing fiber cladding. Thus, a widest possible linear dynamic range is achieved, nevertheless, the sensitivity needed to be further increased. To realize this objective, a sensing configuration allowing exhaustive attenuation of entire guided mode was employed using ZnO nanoparticles (that corresponds to the widest linear dynamic range) immobilized sol-gel microstructured fiber. Almost identical linear dynamic range (5-95%RH) is observed with a manifold (~9 times) increase in the sensitivity as compared to ZnO nanoparticle employed EW fiber sensor. The maximum linear dynamic range decreased to 24-95%RH when the ZnO nanoparticles in sol-gel sensing cladding were replaced with TiO_2 nanoparticles. Nevertheless, the optimized sensitivity improved much in comparison with ZnO nanoparticles immobilized sol-gel sensing cladding RH sensor. In the last sensing scheme (metal as well as metal-dielectric nanoparticles assisted LSPR), a linear dynamic range of 6-90%RH is observed for sensing probe with gold nanoparticle film. The observed linear sensitivity is 0.0213nm/%RH. For sensor based on silver-TiO_2 nanoparticle film, the linear dynamic range decreased to 29-95%RH; nevertheless, sensitivity is improved ~2 times compared to the sensing probe with gold nanoparticle film.

LIST OF CONTENTS

LIST OF FIGURES

LIST OF TABLES

Chapter 1

Introduction

Sensors facilitate the acquisition of valuable information about specific physical parameter that is vital for employing control in various industrial, scientific, and environmental processes. Sensor, in fact, can be termed as a device that converts the change in the magnitude of one physical parameter (termed here after as *measurand*) into the change in the magnitude of another different parameter that can be measured more conveniently and perhaps more accurately [1]. These measurands, in general, span anything from Optical signals (e.g., intensity, wavelength, state of polarization and phase of electromagnetic radiation), mechanical/physical signals (e.g., force, pressure, velocity, mass flow, rotation, vibration, tilt, strain, stress, torsion, refractive index etc.), thermal signals, electrical & magnetic signals (e.g., voltage, current, charge, resistance, inductance, capacitance, pulse duration, frequency and dielectric constant, magnetic flux density, magnetic field direction and permeability etc.) to chemical and/or biological signals (e.g., chemical composition, concentration, pH, malignancy, blood glucose, relative humidity, gas concentration etc.). Hence, almost all areas of science & technological as well as industrial applications rely on the information gathered by sensors for an efficient process control and performance

optimization/structure's health monitoring. This makes them indispensable in today's science & technology and industrial growth age.

Conventional sensors take advantage of the inherent properties of some of the materials that lead to a specific response of these materials when exposed to an applied perturbation. The inherent properties could be thermal, electrical, magnetic, mechanical, chemical etc. For example, the mercury in the thermometer expands when temperature rises and contracts when temperature falls. As another example, a voltmeter measures the voltage in a circuit through the rotation of a coil that is proportional to the voltage. A piezoresisitor measures strain change through resistance variation. A capacitive sensor measures various parameters through the change in capacitance. A moving coil micro-phone converts the sound signal in to electrical signal by the vibration of an induction coil (which is attached to the diaphragm) in a constant magnetic field through the electromagnetic induction. On the other hand, a piezoelectric material produces a potential that is proportional to the applied pressure. This property is exploited for designing a conventional pressure sensor. Some sensors use the chemical properties of material. For example, an approximate measure of pH of solution can be obtained by using pH indicator whose colour changes around a particular pH value. Thus, there are many schemes that are employed to design a sensor capable of measuring a given quantity. However, many of these conventional sensors can perform well only under certain conditions and do not offer the flexibility of multiplexing, remote sensing, etc. There is an ever increasing demand for improving the performance of these sensors in terms of sensitivity, immunity to electromagnetic interference and electrostatic discharge, ability to operate under hazardous environments, remote sensing abilities, long term performance, etc. As a result the conventional designs fall short of expectations on many of the above mentioned aspects.

On the other hand, optical sensors measure the change in magnitude of a parameter by measuring the corresponding change in the optical domain. For example, the optical proximity sensors are being widely used for a variety of consumer based and security applications. The optical proximity sensor works by projecting a beam of light from a transmitter to a receiver across a specific distance. As long as the beam of light maintains a connection with the receiver, the circuit remains closed. If an object obstructs the beam of light, the continuity of the circuit is lost, and the circuit opens. In another example, laser and holographic technology is employed to monitor inclination [2]. Optical sensors for chemical/gas (CO_2 and O_2) concentration detection exploit fluorescence characteristics of certain dyes [3-4]. In other reported optical sensors for detection of various gases such as CO, NO, H_2, optical absorption changes in thin sensing film is employed [5-7]. There are few other optical sensors reported by the researchers [8-9]. In general, these optical sensors overcome certain limitations of existing conventional sensors. Even though, such optical sensors overcome certain limitations of conventional sensors and lead to a better sensitivity, they have their own limitations. They are highly alignment sensitive. If the alignment is disturbed, the performance will be rapidly degraded. Also, they may not work properly in certain situations such as on a foggy or rainy days. Further, it is impossible to deploy such sensors in hazardous conditions like places of intense radiation, high voltage environments, high temperature etc. Thus, being bulky complicated and alignment sensitive, such optical sensors are impractical for real-field applications.

Optical fiber sensors are capable of addressing all the inherent limitations of conventional/bulk optics sensors. Discovery of optical fiber was a major breakthrough in telecommunication industry. During early seventies, when the technology of fiber optics for telecommunication was evolving, it was observed that fibers tend to be sensitive to various

external factors like bends, microbends, pressure etc. Initially, enormous effort was made to reduce the sensitivity of signal carrying fiber to such external perturbations. However, soon it was realized that the exceptional sensitivity of optical fibers to external perturbations can be exploited for sensing various parameters. Thus, the field of optical fiber sensor was born. The exceptional technological advancements in the field of fiber optics as well as in the associated optoelectronic industry leading to the availability of very low loss optical fiber and very sophisticated optical sources/interrogators have given a huge thrust and made a great impact on the development of optical fiber based sensors for various applications spanning engineering (civil, mechanical, aeronautical, chemical, electrical, automobile etc.), biomedical, general sciences to homeland security as an example. Almost all the parameters of practical importance such as pressure [10], temperature [11], liquid level [12], refractive index [13], pH [14], antibodies [15], electric current [16], voltage [17], rotation [18], displacement [19], acceleration [20], acoustic [21], electric and magnetic field measurement [22-23], tilt [24], torsion [25], strain [26] etc. are being successfully and accurately monitored not only in the test-bed set-up but also in the real-field environment. The global thrust in the area of fiber sensor research & development (R&D) is in fact inherited from the following remarkable integrated advantages offered by this technology over the conventional sensors [27]:

1. Fiber optic sensors offer very high sensitivity over the traditional sensors.
2. Ease of miniaturization and hence the possibility of the development of very small, light and flexible sensors.
3. Low-loss optical fibers in conjugation with fiber amplifiers not only allow propagation of light-wave signals over thousands of kilometre but also enable dense wavelength-division-multiplexing (DWDM) to realize over 1Tb/s optical fiber communication systems. Such a large information carrying capacity over

thousands of kilometre enables remote sensing, i.e., enables to receive, monitor and instantaneously perform sensor analysis in remote ultraclean control stations when samples are either hard to reach, or dangerous and/or located in harsh environments, or radio-active.

4. Massive information carrying capacity and hence huge amount of bandwidth offered by an optical fiber which is impossible to realize with an electrical lead enables (a) to achieve high sensing information density through a single optical channel where each optical characteristics (wavelength, phase, intensity etc.) independently and simultaneously encoded through external perturbations. Thus, if various modulation schemes are realized for this optical channel against different and independent external perturbations, multiplexing all such sensors and simultaneous multi-parameter sensing becomes a possibility, (b) to multiplex large number of sensors, each characterised at a particular optical channel over a single fiber transmission line, (c) distributed sensing, i.e. continues sensing along the entire fiber transmission line.
5. Optical fibers are made from insulating materials, therefore, optical fiber sensors are, by their nature, electrically isolated from interrogating electronics.
6. Primary signal is optical, and hence cannot be subjected to electromagnetic interference, radio frequency interference and has zero risk against fire/sparks. This makes optical fiber sensor highly reliable.
7. As a point sensor, they can be used to sense normally inaccessible regions without perturbation of the transmitted signals.
8. Low volume and weight, with excellent stability if brought in permanent contact with electrolyte solution. Second feature enables them to be readily employed in chemical process and biomedical instrumentation.

9. Most fiber optic sensors can be employed over a wider temperature range than electrodes.

Optical fiber sensors can be generally classified as an extrinsic or an intrinsic sensor. In an extrinsic sensor, fiber acts merely as a conduit to guide the light signal to and from the sensing head. Modulation of the optical signal by an environmental/external perturbation takes place outside the fiber. On the other hand, in an intrinsic sensor, fiber itself acts as a sensor. One of the inherent characteristics of the guided optical signal e.g., phase, polarization, wavelength, intensity gets modulated within the fiber by an environmental/external perturbation. As evident, an intrinsic fiber sensor can be further classified on the basis of the employed modulation scheme and can be termed, for example, as an intensity modulation based optical fiber sensor or a wavelength modulation based optical fiber sensor and so on. Most popular schemes among researchers in terms of ease of realization are intensity, phase and wavelength modulation.

Sensors based on intensity modulation have more practical importance due to their simplicity in fabrication and compatibility with multi-mode optical fiber. Intensity modulation in optical fiber can be achieved through various schemes [28-29]. Among these, a scheme that has been widely used by the researchers is evanescent wave based intensity modulation. When the light beam associated with the plane wave is incident from a denser region on the interface between two optically transparent medium of high and low refractive indices, for angle of incidence exceeding the critical angle, light beam is totally internally reflected. Applying boundary condition and carefully solving Maxwell's equation across the interface reveals that there still exists a plane wave in the rarer medium, which is termed as evanescent wave. The field equation of this wave depicts that amplitude of the evanescent wave decreases

exponentially as the distance from the interface increases. An optical fiber comprises cylindrical symmetry; hence, a light beam associated with the plane wave (meridional) that enters the fiber core at a given guided angle θ strikes the core-clad (high index-low index) interface at an angle greater than the corresponding critical angle. Such light beam undergoes successive total internal reflection at upper and lower core-clad interface in the meridional plane. Also, there exists a corresponding light beam travelling at a guided angle of - θ within the fiber. These two beams superimpose to give rise the mode of the fiber. Intensity variation of such mode (fundamental) is shown in Fig. 1.1. The intensity variation is not confined within the core (high index medium) only but extends to the clad (low index medium) owing to the phenomena of evanescent wave associated with total internal reflection.

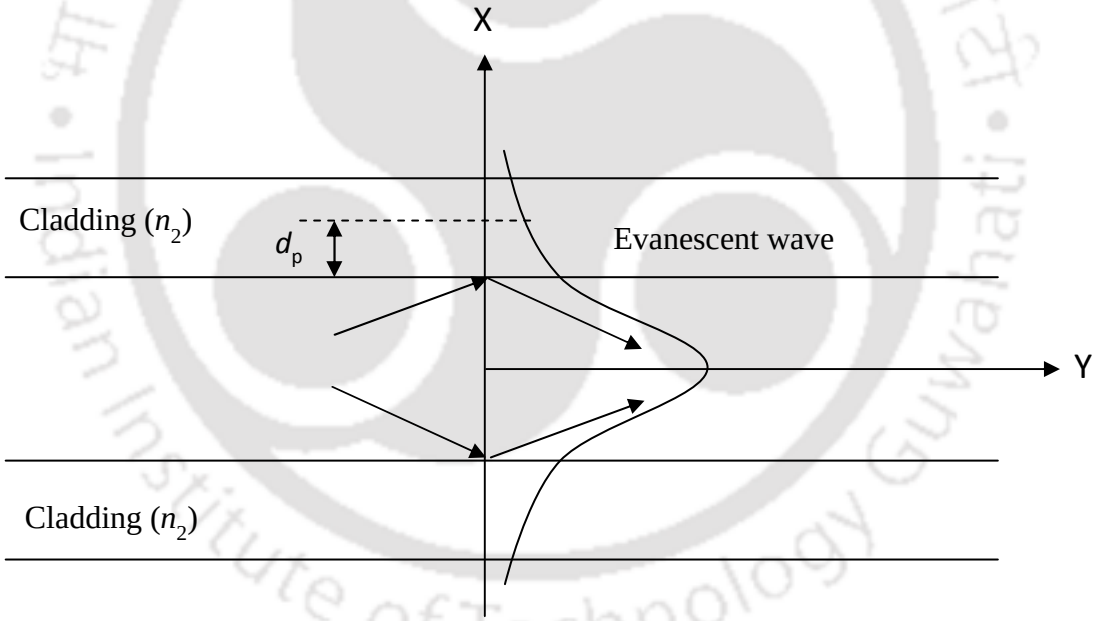

Figure 1.1: *Total internal reflection and evanescent wave in an optical fiber.*

The energy carried by the evanescent tail of the mode diminishes exponentially in the cladding with the distance from the core-cladding interface. A characteristic parameter associated with the evanescent wave is the penetration depth (d_p), that defines the distance

from the core-cladding interface at which amplitude of evanescent wave decreases to 1/*e* of its value at the interface [30]:

$$d_p = \frac{\lambda}{2\pi n_1 \left[\cos^2\theta_{cs} - \cos^2\theta \sin^2\theta_\phi\right]^{\frac{1}{2}}} \tag{1.1}$$

where λ is the free-space wavelength of the light launched into the fiber, n_1 is the refractive index of the fiber core, θ_{cs} is the critical angle of the fiber in the sensing region, θ is the angle of the guided ray with respect to the normal at the core-cladding interface and θ_ϕ is the skewness angle, which is equal to $\pi/2$ for meridional rays. Importantly d_p, which is typically less than operating λ, defines a short range of sensing volume within which the evanescent energy interacts with the measurand and gets attenuated due to the absorption, scattering or refractive index change. Since a multimode fiber can support large number of guided rays, the effective evanescent field around the fiber core is a superposition of the field distribution of all the modes propagating within the fiber. Nevertheless, the quantity of energy available to interact with the measurand in the short range of evanescent wave is described by the fraction of the total guided power (*r*) present in the cladding region, which is defined as [30]:

$$r = \frac{P_{clad}}{P_{total}} \tag{1.2}$$

where P_{clad} is the power in the cladding region and P_{total} is the total guided power. This fraction (*r*) is typically less than 1% for weakly guiding multimode fiber. However, d_p as well as *r*, both, rises sharply as the guided ray angle approaches to the critical angle of the sensing region. This is achieved either by tapering/bending the sensing region or by lower order mode removal. Importantly, d_p as well as *r* are an order of magnitude higher in the case of single-mode fiber (SMF). Hence, SMF should be preferred while designing an evanescent wave based optical fiber sensors (OFS). First step towards designing an OFS based on intensity

modulation by the exploitation of evanescent wave is to gain an access of evanescent wave itself. However, it is difficult to remove the hard silica cladding of single-mode fiber. One method to access the evanescent wave in a single-mode fiber is by preparing side-polished half-block [31]. Here, a single-mode optical fiber is glued inside a curved grove made on a fused silica /quartz block. This entire structure is fixed on the polishing machine and then polished to approach the core-cladding interface to the desired proximity in order to have proper access of evanescent field. A proper alignment and pressure control is required during this process. Another method to access evanescent field in single-mode fiber is by etching the cladding by using Hydrofluoric acid (HF) [32]. However, extreme precaution is necessary while handling HF. Further, the core diameter being of the order of a few micron, alignment and efficient power coupling through such SMF are quite difficult. On the other hand, though d_p and r for multimode fibers are quite less as compared to single-mode fibers, access to the evanescent wave for a specifically fabricated multimode fiber with polymer/plastic cladding and silica core (PCS fiber) is quite easy. One just needs to remove polymer/plastic cladding through razor blade. Further, large throughput power and ease of power coupling to multimode fiber make them more popular in designing evanescent wave based sensors.

There are two ways to exploit such fibers in realizing sensors. If the wavelength of the propagating light falls in the absorption band of the analyte, direct absorption of power carried in the evanescent wave takes place. This is termed as direct sensing. On the other hand for a given source, propagating wavelength in the fiber may not fall in the absorption band of the analyte at all. One needs to switch to the other source of appropriate wavelength then. Even though, it may not be possible to match (within in the feasible domain of) the absorption band with any existing source; or if possible, source might be extremely costly. In such case, the simple/popular source is retained in the sensor system. However, the bare core

is chemically synthesized with optimum configuration and with a proper chemical. The choice of this chemical then became very critical as this chemical must be reactive to the external perturbation and upon exposure of such perturbations, must be capable of modulating its physical or chemical properties that can be mapped at the wavelength of the source. This is termed as indirect sensing. An example of direct sensing is reported by Tai et al. [33], where a fiber optic evanescent wave methane gas sensor using optical absorption of a He-Ne laser has been reported. Similarly, a sensor employing indirect sensing was reported by Sekimoto et al. [34]. In this, an optical fiber hydrogen sensor has been discussed. The sensor utilizes change in the absorption of the evanescent field in the cladding region. The reagent in this case was a platinum or palladium-supported tungsten cladding.

Invention of in-fiber grating made a significant development in the field of optical fiber sensors. Fiber gratings consist of periodic perturbation of core refractive index over a small length of single-mode fiber [35]. They fall into two general classifications based on the period of grating; short period grating or fiber Bragg grating (FBG) and long period grating (LPG). FBG based sensors employ wavelength modulation scheme under the application of strain/thermal perturbation through the strain-optic/thermo-optic effects of the fiber [36-37]. Such sensors are insensitive to fluctuations in the irradiance of illuminating source. Further, the capability of multiplexing a large number of FBG sensing elements on a single fiber as well as the inherently self-referencing nature make FBG based sensors more popular and realistic for structural health monitoring. Apart from strain and temperature, FBG has been used to develop sensors for large number of parameters of practical importance and interest for science and engineering such as ultrasound [38], acceleration [39], pressure [40], tilt [41], torsion [42] and flow rate [43] to name a few. On the other hand, LPGs have also been used to realize all-optical sensing schemes owing to their high sensitivity towards refractive index

of the surrounding medium, strain and temperature [44-47]. However, major issues associated with grating based sensors are their strain and temperature cross-sensitivity and the need of costly and bulky interrogation devices.

Recently, significance of nano-scaling has shown tremendous advancements not only in the area of material science, but also in optical fiber technology as well as in photonics technology as a whole. The interactions that occur in the nano-scale could enhance sensor performance and this could offer significant advantage over conventional sensors [48]. One major factor for this performance enhancement is the high surface-to-volume ratio offered by the nanomaterial which provides more surface area of the sensing material to interact with the analyte. This could result greater sensitivity, reduction in response time, low production costs, reduced power consumption as well as improved stability. Apart from this, nanotechnology leads to a totally different interaction regime termed as localised surface plasmon resonance (LSPR), where light interacts with particles having dimension much smaller than the incident wavelength. This leads to a plasmon that oscillates locally around the nanoparticle with a frequency known as LSPR [49]. Further, nanotechnology also offers the fabrication of new materials whose properties will be different from their bulk and can be tailored specifically for sensing applications. For example, nanoparticles of noble metals such as gold and silver exhibit strong absorption band in the UV-visible region due to localized surface plasmon resonance [50] which is absent in their bulk. Localized surface plasmons are charge density oscillations which happen due to the collective oscillations of free electron cloud in metal nanoparticles. Localized surface plasmons in metal nanoparticles can be excited by light when the frequency of the incident light is in resonance with the oscillation frequency of the conduction electrons and this is called resonance condition. This occurs at a particular wavelength called resonance wavelength. The resonance wavelength is sensitive to

the refractive index of the medium surrounding the metal nanoparticles [49-50]. This property has been used for LSPR based sensing applications. Okamato et al. [51] have reported a LSPR based refractive index sensor using gold nanoparticles. The sensor was developed by immobilizing gold nanoparticles on a glass substrate. Peak absorption wavelength showed a red shift upon increasing the refractive index of the medium surrounding the nanoparticles. LSPR has been realized in conjunction with optical fiber also. For this, the cladding over a certain length of the fiber is removed and this region is coated with metal nanoparticle film. The interaction of evanescent wave of the guided ray with the nanoparticles results in LSPR excitation. Many LSPR based optical fiber sensor have been reported [52-53].

There are various other schemes as well, which have been fused to optical fiber technology such as Cavity-ring-down spectroscopy [54-55] etc. Nevertheless, the choice of scheme in designing an optical fiber sensor is governed by ease of fabrication and the characteristic of the sensor as demanded by its field of application. As mentioned earlier, optical fiber sensors, being versatile, fit to almost all the field of applications. However, one of the most promising and equally important filed of application, which has attracted lots of interest as for as human security is concerned and has a maximum OFS industry share is structural health monitoring (SHM). Complex civil infrastructures, such as bridges, buildings, railways, under-water canal and dams, are often subjected to severe environmental conditions and abnormal loads, e.g. strong winds, heavy rains, high humidity and huge temperature variations that can not be easily anticipated during their design. This results into long term structural deterioration that often is not detected by conventional visual inspection. Moreover, catastrophic events, such as earthquakes, storms or floods can severely affect the health of the structure and induce potential life threatening conditions. Hence, the health of such infrastructures need to be

monitored in real time in order to improve safety and reliability of infrastructure systems by detecting damage before it reaches to a critical state and to allow rapid post-event assessment. SHM is the process of assessing the state of health (e.g., damage) of structures through the measurement of various parameters that affect them. These parameters depend on the construction material, environmental conditions and expected degradation phenomena. Further, they vary from structure to structure. For example, tilt could be more important in the case of an under-water canal or ropeway bridge and vibration for high-rise buildings or railway track. In general, these parameters are classified as mechanical (strain, deformation, displacement, crack opening, stress, and load), physical (temperature, humidity, pore pressure etc.) and chemical (pH, oxidation, corrosion, carbonation, penetration, and timber decay) [56-57]. Humidity is one of the most important parameters to be monitored in SHM as well as in other engineering areas, e.g., semiconductor manufacturing process monitoring, automobile/chemical/biochemical/food processing industries, air conditioning etc. [58-59]. In SHM, concrete is the most widely used construction material in the world. The durability and any structural aging of concrete are governed by moisture content. For example, moisture diffusion during curing may prevent concrete from developing its full strength and might lead to high shrinkage stresses. High moisture content can also promote deterioration process of concrete structure. With aging, the deterioration mechanism in a concrete structure such as bridges, pavements and buildings are more related to the structure characteristics towards moisture variation. In other areas such as semiconductor industry, humidity level is constantly monitored in wafer processing for manufacturing highly sophisticated integrated circuits. In automobile industry, humidity sensors are used in rear-window defoggers and motor assembly lines. In medical field, humidity sensors are used in respiratory equipment, sterilizers, incubators, pharmaceutical processing, and biological products. In agriculture,

humidity sensors are used for green-house air-conditioning, plantation protection, soil moisture monitoring and cereal storage.

Humidity is a general term for the amount of water vapour present in gaseous state in the atmosphere. It is expressed in two different ways; absolute humidity and relative humidity. Absolute humidity is the mass of water vapour contained in unit volume of air. The most common term used for expressing humidity is relative humidity (RH). Relative humidity is the ratio of actual vapour content of the air to the saturated vapour content of the air at the same temperature. This can be expressed as the ratio of the actual water vapour pressure to the saturation water vapour pressure at a specific temperature [60]. When air is fully saturated with water, the pressure exerted by the water vapour present is defined as the saturation water vapour pressure which is a function of temperature. The saturation point also increases rapidly as the temperature of the air rises. This is because the kinetic energy of water molecules is higher at higher temperature. At higher temperature, more water molecules can escape from the liquid water surface into air and this will result higher saturation vapour pressure. In percentage form, RH is expressed as [60]:

$$\%RH = \left(\frac{P_w}{P_{ws}} \right) \times 100$$

where P_w is the partial pressure of water vapour and P_{ws} is the saturation water vapour pressure.

Depending on the need for humidity monitoring, many efforts have been made over the years, employing different schemes to obtain meaningful humidity measurements. The various schemes employed in conventional humidity sensors relate the fundamental properties of

water vapour to different transduction schemes that relay on mechanical and electrical approaches to provide humidity induced measurements [60]. These include mechanical hygrometer, which monitors humidity from the expansion and contraction of materials as a result of surrounding humidity. The commonly used humidity sensing materials include synthetic fibers and human hair. Another device used for humidity measurement is wet and dry psychrometer [60]. It is made of two thermometers (glass or electric) one of which has a wet cotton or linen wick around its bulb to determine the wet bulb temperature and the other to measure the temperature of the sample gas (dry bulb temperature). Evaporation of water from the wick absorbs heat from the thermometer bulb, causing the thermometer reading to drop. The dry bulb temperature simply monitors the temperature of the air. Relative humidity is calculated by comparing the readings using a calculation table that compares the ambient temperature (monitored by the dry bulb) to the difference in temperatures between the two thermometers. However, performance of these sensors is limited by slow response and large size. The demand for low cost, reliable, fast and compact sensor has led to the development of electronic humidity sensor. These are mainly resistive and capacitive types. A resistive humidity sensor converts surrounding humidity variation to impedance change [61]. This can be measured by a current, a voltage or a résistance. Commonly used humidity sensing materials are ceramics, polymer and electrolytes. It is simple and has a fast response, but it is easily contaminated by water soluble salts. Capacitive humidity sensor is most popular among commercial humidity sensors. This sensor determines humidity variation through dielectric constant change of a thin hygroscopic film upon exposure to moisture [62]. The change in dielectric constant is nearly directly proportional to the relative humidity of the surrounding environment. Thus, by monitoring the change in capacitance, relative humidity can be determined. All the techniques discussed so far have their own particular advantages. However, performance of these sensors is limited owing to their inability towards remote and

distributed sensing, multiplexing, deployment in harsh environments and their susceptibility to electromagnetic and radio frequency interference. In order to overcome these limitations, researchers tried develop humidity sensors employing optical technology; especially fiber optics.

Optical fiber sensors are capable of addressing all the inherent limitations of conventional sensors. Hence, various sensing schemes in conjunction with fiber optics have been exploited to develop all-optical RH sensors [63-88]. Russell and Fletcher [63] immobilized a cobalt chloride ($CoCl_2$)/gelatin film on a 12cm-long silica optical fiber to realize an optical fiber RH sensor. A dynamic range of 40-80%RH is reported. Ballantine and Wohltjen [64] reported a humidity sensor using a 9cm long glass capillary waveguide coated with $CoCl_2$/poly(vinylpyrrolidone) (PVP) film. The sensor showed good sensitivity in the RH range of 60-95%RH. Zhou et al. [65] employed the same calorimetric reagent in conjunction with a porous optical fiber for monitoring humidity in the low range. Mitschke [66] has reported an optical fiber humidity sensor based on a porous thin film interferometer (Fabry-Perot) on the tip of the fiber. Humidity variation results in the change of refractive index of the thin film. This causes change in the reflectivity of the interferometer and hence, modulation of the reflected intensity. This sensor measures RH variation in the range of 0-80%. Brook et al. [67] have reported an optical fiber humidity sensor in which Nafion-crystal violet complex immobilized on a glass substrate was used as the sensing element. In this work, optical fiber was used as a light guiding medium to couple light from the source to sensing element and from sensing element to the spectrometer. Experimentally observed sensor responses to different humid environments had been used as inputs to artificial neural network (ANN), and a linear response over a dynamic range of 40-82%RH was achieved. Otsuki et al. [68] have demonstrated an optical fiber RH sensor using curved fiber geometry.

The decladded curved portion was coated by a film of Rhodamine B/hydroxyl-propyl cellulose to realize the sensing probe. A dynamic range of 0-95%RH is reported. Bownass et al. [69] have reported a single-mode fiber based humidity sensor which works in telecommunication wavelength. The sensing principle was based on the humidity induced refractive index change of an organic film which was coated on the cladding of a bent fiber. The sensor was able to measure humidity variation in a high range of 62-80%RH. Another RH sensor reported by Bariain et al. [70] was based on a tapered fiber coated with agarose gel. The reported dynamic range is 30-80%RH. Gupta and Ratnanjali [71] have reported a fiber optic humidity sensor based on the moisture dependent absorption of light by the phenol red doped polymethylmethacrylate (PMMA) film over a small portion of the lower refractive index core of U-shaped plastic-clad-silica (PCS) fiber and had a response time of 5 second with a dynamic range of 20%RH to 80%RH. Arregui et al. [72] have reported an optical fiber sensor configuration for simultaneous measurement of humidity and temperature. It consists of a Fabry–Perot cavity at the fiber tip fabricated by electro-static self-assembled monolayer process for humidity detection and an in-fiber grating for temperature measurement. Experimentally observed dynamic range is from 11%RH to 97%RH. Muto et al. [73] have reported a plastic optical fiber humidity sensor using straight probe geometry by realizing a sensing film of hydroxyl-ethylcellulose/polyvinyl-idenefluoride in the decladded region of a multimode fiber. Observed dynamic range of the sensor is ~20-89% RH. Gaston et al. [74] have reported a fiber-optic RH sensor based on the interaction of evanescent wave in a side-polished single-mode fiber with a poly-vinyl-alcohol (PVA) overlay. The sensor responded linearly in the RH range of 70-90% only. Another side-polished fiber based RH sensor is reported by Herrero et al. [75] where they used overlay of Titanium dioxide (TiO_2) as humidity sensing film. The sensor responded linearly with a high sensitivity in the low humidity range (0-15%RH) only. Tay et al. [76] have reported humidity sensor based on U-

shaped plastic optical fiber. A good sensitivity of 74.85mV/%RH is achieved in a dynamic range of 65-85%RH. Shukla et al. [77] have reported a nano-like magnesium oxide (MgO) film based optical fiber humidity sensor. MgO film has been deposited on a U-shaped glass rod to realize the sensor. Observed dynamic range of the sensor is ~5-80%RH. Khijwania et al. [78] have reported a RH sensor based on a U-shaped probe coated with anhydrous $CoCl_2$ doped PVA film. The sensor was responsive in the RH range 10% to 90%. In reference [30] Khijwania et al. have comprehensively optimized the performance of sensor, reported in their previous study [78], in order to enhance the sensitivity as well as dynamic range. The dynamic range of the optimized sensing probe is found to be 1.6-92%RH with response time of 1second. Matias et al. [79] have reported an optical fiber humidity sensor based on nano-coatings employing electrostatic self-assembly (ESA) technique. The response time of the sensor was shorter than 300 ms, but the dynamic range is 75-100%RH only. Corres et al. [80] have reported a tapered optical fiber based humidity sensor using nanostructured sensitive coating. The sensor showed a variation of 16dB in optical power with a response time of 300 ms for changes in RH from 75% to 100%. Corres et al. [81] have reported another RH sensor using nanostructured coating of Silicon dioxide (SiO_2) nanoparticles at the tip of single-mode fiber. ESA technique has been used to realize multilayer film of SiO_2 nanoparticles. The dynamic range of the sensor is observed to be 40-98%RH with a response time of 150ms. Zhang et al. [82] have reported the fast detection of humidity with a subwavelength–diameter fiber taper coated with gelatin layer. The dynamic range and the response time of the sensor are 9-94%RH and 70ms respectively. Vijayan et al. [83] have reported an evanescent wave fiber optic humidity sensor, which was constructed by depositing Co nanoparticles dispersed in polyaniline over an exposed core region of a multimode fiber. A dynamic range of 20-95%RH is reported. Sreenivasan et al. [84] have reported an optical fiber based humidity detection, using ANN, where they have used the response of the optimized probe in [30] as

the input of ANN for its training. Akita et al. [85] have reported an optical fiber humidity sensor based on a hetero-core optical fiber that was coated with hygroscopic polymer layers. The sensor was developed by splicing a small piece of single-mode fiber between two multimode fiber pieces. Observed dynamic range is 50-92.5%RH. Another hetero-core fiber sensing probe based RH sensor was reported by Wu et al. [86] where they used a small-core single-mode fiber spliced between two single-mode fiber (SMF-28) pieces as the sensing probe. The dynamic range reported is 40-95%RH. Recently, SPR technique is also used to develop optical fiber humidity sensor. Hernaez et al. [87] have reported a SPR based optical fiber humidity sensor by realizing indium tin oxide (ITO) coating onto the decladded portion of a straight fiber followed by a polymeric coating. The dynamic range reported is 20-80%RH with an average sensitivity of 1.08nm/%RH. Another ITO based SPR humidity sensor has been reported by Zamarreno et al. [88] where they turned the thickness of polymeric coating to improve sensor's performance. The observed dynamic range is 20-90%RH. In all these reported sensors, if the dynamic range is large, then the sensor response is nonlinear throughout. If the sensor response is linear, dynamic range is very small. Thus, all these reported fiber based sensors have a nonlinear response with a piece-wise limited linear sensitivity.

With the maturity of optical fiber based devices, other schemes have also been exploited to develop an all-optical humidity sensor with large dynamic range, linear response and a better sensitivity [89-97]. Tan et al. [89] have reported a gelatin-coated Long Period Grating (LPG) sensor for humidity detection in high range. This sensor could respond linearly for the RH variation from 90-99% with sensitivity of 0.833%RH/dB. Konstantaki et al. [90] have reported a LPG humidity sensor utilizing poly (ethylene oxide)/$CoCl_2$ as a hybrid hygrosensitive cladding coating. The sensor could detect RH variation in the range from 50%

to 95% with a resolution better than 0.2%. Liu et al. [91] have reported another LPG based RH sensor in which LPG has been coated with hydrogel for humidity detection. The sensor response is observed to be linear in a range of 38.9-100%RH with the sensitivity of 0.2nm/%RH. Venugopalan et al. [92] have reported a LPG-based humidity sensor in which PVA film was used as sensing material. The sensor could respond over a RH range from 33 to 97%. Viegas et al. [93] have reported a fiber optic humidity sensor based on the change of the grating resonant wavelength of a LPG fiber that has been coated with SiO_2 nanospheres. The range of the sensor was from 20% to 80%. However, since the sensitivity was low, Viegas et al. [94] have reported another sensor where the sensing film was modified to include an intermediate film of higher refractive index to increase the total refractive index. The sensitivity improved by 3 times due to this modification. Miao et al. [95] have reported a humidity sensor based tilted fiber Bragg grating (FBG) where PVA has been used as the humidity sensing film. Sensor response is observed to piecewise linear in the RH ranges 20-74% and 74-98%. Yeo et al. [96] have reported a polymer coated FBG sensor for humidity detection. This sensor could respond linearly in the RH range 23-97 with sensitivity of ~5.6pm/%RH. Another FBG based RH sensor was reported by Huang et al. [97] where they used thermoplastic polyimide coating on FBG for humidity detection. For this the linear dynamic range was extended to 11-98%RH. The observed linear sensitivity is 0.266mV/%RH. The main limitation of gratings based sensors is the temperature as well as strain cross-sensitivities. Furthermore, such sensors require bulky and costly interrogation devices. A simple, inexpensive relative humidity sensor with linear response and optimum sensitivity over widest possible dynamic range is a good choice for real-filed applications.

Main objective of the thesis is to develop a simple optical fiber RH sensor having linear response over widest possible dynamic range and with an optimum sensitivity. Three

different methodologies have been used to fulfill this objective. First methodology is based on the exploitation of evanescent wave for intensity modulation in a straight and uniform PCS multimode fiber. Optical fiber RH sensor is developed in this by chemically synthesizing the decladded portion of the fiber by a reagent (Zinc oxide (ZnO) nanoparticles) and in-house scaled Titanium dioxide (TiO_2) nanoparticles embedded sol-gel sensing film. Second methodology is based on a direct and exhaustive attenuation of guided mode through a ZnO nanoparticles immobilized nanostructure nanoporous sol-gel fiber core which is expected to enhance the sensitivity many fold. The sensor response is compared for sensitivity optimization. In the third and final methodology in an anticipation of further enhancing the sensitivity and having exhaustive comparative analysis, LSPR based RH sensor is developed employing in-house scaled metal and/or dialectic nanoparticles.

Chapter-2 of the present thesis is devoted to develop an optical fiber relative humidity sensor having throughout linear response over a widest possible dynamic range. An evanescent wave absorption based intensity modulation scheme is employed to fulfill this objective. The fiber sensor employs a specific nanoparticle, (ZnO), doped sol-gel nanostructured sensing film synthesized over a short length of a centrally decladded straight and uniform PCS optical fiber of pre-researched core-diameter. A detailed experimental investigation is carried out to optimize the sensor performance in terms of concentration of ZnO nanoparticles in sol-gel sensing film and the film-thickness. To do so, four different compositions were achieved by adding 0.1, 0.2, 0.3 and 0.4g ZnO nanoparticle to the sol solution. For every composition, film thickness was again varied using multiple dip-coating. A humidity chamber has been designed and developed for the proper characterization of the sensing probes. These sensing probes were characterized by exposing them to different humid environments. From the analysis of experimental data it is observed that in all the film-compositions, sensing probe

corresponding to 3-dip coating has best performance. Significantly, responses for the sensor employing 3-dip coated probe carrying 0.4g nanoparticle concentration in the sensing cladding is observed to be linear over a dynamic range of 30-80%RH. In all, a highest linear sensitivity of is 0.0033/%RH also observed for this sensor. Decreasing nanoparticle concentration sol solution showed a decrease in the sensitivity; but an increase in the linear dynamic range. Largest linear dynamic range of 4-96%RH is observed for 3-dip coated probe having 0.1g nanoparticle concentration in the sensing cladding. The observed linear sensitivity is 0.0012/%RH. It is important to mention that a linear response over such a wide dynamic range employing such a simple geometry (straight and uniform optical fiber sensor) is observed for the first time to the best of our knowledge. Further, dynamic performance of the optimized probe was investigated by exposing it to cyclic perturbation of low and high humid environments. An average response time of 0.06 second was observed for humidification, whereas an average response time of roughly 5.5 times less than that of the commercial sensor was observed during the desiccation. A maximum fiber output variation is observed to be of the order of 10^{-5} during the repeatability and reversibility test over a span of few days.

In chapter-3, in order to increase the sensitivity keeping the linear dynamic range close to the maximum as observed in Chapter-2, a novel mechanism of an exhaustive attenuation of entire guided mode through an in-house developed ZnO nanoparticle immobilized nanoporous sol-gel optical fiber is employed to design RH sensor. To fabricate the nanoparticle immobilized sol-gel fiber humidity sensor, sol solution containing optimized ZnO nanoparticles concentration corresponding to the optimum sensor reported in Chapter-2 was used. A proper control/close watch on reaction parameters led to a crack free sol-gel fiber with almost uniform diameter over a length of 14 mm, almost flat end surfaces and nanometer scaled

porosity. To characterize the nanoparticle immobilized sol-gel microstructure nonporous optical fiber as a humidity sensor, it was aligned and mechanically spliced between the two pieces of identical plastic-clad silica (PCS) multimode fiber; and fixed carefully midway inside the humidity chamber. The sensor was exposed to different humid environments. From the analysis of experimental data it is observed that sensor responds linearly in the dynamic range 5-95%RH with sensitivity of 0.0103/%RH. This linear dynamic range is comparable to that of optimized sensing probe based on evanescent wave absorption scheme with ZnO nanoparticles immobilized sol-gel humidity sensing cladding. Most importantly, observed sensitivity is ~9 times higher than that of reported based on evanescent wave absorption scheme with straight fiber geometry. An average response time of the developed sensor was ~0.7 times the average response time of the commercial sensor during desiccating, indicating the sol-gel fiber sensor responses faster than that of the commercial RH sensor. The average response time of sol-gel fiber sensor was observed to be little high during humidification as compared to the response time during desiccation; however it was still faster than commercial RH sensor. In addition, a maximum fiber output variation is observed to be of the order of 10^{-4} only during the repeatability and reversibility test over an interval of few days.

Chapter-4 of the thesis is devoted to comparatively optimize the sensor's response with different sensing agent and to possibly further enhance the sensitivity. For this, sensing probe was developed using a different reagent (TiO_2 nanoparticle) immobilized nanostructured sol-gel humidity sensing film on the centrally decladded optical fiber. A comprehensive experimental investigation is carried out to optimize the design configuration/parameters of the nanostructured sensing film and to achieve the best possible sensor's response. To do so, five different compositions of nanostructured sensing film were achieved by varying nanoparticle colloidal solution concentration to 6, 8, 9 10, and 12 % (v/v) in the sol solution

during the film preparation stage. Multiple dip coating was employed for each composition to prepare the optical fiber sensing probes with varying film thickness to approach a maximum sensitivity. From the analysis of experimental data it is observed that 3-dip coated probe of 9% (v/v) nanoparticle concentration in sol has the optimum performance. The observed linear dynamic range of this probe is 24-95%RH with enhanced sensitivity of 27.1mV/%RH. Response characterizes of the optimized probe is compared against other optical fiber RH sensors reported in the literature employing various schemes. It is observed that linear dynamic range of the developed sensor is slightly lower than the largest reported in the literature. Nevertheless, its sensitivity is 102 times higher than the sensing probe having largest linear dynamic range. Average response times of humidification and desiccation cycles are observed to be 0.01 second and 0.06 second respectively. Furthermore, maximum fiber output variation is observed to be of the order of 10^{-4} only during the repeatability and reversibility test over an interval of few days.

Finally, in Chapter-5, for an exhaustive comparative analysis, another optical fiber RH sensor was developed employing metal as well as metal-dielectric nanoparticle assisted LSPR. A U-shape probe geometry, rather than the straight and uniform geometry, was used to ease out the realization of nanoparticle film on the fiber surface for sensor development. The decladded portion of the fiber (U-shaped region) was chemically synthesized with metal as well as metal-dielectric nanoparticle films to realize the LSPR humidity sensing probes. A detailed experimental investigation is carried out employing nanoparticle films of gold and silver. The sensing probe was carefully fixed inside the humidity chamber for its characterization. Fiber sensor output spectra corresponding to different humid environments were recorded using the spectrometer. It was observed that the peak absorption wavelength shifted towards higher wavelength upon increasing the humidity. From the analysis of

experimental data, a linear dynamic range of 6-90%RH with a sensitivity of 0.0213nm/%RH was achieved for gold nanoparticle assisted LSPR optical fiber sensor; whereas for metal-dielectric (gold-TiO_2) nanoparticles assisted LSPR optical fiber RH sensor, a linear dynamic range of 12-80%RH with a sensitivity of 0.0177nm/%RH is observed. For (silver-TiO_2) nanoparticles assisted LSPR optical fiber RH sensor, a linear dynamic range of 29-95%RH is observed with an enhanced sensitivity of 0.0412nm/%RH. Response characterizes of the developed sensors are compared against other optical fiber RH sensors reported in the literature employing wavelength interrogation scheme.

Above work has resulted in following publications:

(A) IN INTERNATIONAL JOURNALS

1. R. Aneesh and Sunil K. Khijwania, "Zinc oxide nanoparticle based optical fiber humidity sensor having linear response throughout a large dynamic range", **Applied Optics**, 50, 5310-5314 (2011).
2. R. Aneesh and Sunil K. Khijwania, "Titanium dioxide nanoparticle based optical fiber humidity sensor with linear response and enhanced sensitivity", **Applied Optics** (Accepted) (2011).
3. R. Aneesh and Sunil K. Khijwania, "Zinc oxide nanoparticle doped sol-gel fiber as humidity sensor with wide linear dynamic range and enhanced sensitivity", (Communicated).
4. R. Aneesh, Abhinav Rastogi and Sunil K. Khijwania, "Metal-dielectric-nanoparticles assisted Localized-Surface-Plasmon-Resonance based U-shaped optical fiber humidity sensor with linear response over a wide dynamic range", (Communicated).

OTHER PUBLICATIONS

5. R. Aneesh, Meeth Maharana, Pathi Munendhar, H. Y. Tam and Sunil K. Khijwania, "Simple temperature insensitive Fiber Bragg Grating based tilt sensor with enhanced tunability", **Applied Optics**, 50, E172-176, (2011).

(B) IN INTERNATIONAL CONFERENCES

1. R. Aneesh, Sunil K. Khijwania, "An optical fiber humidity sensor with linear response throughout its dynamic range", International Conference on Optics and Photonics "**ICOP 09**", Chandigarh, India, 30 October-01 November, (2009).
2. R. Aneesh, Sunil K. Khijwania, "Zinc oxide nanoparticle based optical fiber humidity sensor", International Conference on Advanced Nanomaterials and Nanotechnology "**ICANN 2009**", Guwahati, India, 9-11 December, (2009).
3. Sunil K. Khijwania, R. Aneesh, "Design and development of simple Fiber Bragg Grating based tilt sensor", 12th International Symposium on Microwave and Optical Technology "**ISMOT 2009**", Delhi, India, 16-19 December, (2009).
4. R. Aneesh, Meeth Maharana, H. Y. Tam and Sunil K. Khijwania, "Simple temperature insensitive Fiber Bragg Grating based tilt sensor with a tunale response and a large dynamic range", International Conference on Fiber Optics and Photonics, "**PHOTONICS 10**", Guwahati, India, 11-15 December, (2010).
5. R. Aneesh, Abhinav Rastogi and Sunil K. Khijwania, "Surface Plasmon Resonance based U-shaped optical fiber humidity sensor", International Conference on Fiber Optics and Photonics, "**PHOTONICS 10**", Guwahati, India, 11-15 December, (2010).
6. R. Aneesh, Sunil K. Khijwania, "Titanium dioxide nanoparticle based optical fiber humidity sensor with linear response over a large dynamic range",

International Conference on Fiber Optics and Photonics, "**PHOTONICS 10**", Guwahati, India, 11-15 December, (2010).

7. R. Aneesh, Sunil K. Khijwania, "Nanoparticle doped sol-gel optical fiber as a humidity sensor with linear response over a large dynamic range", 7th International Workshop on Fiber Optics and Passive Components, "**WFOPC 11**", Montreal, Canada, 13-15 July, (2011).

Chapter 2

ZnO Nanoparticle based Simple Optical Fiber Relative Humidity Sensor: Realization of Wide Dynamic Range

2.1 Introduction

Relative humidity is one of the most important parameters to be monitored in numerous areas such as structural health monitoring, semiconductor manufacturing process, chemical/biochemical/food processing industries, air conditioning etc. Most of the conventional humidity sensors, which are resistive and capacitive type, are based on the electrical properties of the sensing material. The main hindrance of these sensors for real-field applications is their inability towards multiplexing, remote sensing, deploying in a harsh environment, and a very high sensitivity towards electromagnetic/radio frequency interference to name a few. Relying on a very high sensitivity of the optical signal propagating through an optical fiber to the external perturbations, optical fiber sensors have emerged as a strong alternate to the conventional/bulk optics sensors with a capability to address all the inherent limitations of these sensors. Optical fiber sensors with inherent advantages such as remote & distributed sensing, multiplexing capabilities, very high sensitivity, small volume, light weight, potentially resistant to ionizing radiation etc., have found wide range of real field applications in structural health monitoring (deformations owing to internal strain, temperature, tilt, vibration, torsion effects, and deterioration processes such as steel reinforcement corrosion and alkali-silicate gel formation in concrete

owing to internal humidity effects), environmental (pollution, hazardous gases, humidity etc.) monitoring and bio/chemical diagnosis to name a few [27-28]. Hence many researchers over the years exploited various schemes to design and develop optical fiber RH sensors. Russell and Fletcher [63] immobilized $CoCl_2$/gelatin film on a 12cm-long silica optical fiber, whereas Ballantine and Wohltjen [64] employed the same calorimetric reagent/polymer system on 9cm glass capillary to realize an optical waveguide humidity sensor. Gupta and Ratnanjali [71] have reported a fiber optic humidity sensor based on the moisture dependence absorption of light by the phenol red doped PMMA film over a small portion of the core of U-shaped plastic-clad-silica fiber. Gaston et al. [74] have reported a fiber-optic RH sensor based on the interaction of evanescent wave in a side-polished single-mode fiber with a PVA overlay. Khijwania et al. [30] have reported a RH sensor based on a U-shaped probe coated with anhydrous $CoCl_2$/PVA film. Matias et al. [79] have reported an optical fiber humidity sensor based on nano-coatings employing ESA technique. Corres et al. [80] have reported a tapered optical fiber based humidity sensor using nanostructured sensitive coating. Zhang et al. [82] have reported the fast detection of humidity with a subwavelength–diameter fiber taper coated with gelatin layer. Akita et al. [85] have reported an optical fiber humidity sensor based on a hetero-core optical fiber that was coated with hygroscopic polymer layers. Liu et al. [91] have reported a LPG based RH sensor in which LPG has been coated with hydrogel for humidity detection. Huang et al. [97] have reported a FBG based RH sensor in which the FBG has been coated by thermoplastic for humidity detection. However, all most all non-fiber grating based optical fiber RH sensors, reported in the literature, employing different mechanisms exhibit nonlinear response with a piece-wise limited linear sensitivity. Though fiber-grating based humidity sensors have wide linear dynamic range, performance of these sensors is limited by temperature as well as strain cross sensitivity and the need of

costly and bulky interrogation devices. Ideally a sensor should have a wide dynamic range and a linear response throughout its observed dynamic range with a high sensitivity.

This chapter describes the development of a simple optical fiber humidity sensor with a linear response over a very wide dynamic range. Owing to the fact that the nanoparticle has unique structure and high surface to volume ratio, optical fiber humidity sensor is developed using ZnO nanoparticles immobilized nanostructured sol-gel sensing film onto the centrally decladded plastic-clad-silica optical fiber and an evanescent wave based intensity modulation technique. A comprehensive experimental study is carried out in order to achieve the optimum humidity sensing cladding configuration. Performance of the optimized probe is compared against a commercially available relative humidity sensor. The response characteristics of the sensor are observed to be usually very fast, repeatable and fully reversible. Most importantly, the response is observed to be linear throughout the dynamic range as wide as 4% to 96%RH. A linear response over such a large dynamic range is observed for the first time to the best of our knowledge in such a simple approach. Even following the testing of the sensor in extreme conditions for more than 10 days, the sensing characteristics are observed absolutely invariable.

2.2 Experimental

2.2.1 Sol-gel process

Sol-gel process is a method used for the synthesis of glassy material at room temperature. Generally, sol-gel process consists of hydrolysis and condensation of a metal alkoxide. The commonly used metal alkoxides are silicon alkoxides, e.g., $Si(OC_2H_5)_4$, Tetraethyl orthosilicate (TEOS) and $Si(OCH_3)_4$, Tetramethylorthosilicate (TMOS). Silica glass prepared by the sol-gel method is a nanoporous glass matrix that contains inter-connected pores formed by a three-dimensional SiO_2 network [98]. Sol-gel process can be divided into

following steps: mixing (to form a solution), gelation, aging and drying. In solution stage, for example, suitable volumes of TEOS, ethanol and water are mixed. A suitable volume of HCl that serves as a catalyst, is added to this solution under continues stirring/sonication to get a solution termed as sol. This sol is kept for gelation for several hours/days under a stable environment. The hydrolysis and condensation reactions take place are as following:

Hydrolysis: this results in the formation of silanol group (Si–OH)

$$Si(OC_2H_5)_4 + H_2O \rightarrow Si(OC_2H_5)_3(OH) + C_2H_5OH$$

Condensation: silanol group further react to form siloxane polymers

$$Si(OC_2H_5)_3(OH) + Si(OC_2H_5)_3(OH) \rightarrow (OC_2H_5)_3Si{-}O{-}Si(OC_2H_5)_3 + H_2O$$

During the aging process, poly-condensation reaction (condensation polymerization) takes place which results in a cross linkage of silanol with siloxane leading to the formation of SiO_2 nanostructure network (with silanol groups on the surface). The resulting gel contains ethanol and water as byproducts. These solvents can be evaporated by annealing the gel at higher temperature. A sensing agent added to the mixture at some time during the formation of sol can be securely trapped within the nanoporous glass matrix. The porosity of the nanostructure sol-gel glass allows an analyte to diffuse readily in and out of the pores of sol-gel glass matrix. Apart, the sol-gel derived nanostructure glass matrix has the following advantages: (a) sol-gel derived glass is made of silica, which is chemically inert; hence the sensing probe, based on such glasses can be used in harsh environments, (b) it is compatible with many inorganic and organic reagents; hence various sensing agents can be entrapped within the nanostructure glass matrix, (c) the low temperature synthesis also allows the entrapment of molecules with low chemical and thermal stability. To design an optical fiber sensor, the sol-gel film containing the sensing agent can be realized on the bare core of the optical fiber

employing dip-coating method. Several sol-gel based optical and optical fiber sensors have been reported in the literature [99-102].

2.2.2 Humidity sensing probes preparation

Sensitivity of an evanescent wave absorption based optical fiber sensor, for a straight and uniform probe, depends on the fiber core diameter [103]. The sensitivity is inversely proportional to the core diameter of the sensing probe. This is due to the fact that as the core diameter decrease, number of ray reflection per unit length increases. As a result, more power is available with the evanescent field in the sensing region to interact with the analyte. Hence, plastic-clad-silica multimode fiber of pre-researched optimum core diameter of 125µm [103] was used to develop the sensor. Fiber has a core refractive index of 1.457 and cladding refractive index of 1.404, which give the critical angle of the fiber roughly equal to 75^{o}. The total length of the fiber used was around 60cm. Fiber ends were prepared properly to get optically-flat end faces perpendicular to the axis of the fiber which provides the efficient coupling of light from source to fiber and fiber to the detector. About 5 cm of the cladding was carefully removed from the central portion of the fiber. After that, it was sonicated in soap solution (Merk) and then in de-ionized water. Finally, it was cleaned with acetone. ZnO nanoparticles were then synthesized through a sol-gel matrix over this centrally decladded portion of the fiber to fabricate the sensing film. It's worth mentioning that the properties of sol-gel glass matrix film, e.g, nanostructures pour size, porosity, film thickness, refractive index, appearance (crack free) can be tailored by carefully controlling the chemical composition and process during the sol-gel synthesis stage. To do this, chemical compostion of the sol was first optimized. TEOS, de-ionized water, ethanol and hydrochloric acid were mixed in a proper volume ratio under continuous stirring to prepare sol. This solution was further stirred for another 30 min. A small volume of this sol was poured into a beaker and

kept for several days for gelation under a stable environment. A crack free sol-gel matrix was achieved for an optimized volume ratio of 3: 2: 1: 0.01 for TEOS, de-ionized water, ethanol and hydrochloric acid. Hence, to prepare optical fiber humidity sensing probe, the sol solution was prepared by mixing 15 mL of TEOS, 10 mL of de-ionized water, 5 mL of ethanol and 50 µL of hydrochloric acid (in optimum ratio). The solution was then stirred for 30 min and kept for 36 hours to make it more viscous. Afterwards, ZnO nanoparticles (reagent) of size less than 100nm (Sigma-Aldrich) were added to the sol under continues stirring to have a uniform distribution of nanoparticles in sol solution. The decladded potion of the fiber was dip-coated at a pre-determined speed to ensure a uniform coating of the reagent immobilized sol. In order to study the effect of nanoparticle concentration on sensor performance, three different compositions were achieved by adding 0.2g, 0.3g and 0.4g ZnO nanoparticle to the sol solution. For the performance optimization of the sensor, multiple dip coating (2-dip, 3-dip and 4-dip) was employed for each composition. This way sensing probes with identical film thickness, but varying film's chemical composition, as well as, sensing probes with identical film's chemical composition, but varying film thickness were practically realized. The sensing probes were dried at the room temperature for two days. Afterwards, they were annealed at 160ºC in an oven for 4 hours in order to remove trace ethanol and water molecules (resulted by condensation reaction) from the pores of the film.

2.2.3 Design and development of humidity chamber

A humidity chamber has been designed and developed for the proper characterization of optical fiber humidity sensor. It was made of perpex sheet of thickness 1cm. The total dimension of the chamber was 11 cm × 9 cm × 7 cm. The schematic diagram of experimental set up is shown in Fig. 2.1. In this provision, dried air was first divided into two channels. Dry air coming from one channel was passed through a water bath using a flow meter to

make it humid and then fed to the humidity chamber. Dry air coming from the other channel was directly fed to the humidity chamber using another flow meter. Flow meters were used to properly mix dry and humid air in the humidity chamber to control RH within the chamber. A small outlet valve was made in the humidity chamber in order to maintain the proper air flow. A commercially available humidity sensing probe (Rotronic-*HygroClip*), which can monitor humidity as well as temperature, was fixed inside the humidity chamber. The output of this probe was connected to one of the input channels of a data acquisition card (DAQ) which was interfaced to the computer using LABVIEW programming.

2.2.4 Sensing probe characterization

Optical fiber humidity sensing probe was fixed inside the humidity chamber in such a way that the sensing region comprising nanoparticle immobilized sol-gel nanostructured film was in the middle of the chamber. Light from a He-Ne laser, operating at 632.8nm, was coupled to the one end of the fiber. The distal end was connected to a photodetector using SMA (sub-miniature version A) connector. The photodetector was interfaced to the computer using DAQ card and LABVIEW programming as explained earlier. The schematic diagram of experimental setup for sensor characterization is shown in Fig.2.1. To start the measurement, humidity was reduced by passing the dry air inside the chamber. For this, dry air flow meter was completely opened and humid air flow meter was completely closed. The dry air reduced the humidity level to the minimum possible value. After that, the humidity was slowly increased to the maximum possible value in suitable steps. The fiber output and humidity were measured, in each step, after sufficient time needed for them to get stabilized. The fiber output as well as commercially available probe output was recorded as a function of time with a resolution of 1second.

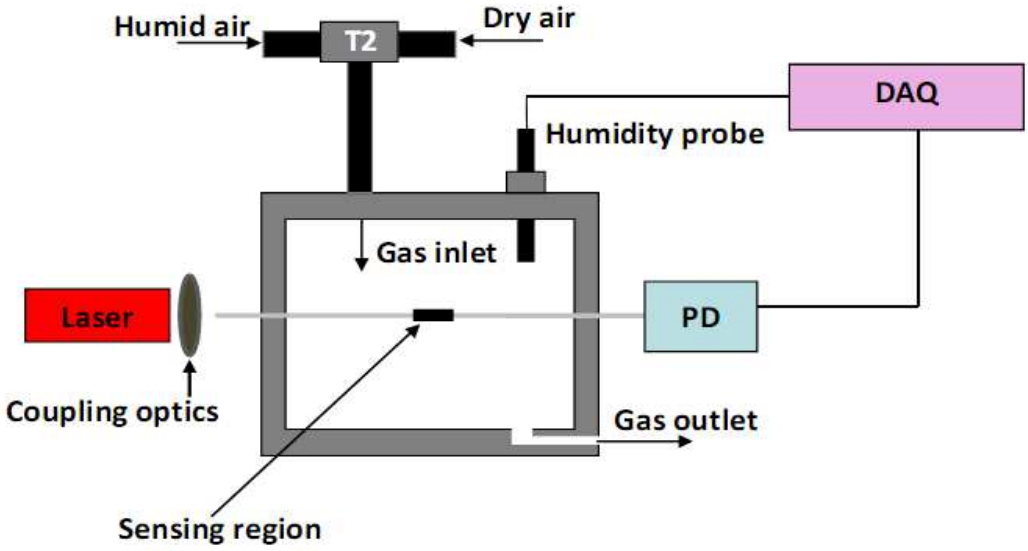

Figure 2.1: *Schematic diagram of experimental setup for optical fiber humidity sensor characterization.*

2.3 Results and Discussion

The sensor is based on the phenomenon of intensity modulation through evanescent wave absorption where a small portion of the optical power in the cladding region interacts with the sensing ZnO nanoparticles embedded nanostructured sol-gel thin film. To carry out the experiment and to study the sensor response, the fiber output as well as the commercial sensor's output was recorded as a function of time with a resolution of 1 second. Measurements were carried out for both increasing and decreasing humidity cycles. All these measurements were recorded at a constant temperature (25^{o}C). A slow and step humidity variation was made inside the chamber by keeping constant value of humidity for sufficient time. A typical time response of optical fiber sensor (3-dip coated probe of 0.2g ZnO nanoparticle concentration in sol solution), as an example, is depicted in Fig. 2.2 while

increasing RH. It may be noted that as the humidity increases, fiber output decreases. This is because of the fact that the nanoparticles immobilized dry sol-gel has almost negligible absorption at a low humidity for 632.8nm; whereas the absorption within the sensing sol-gel film increases at high humidity at the same wavelength. As the surrounding humidity increases, absorption increases**,** hence the output power decreases. Similar qualitative behaviour was observed for the other probes also and for decreasing RH variation. From these data, fiber output corresponding to the applied humidity (commercial sensor output) was read from the stabilized portion (on the time scale) and plotted against the applied RH values to investigate/ analyse fiber sensor response.

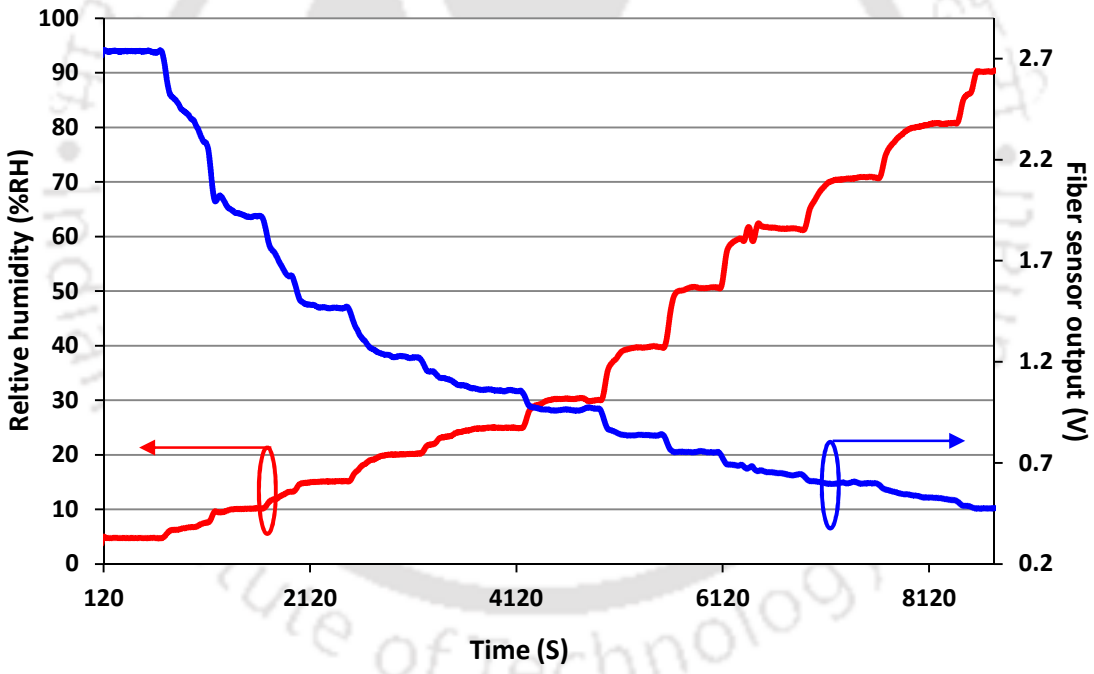

Figure 2.2: *Responses of commercial humidity sensor and fiber optic humidity sensor (3-dip coated probe of 0.2g ZnO nanoparticle concentration in sol solution).*

In order to optimize the sensor performance, response characteristics of all sensing probes with varying film thickness for each varying film composition is studied. Since the sensing

film in each case is deposited from the same respective solution, any difference in response should be attributed to the difference in the film thickness. To analyze the effect of film thickness on the fiber sensor response, normalized fiber sensor output against %RH is plotted in Fig. 2.3, for all three probes (2-dip, 3-dip and 4-dip) corresponding to 0.4g nanoparticle concentration in sol solution. Fiber sensor output and %RH values, both, were extracted from the stabilized portion of their response characterizes. As can be observed from the figure, 2-dip coated probe responds linearly from 40%RH to 67%RH. Observed linear sensitivity of this probe is 0.0012/%RH. Increasing film thickness (from 2-dip to 3-dip) improved sensitivity as well as dynamic range of the sensor. The linear dynamic range of 3-dip coated probe is observed to be 30-80%RH, which is higher than the one for 2-dip coated probe. 3-dip coated probe is observed to have a sensitivity of 0.0033/%RH in the observed linear dynamic range. Compared to 2-dip coated probe, sensitivity of 3-dip coated probe is improved by factor 2.75. Further increase in the film thickness (from 3-dip to 4-dip) decreased the sensitivity to 0.0012/%RH without affecting the linear dynamic range. This shows that there exists an optimum film thickness for 0.4g nanoparticle film composition. In this case, the optimum film corresponds to 3-dip coated probe. Following reasons could be attributed to the observation of an optimum film thickness. For 2-dip coated probe, the film thickness was much less than that of the penetration depth of the evanescent wave [30]. Correspondingly, less number of immobilized nanoparticles were available in the sol-gel sensing cladding to interact with the evanescent wave. Equally importantly, the evanescent wave extended beyond the sensing film and remained unexhausted as for as its interaction with the nanoparticle, and hence, with the water vapour is concerned. With the increase in the humidity, water molecules that are diffused into the pores of the sensing film could interact with a limited number of nanoparticles only, resulting in a limited absorption of the optical power carried by the evanescent field in the sensing region. Thus, a low sensitivity was

observed. The thickness of the sensing film corresponding to 3-dip coated probe was of the order of the penetration depth and hence higher than that for the 2-dip film.

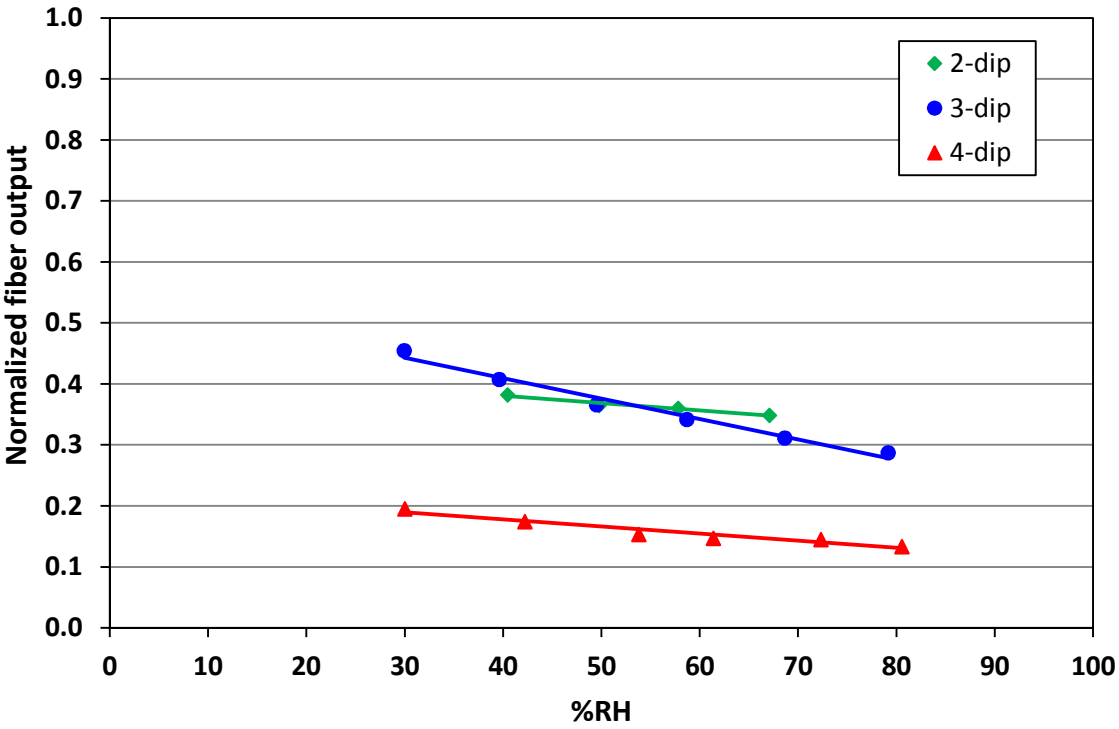

Figure 2.3: *Linear response of 2-dip, 3-dip and 4-dip coated probes corresponding to 0.4g ZnO nanoparticle concentration in sol solution.*

With higher nanoparticles within the sol- gel film to interact with the optical power and with complete exploitation of the optical power available in the evanescent field, optimum optical absorption was observed in this case. This led to the higher sensitivity as compared to the 2-dip coated probe. Thickness of the sensing film for 4-dip coated probe was more than the evanescent wave. Thus, less number of water molecules could diffuse into the volume of the film spanned by the evanescent wave to interact with the corresponding optical power in the wave. This reduced the sensitivity compared to 3-dip coated probe.

In the next step, sensing probes corresponding to 0.3g nanoparticle concentration in sol solution were characterized. Normalized fiber sensor output against applied %RH for three probes (2-dip, 3-dip and 4-dip coated probes) for this film composition are shown in Fig.2.4. As can be observed from the figure, linear dynamic range of 2-dip coated probe is 31-80%RH with a sensitivity of 0.002/%RH. Once again, increasing film thickness from 2-dip to 3-dip increased the sensitivity of the probe as observed for the pervious film composition. 3-dip coated probe has sensitivity of 0.003/%RH in the observed linear dynamic range (30-80%RH). Further increasing film thickness from 3- dip to 4-dip decreased the sensitivity to

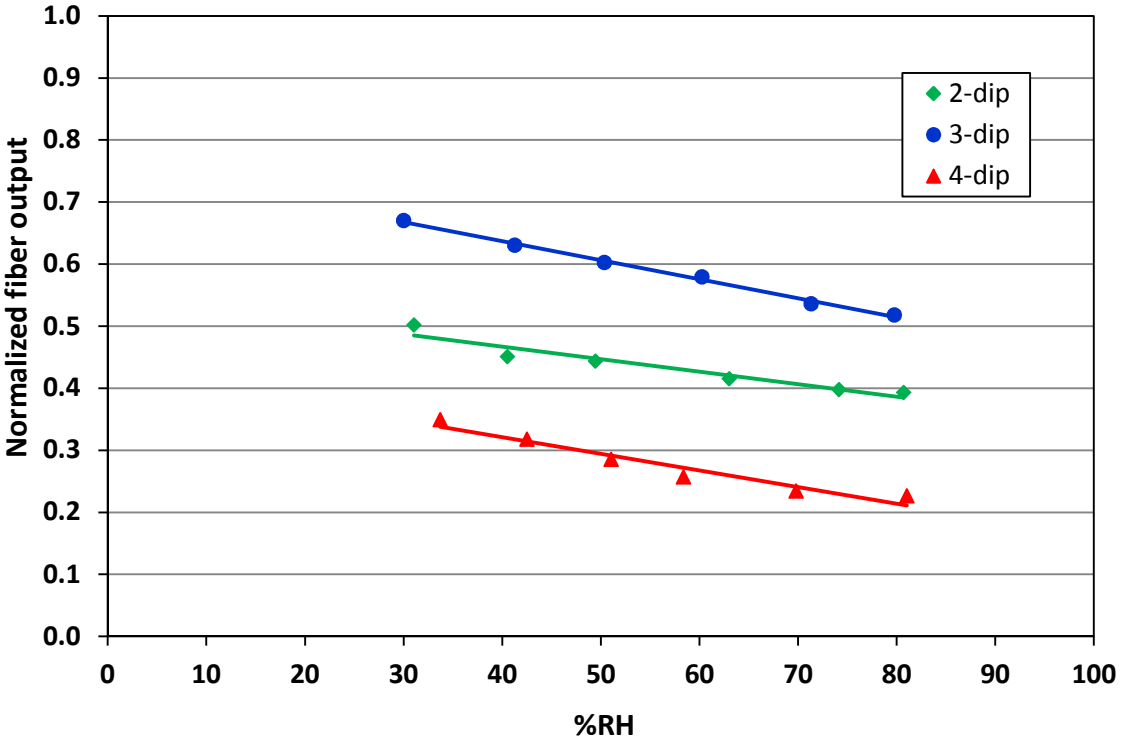

Figure 2.4: *Linear response of 2-dip, 3-dip and 4-dip coated probes corresponding to 0.3g ZnO nanoparticle concentration in sol solution.*

0.0027/%RH. Thus, again, 3-dip coated probe showed a better performance characteristics compared to the 2-dip and 4-dip coated probes, which establishes the existence of optimum film thickness corresponding to 3-dip coated probe even for this film composition. However,

compared to previous composition, sensitivity of 3-dip coated probe decreased without affecting the dynamic range. This is expected to be due to the decrement in number of nanoparticles in the humidity sensing film.

Optical fiber sensing probe corresponding to 0.2g of ZnO nanoparticle immobilized sol-gel silica matrix as a sensing cladding of varying film thickness (2-dip, 3-dip and 4-dip) were similarly characterized afterwards. 3-dip coated probe for this film composition showed a better sensitivity as compared to the 2-dip and 4-dip coated probes, confirming the existence of optimum film thickness for this case as well. A linear dynamic range of 30-90%RH with a sensitivity of 0.0027%RH was observed for 3-dip coated probe having film composition corresponding to 0.2g ZnO nanoparticle in the sol. Comparing the response of optimum film thickness with film composition corresponding to 0.4g, 0.3g, 0.2g ZnO nanoparticle concentration in the sol, following observations were made: (1) maximum sensitivity was observed for 0.4g ZnO nanoparticle concentration. The sensitivity decreases with decrease of ZnO nanoparticle concentration in the film; (2) linear dynamic range increases as the ZnO nanoparticle concentration reduces in the film. Hence, in order to increase the linear dynamic range further, another sensing probe was fabricated with ZnO nanoparticle concentration of 0.1g in sol solution with 2-dip, 3-dip, and 4-dip coatings. Response corresponding to the 3-dip coated probe appeared to be the best for 0.1g ZnO nanoparticle composition also, which is depicted in Fig.2.5. Importantly, as can be observed from Fig.2.5, sensor corresponding to 0.1g ZnO nanoparticle film composition and 3-dip coating responded to an applied humidity as low as 4%RH to as high as 96%RH, thus spanning a dynamic range of 4%RH – 96%RH. The most striking feature of the fiber sensor characteristics is the fact that the fiber sensor responded to the applied humidity changes within this dynamic range linearly. Further reduction of ZnO nanoparticle concentration did not pay any dividend, sensitivity further

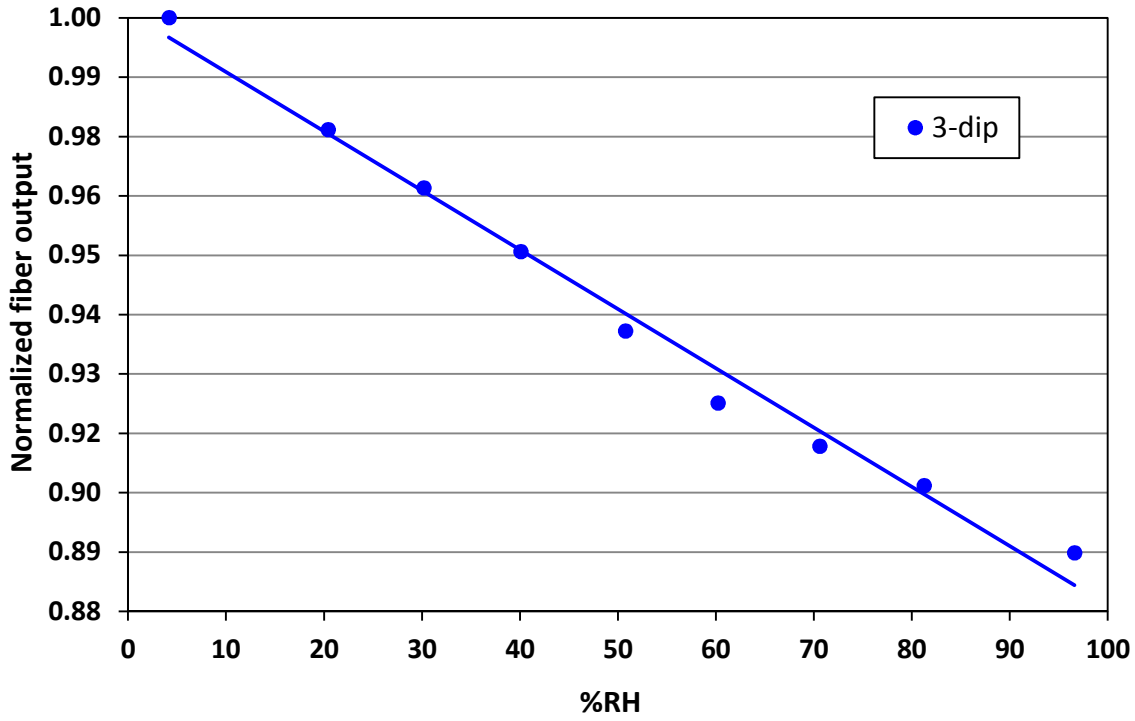

Figure 2.5: *Experimentally observed sensor response of 3-dip coated probe of 0.1g ZnO nanoparticle concentration in sol solution.*

reduced and linear dynamic range remained the same. A linear response throughout over a dynamic range as wide as 4%RH – 96%RH was achieved for the first time to the best of the authors knowledge with such a simple geometry employing nanoparticle embedded sol-gel nanostructured sensing film on a straight and uniform decladded optical fiber (see Table 2.1). A linear sensitivity of 0.0012 RH^{-1} was observed in this case. It is worth mentioning that the sensitivity can be further increased manifold by synthesizing the same nanostructured sensing film on a bi-conical taper [104] or a U-shaped geometry of a pre-researched [103] optimized bending radius made of the same optical fiber.

Table-2.1: Dynamic range comparison of developed sensor with other reported sensors in the literature.

Authors	Sensing element	Linear dynamic range (%RH)
Gaston et al. [74]	Side polished SMF	70-90
Herrero et al. [75]	Side polished SMF	0-15
Tan et al. [89]	LPG	90-99
Liu et al. [91]	LPG	38.9-100
Yeo et al. [96]	FBG	23-97
Huang et al. [97]	FBG	11-98
Vijayan et al. [83]	U-shape plastic fiber	80-92
Tay et al. [76]	U-shape plastic fiber	65-85
Sensor-1 (*3-dip coated probe of 0.4g nanoparticle in sol*)	Straight and Uniform PCS fiber	30-80
Sensor-2 (*3-dip coated probe of 0.1g nanoparticle in sol*)	Straight and Uniform PCS fiber	4-96

Linear dynamic range and the sensitivity for the optimized film thickness (3-dip probe) for various film's chemical composition (ZnO nanoparticle concentration) is compiled in Table-2.2. for an easy comparison. Corresponding sensors are named as S1, S2, S3 and S4. 3-dip coated probe of 0.4g nanoparticle concentration in sol solution is characterized with highest sensitivity. However, its linear dynamic range is only 30-80%RH. Decreasing nanoparticle concentration in sol decreases sensitivity, but increases the linear dynamic range substantially. Three-dip coated probe of 0.1g nanoparticle concentration in sol has largest linear dynamic range (4-96%RH). Nevertheless its sensitivity is lower than the 3-dip coated probe of other compositions. This lead the foundation of remaining investigations in the thesis – possibility of retaining this widest possible linear dynamic range achieved here and to enhance the sensitivity! Coming back to the present observation, if the application requires

Table-2.2: Response comparison of 3-dip coated probes in all compositions.

Sensor	Concentration of ZnO nanoparticle in sol solution	Linear dynamic range (%RH)	Sensitivity (Normalized/%RH)
S1	0.1g	4-96	0.0012
S2	0.2g	30-90	0.0027
S3	0.3g	30-80	0.0030
S4	0.4g	30-80	0.0033

high sensitivity, S4 should be deployed, however if RH required to be monitored in a wide range, S1 should be deployed.

In the next step, dynamic performance of the optimized sensing probe (corresponding to the achievable widest dynamic range) was investigated by exposing the fiber sensor to a repeat and quick RH step changes between 5%RH to 95%RH. The humidity chamber was first desiccated to 5%RH and then quickly humidified to 95%RH by passing air from the mouth (human breathing contains more water vapor) through the pipe to the chamber. The observed time response is depicted in Fig. 2.6. As can be observed from the figure, humidity (commercial sensor output) increases almost linearly, and quickly stabilizes afterwards during the forward cycle of the humidity variation (5%RH to 95%RH); whereas it changes almost linearly only up to the two-third (95%RH to 35%RH) of the reverse cycle of the humidity variation (95%RH to 5%RH) and afterwards changes slowly and exponentially before stabilizing to 5%RH. Importantly, the relative intensity (fiber sensor output) almost instantly and smoothly changes during the forward cycle of the humidity changes. During the

reverse cycle of the humidity change, it varies exponentially but at much faster rate in comparison to the commercial sensor. Also, the relative intensities in the fiber output are

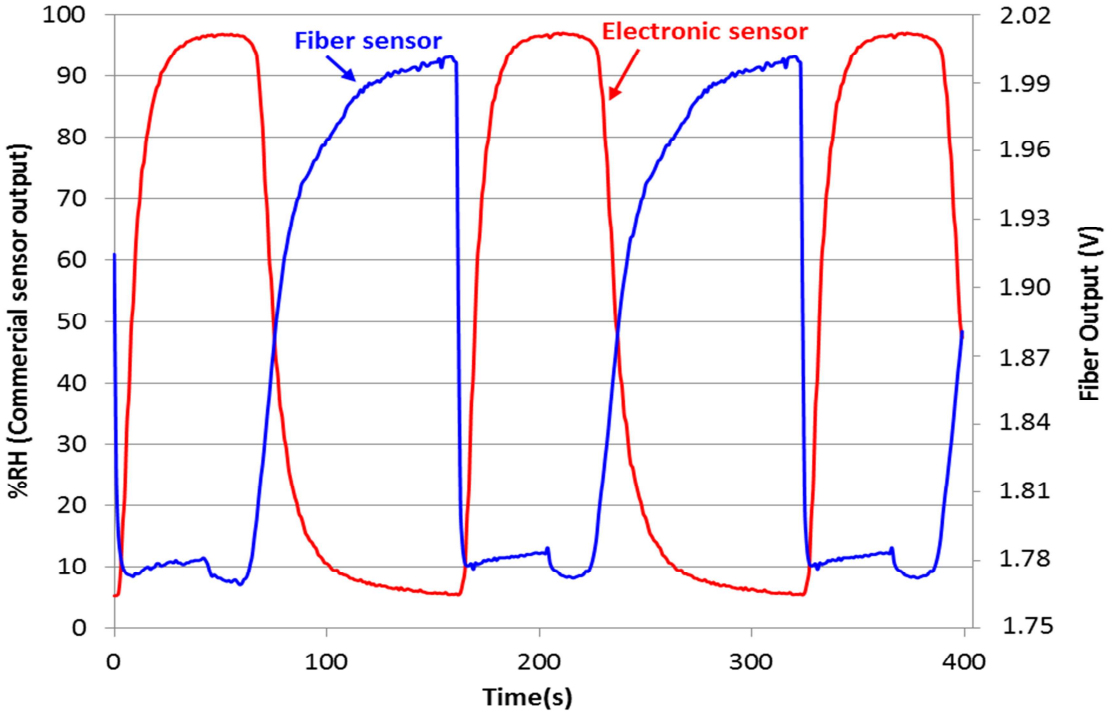

Figure 2.6: *Observed time response behaviour of the optimized fiber humidity sensor for a cyclic perturbation.*

closely identical to extreme RH values in the humidification and desiccation cycles. An average response time of 0.06 second was observed for humidification, whereas an average response time of roughly 5.5 times less than that of the commercial sensor was observed during the desiccation. Ideally, the response time of the sensor should have been the same irrespective of the humidification or desiccation processes. A possible reason could be the fact that we could not make a step-down variation during the reverse cycle of the humidity change while decreasing the humidity to the lowest value (5%RH). It took longer time to reach to this minimum. This was in contrast to an almost quick step-up variation while switching the humidity to the upper (high) value in the chamber and hence the approach we

followed to find the response time was not exactly applicable for the reverse cycle. In any case, the observed response times of the fiber sensor for the forward as well as the reverse humidity cycles were much lower than the response times of the commercial sensor. Similar observations were made for sensors S2, S3 and S4 as well. This establishes the fact that the developed fiber sensor is much faster than the commercial sensor.

Finally, repeatability and reliability tests were carried out to rigorously analyze the sensor (corresponding to widest achievable dynamic range) performance. For this, experiments with the optimized fiber humidity sensing probe were repeated at an interval of 4 days. A total of 3 such repeat experiments on three different days were carried out in a span of 11 days. Fiber sensor outputs corresponding to the three different humility values (25, 55 and 85%RH) as an example are shown in Fig. 2.7.

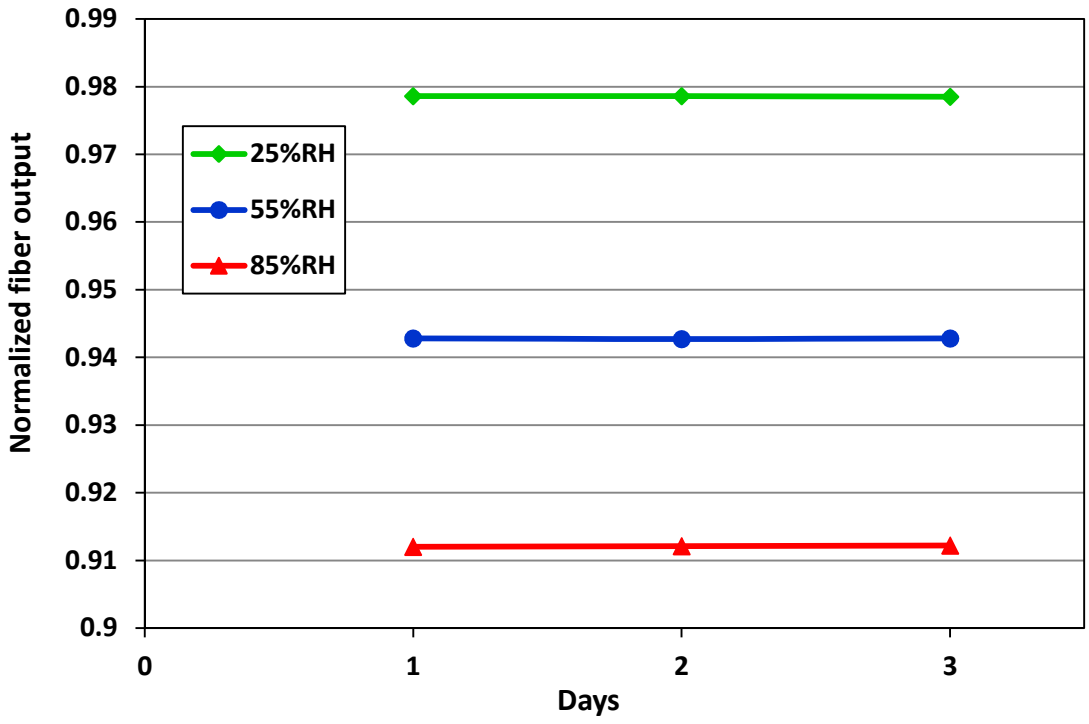

Figure 2.7: *Repeatability test of the sensor on different days.*

As can be observed from the figure, sensor output is almost constant over a span of 11 days. The maximum variation in the optical fiber sensor output, compared to day-1, at the three different humidity values of 25%RH, 55%RH and 85%RH is observed to be of the order of 10^{-5}. Similar observations were made for sensors, S2, S3 and S4. This shows a great reliability and repeatability of the developed sensor. Thus, the developed sensor employing evanescent-wave absorption scheme through a nanoparticle immobilized sol-gel silica sensing film synthesized over a 5 cm length of a centrally decladded straight and uniform optical fiber and having a reliable, repeatable and throughout linear response achieved over an almost widest possible dynamic range is of great importance for real applications.

2.4 Conclusion

This chapter explained the development of a simple nanoparticle based fiber optic relative humidity sensor employing evanescent wave based intensity modulation scheme. The sensor comprises ZnO nanoparticles immobilized nanostructured sol-gel sensing film (cladding) synthesized over a centrally decladed straight and uniform optical fiber. A rigorous experimental analysis was carried out in order to optimize the sensing film (cladding) configuration for the best possible sensor response. This was done by varying the film chemical composition as well as film thickness. From the analysis of the experimental data, it is concluded that in all the film compositions (chemical composition and thickness), sensing probes with film thickness corresponding to 3-dip coating showed best response. 3-dip coated probe of 0.4g ZnO nanoparticle concentration in sol solution showed the best linear sensitivity. Decreasing the nanoparticle concentration in sol solution decreased the sensitivity, but increased the linear dynamic range. Response of 3-dip coated probe of 0.1g ZnO nanoparticle in sol solution is observed to be linear throughout the range as wide as 4%

to 96%RH. A linear response over such a large dynamic range is observed for the first time to the best of our knowledge in such a simple approach. The average response time of the optimized sensor is observed to be much less as compared to the commercial sensor. Further, the sensor response is observed to be highly reversible, reliable and repeatable. A maximum fiber output variation upon applying the humidity change that could be observed over a span of more than 11 days is of the order of 10^{-5} only. Hence the reported sensor is of great practical importance and use. Next chapter of the thesis is devoted to enhance the sensitivity while possibly keeping the widest RH range observed in the present chapter intact.

Chapter 3

Exhaustive Guided Mode Attenuation based Optical Fiber Humidity Sensor: Enhanced Sensitivity and Wide Linear Dynamic Range

3.1 Introduction

There have been numerous scientific works reported in the literature to realize an effective all-optical relative humidity (RH) sensor. Owing to the inherent advantages offered by fiber optics towards sensing technology [28], over the past few decades a major research in this class (all-optical sensing) is focused on the development of optical fiber RH sensor. Both the techniques – extrinsic [81] as well as intrinsic – have been employed to develop these sensors. Especially in intrinsic techniques, intensity modulation through evanescent wave absorption/scattering [64, 69, 73, 75] and the wavelength modulation through long period gratings (LPG) [89, 92] /fiber Bragg gratings (FBG) [96-97] or an interferometric structure [86] have emerged as the most popular technique to realize optical fiber RH sensor. It's worth mentioning that the optical signal propagating in the fiber at an operating wavelength such as ~632.8 nm or ~1550 nm does not directly interact with applied humidity perturbations; and hence cannot lead to an intensity/wavelength modulation. To realize RH sensor at these wavelengths, such interactions are indirectly conceived by bringing a suitable chemical

reagent into the interaction range of the propagating signal in the fiber. This reagent undergoes a chemical transformation when exposed to RH perturbations, which leads to either in the change of its mechanical properties or to an altogether different chemical species optically active (directly interacts) at these wavelengths – enabling intensity/wavelength modulation. For this reason, wavelength modulation sensors in [89, 92] have used polymer coated LPG/FBG. For LPG based RH sensors, highest dynamic range of 33–97%RH was observed in [92], but the sensor response was nonlinear throughout. For FBG based RH sensors, highest linear dynamic range of 11–98%RH was observed in [97] with a sensitivity of 0.266mV/%RH. Though a wide dynamic range is achieved, performance of all these grating based RH sensors is limited by temperature as well as strain cross-sensitivities. Requirement of sophisticated grating writing techniques as well as costly and bulky interrogation devices further complicates designing of such sensors from practical point of view, where a cheap and easily fabricate-able sensor would be preferred. On the other hand, RH sensors employing intensity modulation through evanescent wave absorption/scattering exploits chemically modified cladding (owing to the reason explained earlier). In general, the penetration depth of the evanescent wave in the cladding region is typically less than the wavelength of operation [30]. This depth defines a short range of sensing volume within which, power carried by evanescent wave interacts with the measurand and gets attenuated due to absorption/scattering/refractive index change. Consequently, the fraction of the total guided power present in the cladding region is generally less than 1% (w.r.t. the total guided power) for weakly guiding multimode fiber. This imposes main limitation for sensors based on intensity modulation through evanescent wave employing straight & uniform fiber geometry and, in general, leads to a poor sensitivity. To overcome this limitation, one needs to replace the fiber cladding by a synthesized cladding over a large portion of fiber to have detectable change at the output end. If the length of the modified cladding is to be kept small,

one needs to replace the fiber either by a single mode fiber (which carries higher fractional guided power in the cladding) or by a bent/tapered fiber geometry to increase the sensitivity. However, irrespective of the employed fiber geometries, all most all such evanescent wave based RH sensors reported in the literature [64, 69, 73, 75] exhibit nonlinear response with a piece-wise limited linear sensitivity over the observed dynamic range. In the previous chapter, an optical fiber RH sensor having a throughout linear response over the dynamic range as wide as 4-96%RH employing straight and uniform fiber geometry in conjugation with ZnO nanoparticle immobilized sol-gel sensing cladding is reported. The observed linear sensitivity was 0.0012/%RH. It's worth mentioning that the reagents used in all such studies (e.g., ZnO nanoparticle in [chapter-2], SiO_2 nanoparticles in [81], $CoCl_2$ in [30, 64], hydroxyethylcellulose in [73], TiO_2 in [75], MgO in [77], Co nanoparticles in [83], etc.) to conceive an indirect interaction with RH perturbations at the operating wavelength were immobilized in certain polymer matrix and hence their concentration was limited even in the optimized composition of synthesized cladding. Further, they were accessible only in the minuscule volume of this cladding. This limited the resulting sensitivity of the sensor. Certainly, if the reagent can be made accessible by some method even in the core region of the fiber, the only way left to increase the extent of interaction with the guided signal, sensitivity is bound to increase manifold. However, this is not possible if the fiber used in the sensor development is solid silica core standard fiber. Interestingly, Zhou et al. [65] showed a way by employing a bare optical fiber with porous core. The advantage of this approach is the fact that the reagent is allowed to diffuse into the fiber core. Importantly, the entire guided mode is allowed to interact with this reagent, leading to an enhanced sensitivity. However, the fabrication of bare fiber with porous core was very complicated and the resulting sensor response was piece-wise limited to a very short RH span in [65].

The motivation of the work reported in the present chapter is to develop an all-optical RH sensor with linear response over a wide dynamic range (close to the largest reported in chapter 2) and to enhance the sensitivity. To realize this, mechanism of exhaustive attenuation of entire guided mode is exploited. This is done by employing reagent immobilized bare fiber with porous core having straight and uniform geometry as a sensing element. A very simple methodology is used to fabricate ZnO nanoparticle (reagent) immobilized nanoporous microstructured sol-gel bare, straight and uniform optical fiber core. Performance of the developed sensor is characterized against the commercially available relative humidity sensor. The response characteristics of the sensor are analysed, and compared with the RH sensor based on evanescent wave absorption scheme employing an identical humidity sensitive porous nanostructure (ZnO nanoparticle immobilized sol-gel matrix with identical chemical composition) as the synthesized cladding. The sensor repose is observed to be linear over a dynamic range of 5-95%RH, which is comparable to the widest dynamic range observed in Chapter 2. Most importantly, linear sensitivity is observed to be 0.0103/%RH, which is ~9 times higher than the sensitivity observed for the sensor employing evanescent wave absorption scheme. In addition, sensor response is observed to be fast, reversible, and repeatable.

3.2 Experimental

3.2.1 Fabrication of ZnO nanoparticles immobilized sol-gel nanoporous optical fiber

Sol-gel technology provides an effective tool to produce silica glass matrix from liquid phase. The main advantage of this technique is the fact that various properties of sol-gel derived glass e.g., refractive index, porosity, microstructure, hydrophobicity, stability etc. can be

desirably engineered by controlling experimental conditions e.g., reaction process, precursor's characteristics, catalysis etc. In addition, sol-gel glass is characterized with high optical transmission coefficient over a broad wavelength range (UV to near IR) and high thermal/chemical stability [105-106]. Another advantage is, one can easily immobilize any chemical reagent in sol-gel glass matrix while deciding the chemical composition at the sol preparation stage itself. Owing to these reasons, sol-gel technology is used in the present work to fabricate bare, straight & uniform optical fiber sensing element with reagent immobilized porous microstructured silica core. It's worth mentioning that the realization of a crack free sol-gel silica fiber core having flat end surfaces, uniform diameter throughout its length and controlled porosity is quite challenging. For this purpose, a precursor solution was prepared by mixing Tetraethyl orthosilicate (TEOS), de-ionized water, ethanol and hydrochloric acid in the ratio 3: 2: 1: 0.01 (same as used in chapter-2). Preserving this solution at room temperature for few hours to have hydrolysis and condensation polymerization leads to a viscous sol solution. At this stage, 0.1g ZnO nanoparticles (corresponding to the largest dynamic range in chapter-2) of size less than 100nm (Sigma-Aldrich) was added to this solution under continuous stirring. After a proper mixing, this final solution was poured into a small Tygon tube of the lowest available inner diameter. Subsequently, it was preserved for two weeks in the stable environment for gelation, which led to a porous silica glass matrix. This sol-gel derived glass matrix was then gently pushed out of the Tygon tube and annealed at 160^{o}C in order to remove trace ethanol and water molecules from the porous structure. Thus a bare, straight (having cylindrical shape), reagent immobilized porous silica optical fiber core was achieved. The total length of the bare fiber core was observed to be ~14mm, which can easily be tailored to other values.

Before attempting to realize RH sensor employing this sol-gel derived porous silica optical fiber core as an optical waveguide, its structural properties are needed to be examined. This is

because of the fact that the wave-guidance through any given medium/device is bound to get affected by the structural properties of that medium/device. For an effective and loss-less wave-guidance, the cylindrical shaped fiber core needs to be free from (a) small-scale (small, compared to the wavelength of operation) inhomogeneities arising from density and composition fluctuation within the core, (b) imperfections at the fiber core surface and (c) fiber core diameter fluctuation. Small-scale inhomogeneities are inherently frozen in the sol-gel derived reagent immobilized silica fiber core owing to (a) a cross-linked microstructure of the sol having interspaces that is converted into a microstructure with nano-scale pores after gelation, (b) the presence of immobilized reagent (in the present case, ZnO nanoparticles) and (c) the use of Tygon tube whose inner surface at wavelength-scale is not smooth but carries imperfections. One such inhomogeneities, namely the presence of pores, makes sol-gel glass permeable to the analyte to be sensed, an essential requirement for sensing application. However, these pores along with the immobilized reagent also play the role of the scattering centers within the sol-gel fiber core; making such structures heavily lossy. Thus, one needs to design such structures very carefully by effectively controlling the porosity of such structures. To examine these characteristics of the developed sol-gel silica bare fiber core, its microstructure was studied through a field emission scanning electron microscope (FE-SEM) (Sigma FE-SEM, Carl Zeiss NTS, USA, resolution 2.5nm). Fig. 3.1 shows the FE-SEM image of the sol-gel fiber. The diameter of the fiber is observed to be ~800µm. Also, the diameter is observed to be uniform throughout the length of the sol-gel fiber. It's worth mentioning that a lower diameter, which is certainly possible to realize, could not be achieved in this study owing to the non-availability of Tygon tube of lower inner diameter in the laboratory. Further, the end-faces of the sol-gel fiber are observed to be almost flat and the fiber is free from any crack. Importantly, observing the central region (excluding the near surface region) in the cross-section of the developed sol-gel fiber, pore size is observed to be

smaller than the resolution of FE-SEM. This is in accordance with the reported pore size (~3.8 nm) for the nanostructure of a sol-gel silica thin film [106]. Surface morphology of the sol-gel fiber is shown in Fig. 3.2, which depicts an interconnected uniform and porous structure having moderate roughness. Pore size on the surface of the sol-gel fiber core is

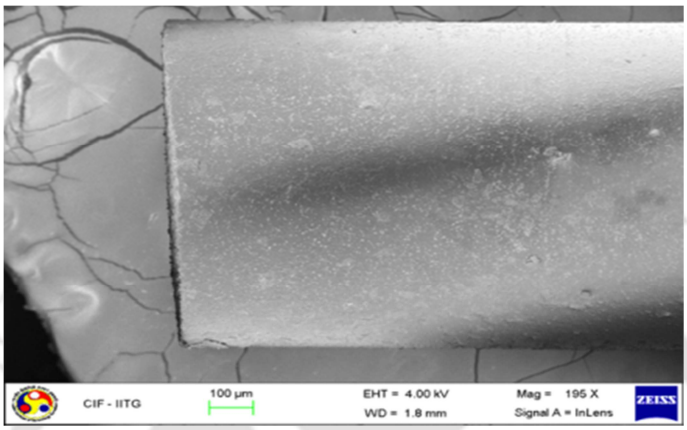

Figure 3.1: *FE-SEM image of ZnO nanoparticle immobilized microstructured sol-gel silica fiber core.*

observed to be in the micron (µm) range. Further, the surface porosity was observed to be higher than the volume porosity. These observations might be due to the large-scale roughness involved with the inner surface of the Tygon tube, as the outer surface of the sol-gel fiber core was in touch with it during the fabrication procedure.

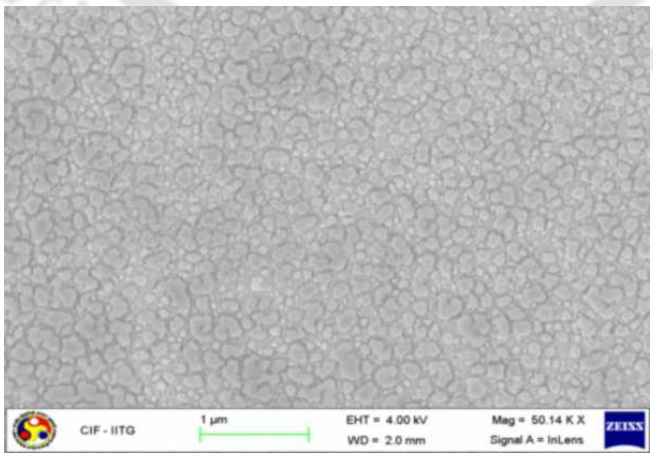

Figure 3.2: *FE-SEM pattern of surface morphology of ZnO nanoparticle immobilized microstructured sol-gel silica fiber core.*

3.2.2 Designing of RH sensor

Schematics of the methodology for realizing an all-optical RH sensor employing the sol-gel derived nanoporous silica optical fiber core as the sensing element is shown in Fig. 3.3. A small piece (~10mm) of the nanoporous sol-gel microstructure fiber core was carefully aligned and mechanically spliced between the two pieces of identical plastic-clad-silica

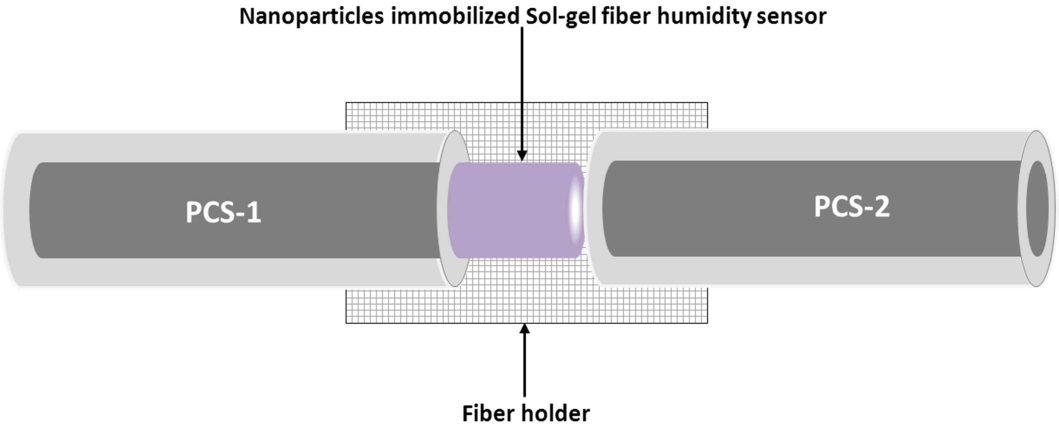

Figure 3.3: *Schematic diagram of alignment of sol-gel fiber sensor between two multimode fiber pieces.*

multimode fiber. Ideally, the core diameter of the PCS fiber should be exactly the same as that of the sol-gel fiber for efficient power coupling and correct alignment. However, PCS fiber used in the sensor designing was having a core diameter of 600µm – much less than the core diameter of the sol-gel fiber (~800µm), but available maximum in the lab. This resulted in a core diameter mismatch owing to the experimental constraints (unavailability of Tygon tube of 600µm inner diameter/unavailability of a PCS fiber of ~800µm core diameter). There would be additional losses due to mechanical splice and not-so-perfect end-faces of the sol-gel fiber. The core diameter mismatch, along with these factors, greatly affects the efficiency of the sensor. Nevertheless, experimental characterization of the sensor was carried out to

show the proof of concept. The three fibers were aligned in a way to possibly maintain a common central axis for all of them. A small piece of stainless steel grid was used to provide support to both the splice points and this way, to maintain the alignment while characterizing the sensor during experiment.

3.2.3 Sensing probe characterization

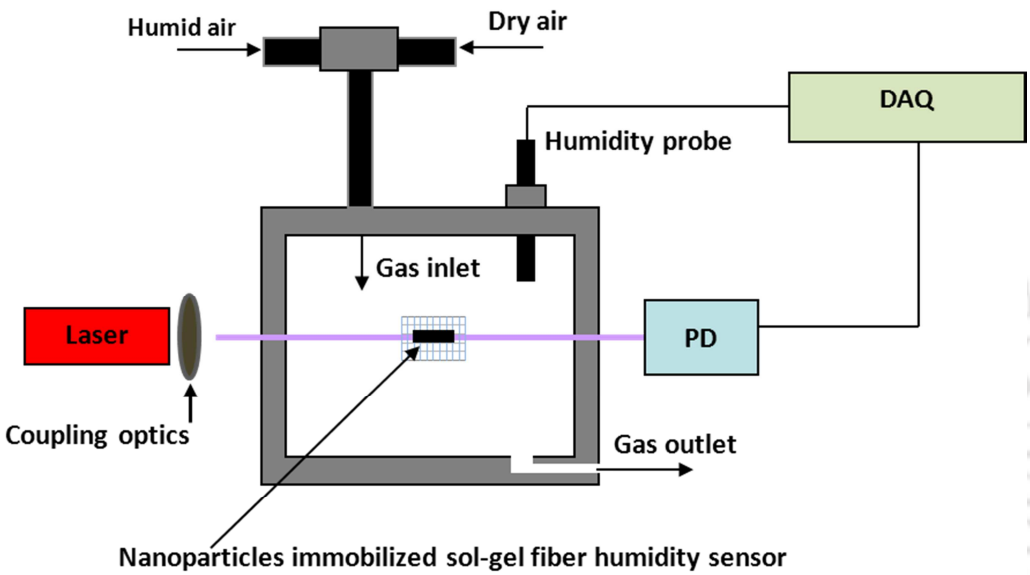

Figure 3.4: *Schematic diagram of experimental setup for sensor characterization*

Developed sol-gel fiber humidity sensor was carefully fixed at the center of humidity chamber via PCS fibers. Free end of one PCS fiber was coupled to a He-Ne laser (632.8nm) and free end of the other fiber that carries the transmitted light was coupled to a photodetector using SMA connector. The schematic diagram of the experimental set up for sensor characterization is shown in Fig. 3.4. The sensor was exposed to different humid environments as explained in chapter-2

3.3 Results and Discussion

The proposed sensor works on the principle of exhaustive attenuation of entire guided mode in a ZnO nanoparticles immobilized nanoporous sol-gel bare, straight and uniform optical fiber, which results in an intensity modulation to a higher extent at the fiber output end. For proper characterization of the developed nanoparticles immobilized nanoporous sol-gel-fiber

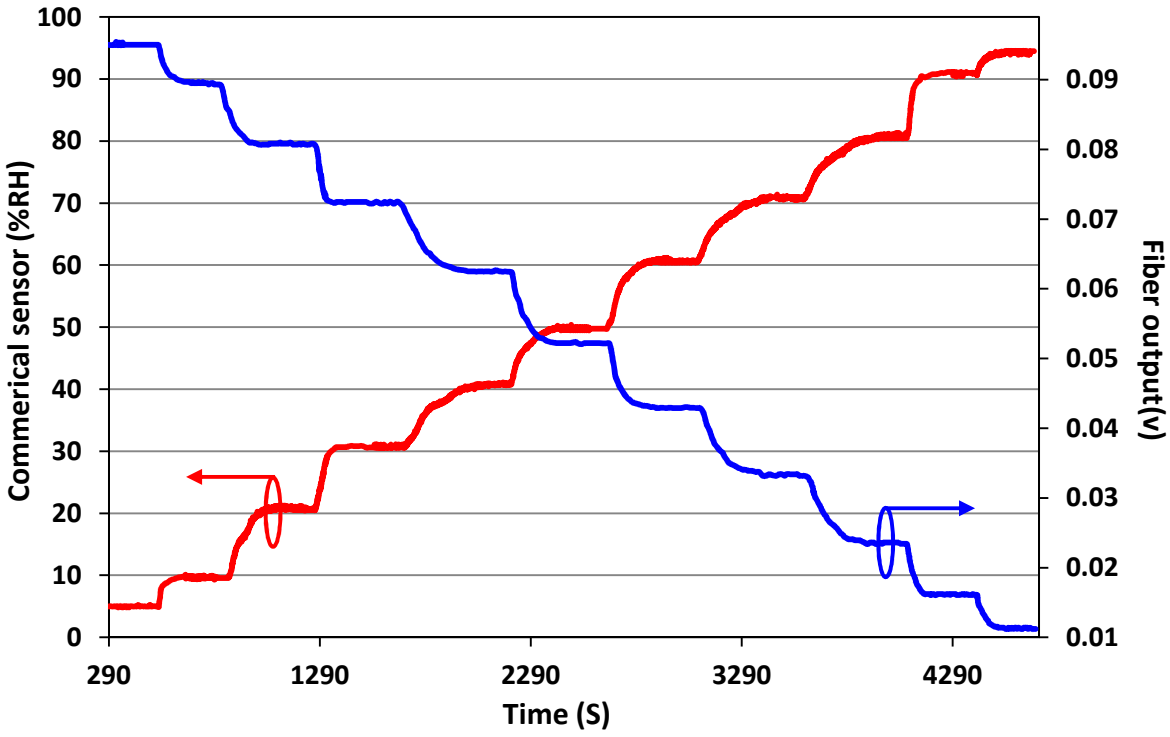

Figure 3.5: *Time variation of commercial humidity sensor and sol-gel fiber humidity sensor.*

as a humidity sensor, it was carefully fixed inside the humidity chamber and exposed to different humid environments by controlling the flow rates in humid and dry flow meters. During this, the transmitted light through the sol-gel fiber sensor was monitored against humidity variation inside the chamber. Fiber output as well as commercial sensor outputs was simultaneously recorded as a function of time with a resolution of 1second. Measurements were carried out for increasing and decreasing humidity cycles at a constant temperature (25^{o}C). A typical fiber sensor response while increasing humidity is shown in Fig. 3.5. As

can be observed from the figure, as the humidity increases, transmitted light intensity through the sol-gel fiber sensor decreases. This is because of the fact that the nanoparticles immobilized dry sol-gel fiber has almost negligible absorption at a low humidity at 632.8nm; whereas the absorption within the sensing fiber increases at high humidity at the same wavelength. This causes attenuation of the propagating mode of the PCS fiber through the

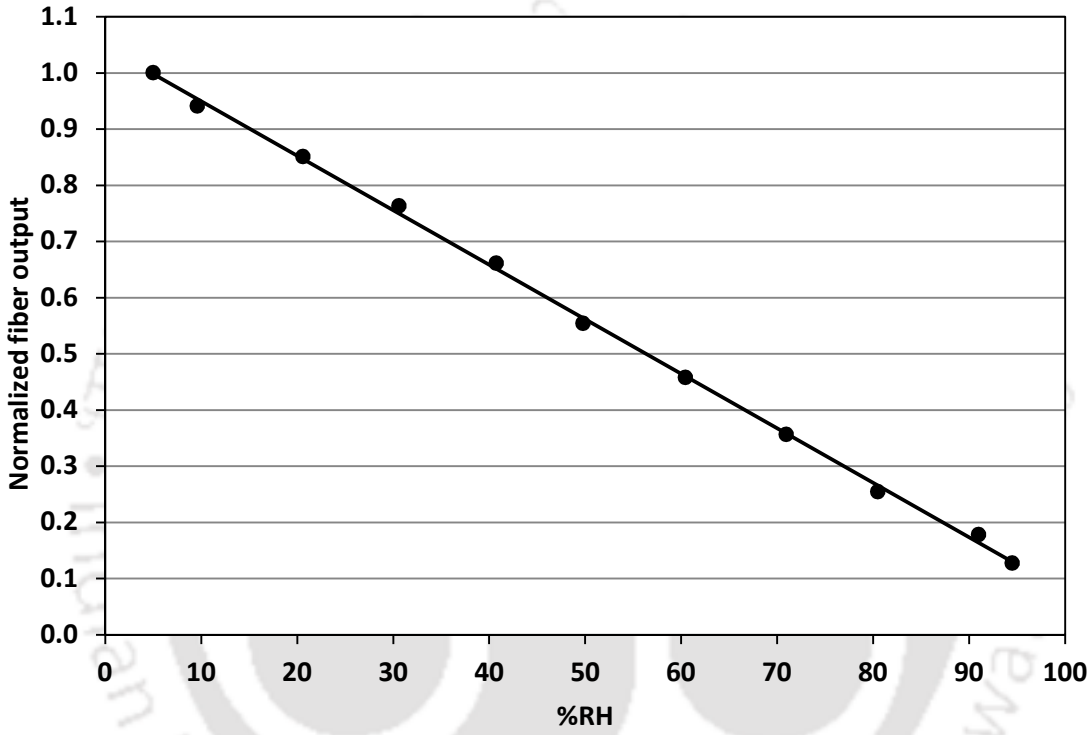

Figure 3.6: *Experimentally observed sensor response of the ZnO nanoparticles immobilized nanoporous sol-gel fiber sensor.*

sol-gel fiber sensor, and hence decreases in the transmitted light intensity. To have a proper idea about fiber sensor response, fiber sensor output is plotted against %RH in Fig. 3.6. Fiber senor output and %RH values, both, were extracted from the stabilized portion of their time response characteristics. As can be observed from the figure, the ZnO nanoparticles immobilized nanoporous sol-gel fiber sensor responds linearly to applied perturbations over a wide RH range of 5-95%. The observed linear sensitivity is 0.0103/%RH.

The observed linear dynamic range of the sol-gel fiber humidity sensor is comparable to the one, observed with an identical sol-gel sensing matrix synthesized as the fiber cladding on a solid silica standard fiber core (sensor S1, Table 2.2 of Chapter 2). Importantly, sensitivity increased manifold (~9 times) compared to the probe based on evanescent wave absorption scheme (sensor S1). The sensitivity enhancement is due to the fact that, for sensor employing evanescent wave absorption scheme, only a small fraction of the power carried by the mode (in the evanescent wave) can interact with the sensing material. This results in an intensity modulation to a lesser extent; and hence, a lower sensitivity. However, in nanoparticle immobilized nano structured sol-gel fiber humidity sensor, the sensing material (reagent) is infused uniformly in the entire core within the sensing region. Further, the nanoporous structure of this sensing region with good porosity also ensures the diffusion of perturbation (humid air) to the greater depth within the sensing region (sol-gel nanoporous fiber core). It is worth to mention that performance of the sensor can be furthere improved by making sol-gel fiber core whose diameter matches with the core diameter of multimode fiber. Thus, the guided mode of the standard fiber, upon entering into the sol-gel fiber, are completely exposed to the reagent and the analyte, which enables a huge extent of interaction that is impossible to realize with an identical structure as a sensing cladding (rather than a sensing core). Also, the corresponding absolute sensitivity of sol-gel fiber sensor was 0.93mV/%RH which is ~3.5 times the maximum sensitivity observed with FBG based RH sensor (dynamic range 11-98%RH, sensitivity 0.266mV/%RH) [97]. A detailed comparison of this sensors response is carried out in section 4.3 of the next chapter.

In the next step, dynamic performance and the repeatability characteristics of the ZnO nanoparticle immobilized nanoporous sol-gel fiber humidity sensor were investigated in an identical way reported in Chapter 2. An average response time of 0.54 second was observed

for humidification whereas an average response time of 0.68 second for the desiccation. These were smaller than the average time response of the commercial sensor, but almost 10 times higher than the one observed for sensors in Chapter 2. Owing to the porosity down till the axis of the fiber in the sensing region, later observation is expected. Further, the response time of the sensor should ideally have been identical irrespective of the humidification or desiccation processes. A possible reason could be the fact that, once again, we could not make a step-down variation during the reverse cycle (desiccation) of humidity variation. Exposure to the cyclic variation of RH changes once again established that the response of sol-gel fiber sensor is highly reversible and repeatable. In addition, a maximum fiber output variation during the repeatability and reversibility test over an interval of few days is observed to be of the order of 10^{-4} only. This shows a high reliability and repeatability of the reported sensor.

3.4 Conclusion

This chapter described the development of an all optical humidity sensor based on exhaustive attenuation of guided mode in ZnO nanoparticles immobilized nanoporous sol-gel fiber. Sensor response was investigated for different humid environments. A linear response over a wide dynamic range of 5-95%RH with a sensitivity of 0.0103/%RH is observed for this sensor. The observed linear dynamic range is comparable to the optical fiber humidity sensor based on evanescent wave absorption scheme with ZnO nanoparticles immobilized sol-gel film as humidity sensing cladding. In addition, sensitivity is improved by factor ~9 compared to sensor employing evanescent wave absorption scheme. Further, the observed linear sensitivity is ~3 times higher than the highest reported in chapter 2. It is worth to mention that the performance of the sensor can be further improved by reducing the diameter mismatch

between sol-gel fiber sensor and core of the multimode fiber used for the experiment. Additionally, with an average time of 0.54 second for humidification and 0.68 second for desiccation, a maximum fiber output variation of the order of 10^{-4} over a sufficiently long period the developed sensor is most suitable for real-field applications.

Chapter 4

TiO_2 Nanoparticle based Simple Optical Fiber Relative Humidity Sensor: Sensitivity Enhancement with Linear Response

4.1 Introduction

Last two chapters described the development of optical fiber RH sensor with ZnO nanoparticles immobilised sol-gel nanostructure as a humidity sensing clad and the core. A good sensitivity over a wide dynamic range was realized. In order to further enhance the sensitivity, while keeping the sensor response linear possibly over a wide RH range, RH sensor employing simplest fiber geometry (straight and uniform optical fiber) is developed exploiting a different sensing reagent (TiO_2 nanoparticle). As was established in Chapter 3, the exhaustive guided mode attenuation through reagent immobilized nanoporous sol-gel silica glass core is bound to result in a manifold sensitivity enhancement in comparison to the reagent immobilized nanoporous sol-gel silica glass clad over a solid standard silica fiber core. Hence, evanescent wave absorption based intensity modulation scheme was employed for the new reagent in the work reported in this chapter. TiO_2 has high adsorption towards water molecules. When nano-scaled, it will have high surface to volume ratio and hence, more surface area to interact with the water molecules. The exposed sensing region (central decladded fiber core that carries TiO_2 nanoparticle immobilized nanostructured sol-gel thin film) to the humid environment induces an absorption of the optical power carried by the evanescent field. This absorption of the optical power increases with the increase in the

humidity; and finally results in a modulated fiber output, which is used as the criterion for detecting and determining relative humidity of the surrounding environment. A comprehensive experimental investigation is carried out in order to optimize the sensor performance by suitably controlling various potential experimental/sensor parameters of interest that can influence the sensor's response. Importantly, a much improved sensitivity of 27.1mV/%RH is observed, for the optimized probe, along with the throughout-linear sensor response over a dynamic range as wide as 24% to 95%RH with an average response time of 0.01 second for humidification and 0.06 second for the desiccation. Furthermore, a maximum fiber output variation during the repeatability and reversibility test is observed to be of the order of 10^{-4} only. Thus, the response characteristics of the optimized sensor are observed to be very fast, reversible and repeatable. These characteristics of the sensor make the developed sensor very useful for many practical real-field applications.

4.2 Experimental

4.2.1 Preparation of colloidal TiO_2 nanoparticles

TiO_2 nanoparticles (10 – 15 nm size) were developed in the laboratory in a way to fine tune their size. For this, Titanium (IV) isopropoxide was used as the precursor solution. A suitable

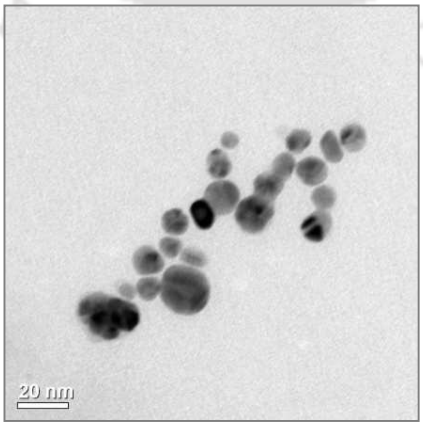

Figure 4.1: *TEM image of in-house developed TiO_2 nanoparticles.*

volume of Titanium (IV) iso-propoxide was added to ethanol. A controlled volume of this solution was then added to de-ionized water in different volume ratio under vigorous stirring. The stirring was continued for 12 hours. Stirring speed, pH of the de-ionized water and the solution composition were carefully controlled. An optimum composition with a volume ratio of 0.1:1:9 is observed for Titanium (IV) isopropoxide, ethanol and de-ionized water. A Transmission Electron Microscope (TEM) image of the prepared TiO_2 nanoparticles is shown in Fig. 4.1.

4.2.2 Humidity sensing probes preparation

PCS fiber having same specifications used in Chapter-2 was used to develop the sensing probe. Once again, about 5 cm of the cladding was removed from the central portion of the fiber. The probe was first sonicated in soap solution (Merk) and then in de-ionized water. Finally, it was cleaned with acetone. In-house developed TiO_2 nanoparticles were then synthesized through a sol-gel nanostructured matrix over this centrally decladded straight fiber to fabricate the sensing film. To do so, the sol was prepared by mixing tetraethyl orthosilicate (TEOS), de-ionized water, ethanol and hydrochloric acid in the ratio of 3: 2: 1: 0.01 (same as used in Chapter 2). A suitable volume of TiO_2 nanoparticle colloidal solution was added to the sol under constant stirring. In order to investigate the effect of nanoparticle concentration on the sensor performance, concentration of TiO_2 nanoparticle colloidal solution was varied to 6, 9 and 12 %(v/v) in the sol. This way, three sol solutions were prepared with varying TiO_2 nanoparticle concentration. Dip coating method was used to deposit a TiO_2 nanoparticle immobilized nanostructured sol-gel film onto the bare fiber core for each sol solutions. For further optimization and investigation of the sensor performance, multiple dip coating was employed to prepare the fiber optic probes with varying film thicknesses for the three sol solutions of varying nanoparticle concentrations. All sensing

probes were annealed at 160ºC in order to remove ethanol and water from the pores of the film.

4.2.3 Sensing probe characterization

Similar procedures as explained in Chapter 2 were followed in order to characterize each sensing probe.

4.3 Results and Discussion

In the process of characterization and optimization of the sensor's response, the effect of film composition and film thickness were examined in detail once again. As mentioned earlier, varying film compositions through 6, 9 and 12 %(v/v) of TiO_2 nanoparticle colloidal solution in the sol were prepared. Sensing film of three different thicknesses with each solution were deposited on the centrally decladded fiber. The latter was done using two-dip, three-dip, and four-dip coatings. Fiber sensors were fixed in the test-chamber. Humidity was varied in steps and that too, very slowly inside the chamber. Experiments were carefully carried out for increasing as well as decreasing humidity cycles and the data were recorded only after the stabilization of humidity in the test-chamber. Further, these data (fiber output as well as the commercial probe output) were recorded once again as functions of time with a resolution of 1 second. A constant temperature of 25^{o}C was maintained throughout the experimental investigations for all sensing probes. Fig. 4.2 depicts a typical sensor response, as an example, for the sensing probe having film composition corresponding to three-dip coating of 9 %(v/v) TiO_2 nanoparticle colloidal solution concentration in the sol onto the centrally decladded straight and uniform optical fiber. As can be observed from this result, fiber output decreases as the humidity increases within the chamber. This can be physically understood as following: water molecules being diffused into the nano-scaled pores of the pure sol-gel

matrix get adsorbed in these pores. The rate of adsorption is stimulated (greatly enhanced) owing to the presence of the metal-oxide cations [108-109]. Thus, increase in the humidity increases adsorption of water vapour and the condensation in the pores of the sensing film manifolds. This leads to a greater change of refractive index in the sensing region in comparison of a pure sol-gel sensing film. Corresponding leakage of the guided power to the cladding modes results in a comparatively intense intensity modulation. A similar qualitative behavior was observed for the other film configurations as well.

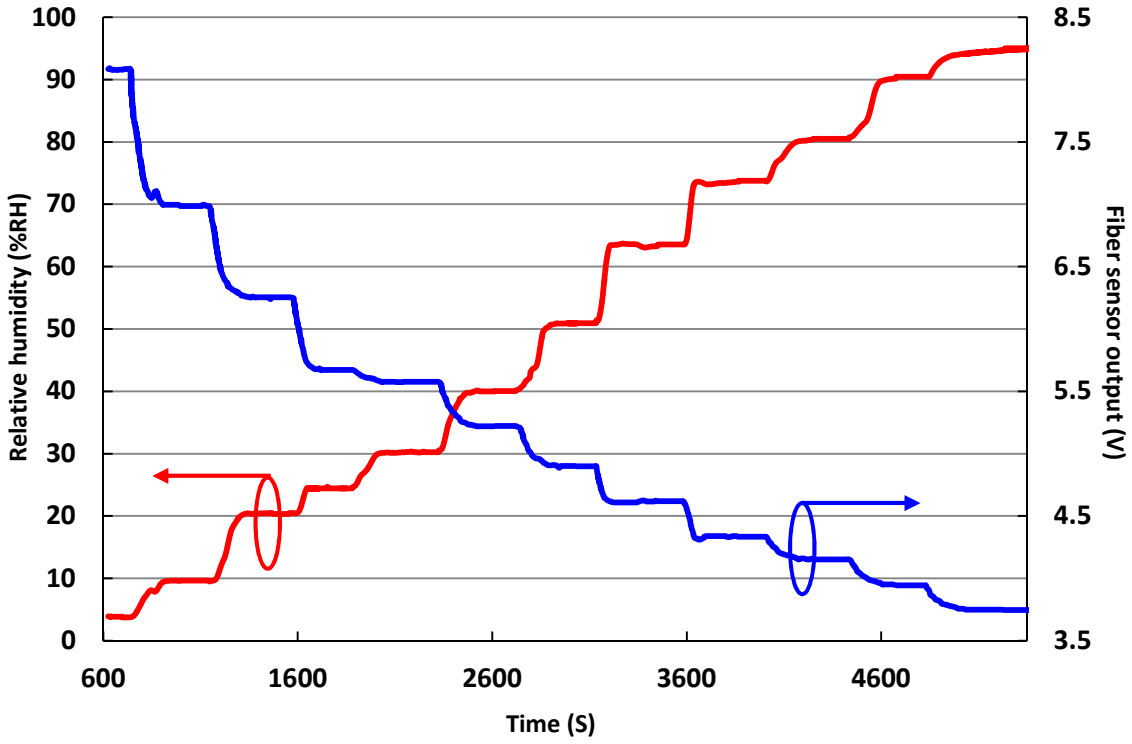

Figure 4.2: *Time variation of commercial humidity sensor and fiber optic humidity sensor (3-dip coated probe of 9 %(v/v) nanoparticle concentration in sol).*

Coming back to the optimization process, response characteristics for all the sensors with varying film thicknesses for each varying film composition were studied. Since the nanoparticle doped nanostructured films in each case is deposited from the same respective

solutions, any difference in response should be attributed to the difference in the film thickness. To explicitly observe this effect, fiber output is plotted against %RH (measured through the commercial sensor) for each case. Fig. 4.3 depicts the effect of varying film thickness for 6%(v/v) TiO_2 nanoparticle colloidal solution concentration in the sol. As can be noticed from this result, a throughout-linear response in the humidity range of ~25-94%RH is observed for all the sensors of varying film thickness with this film composition. A sensitivity of 2.0mV/%RH is observed for two-dip coated sensor. Increase in film thickness from two-dip to three-dip improves sensitivity to 9.5mV/%RH, which is ~4.7 times higher to the one observed for two-dip coated sensor. Increasing the film thickness from three-dip to four-dip does not result in the same trend; rather sensitivity ceases to improve and drops down to 1.0mV/%RH. Three-dip coated sensor once again exhibited the best achievable sensitivity for this composition, whereas, two-dip coated sensor exhibits better sensitivity

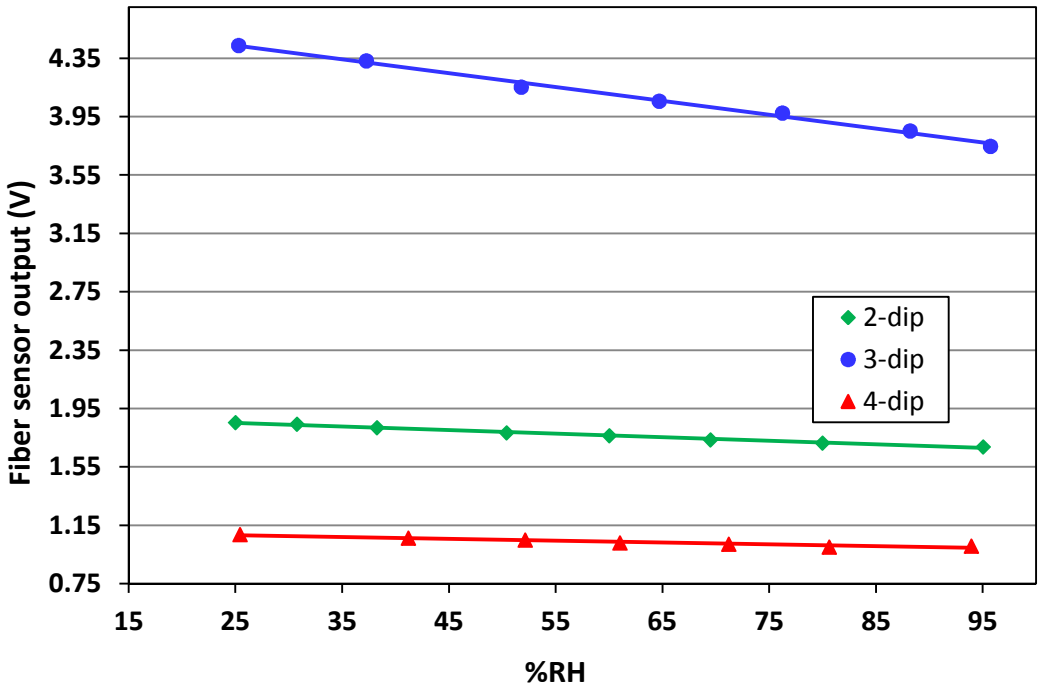

Figure 4.3: *Experimentally observed sensor responses of 2-dip, 3-dip and 4-dip probes with 6%(v/v) nanoparticle concentration in sol.*

than four-dip coated sensor. This observation establishes the fact that there exists an optimum film thickness corresponding to three-dip coated sensor for this film composition (as was observed in Chapter 2 for ZnO nanoparticles immobilized sol-gel sensing clad).

Next, fiber output is plotted in Fig. 4.4 for the sensor with a film composition corresponding to 9%(v/v) TiO_2 nanoparticle colloidal solution concentration in the sol. As can be observed, sensor response remains throughout-linear. Further, increasing the nanoparticle concentration in nanostructured sensing film hasn't affected the dynamic range of the sensor, which remains the same as it was for lower nanoparticle concentration. Nevertheless, increasing the nanoparticle concentration in the sensing film does improve an overall response of the sensor. Sensitivity for the two-dip coated sensor increased to 5.8mV/%RH (~3 times) as compared to

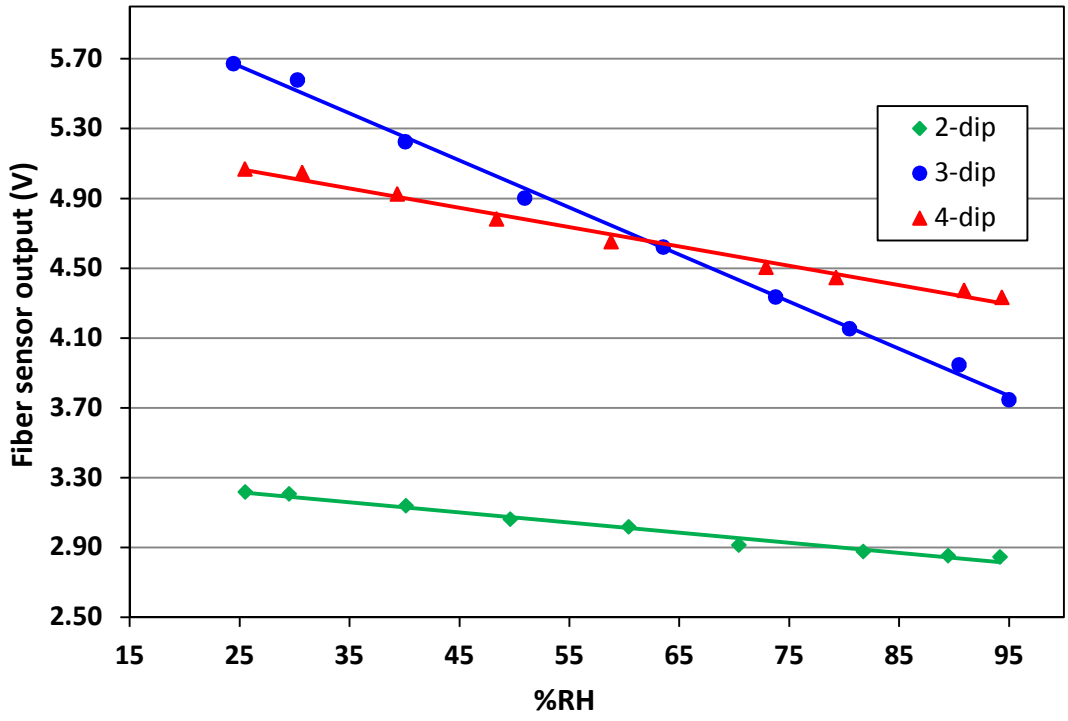

Figure 4.4: *Experimentally observed sensor responses of 2-dip, 3-dip and 4-dip probes with 9%(v/v) nanoparticle concentration in sol.*

2.0mV/%RH for 6%(v/v) TiO_2 nanoparticle colloidal concentration. Once again, increasing the film thickness from two-dip to three-dip for this film composition improves sensitivity, which is observed to be 27.1mV/%RH.

The ratio of increment for three-dip sensitivity of 9% composition film is ~4.7 as compared to the two-dip coated sensor of same film composition and is 2.85 as compared to the three-dip coated sensor of lesser (6%) film composition. That is, trend of sensitivity enhancement remains the same while either increasing the film thickness keeping film composition constant, or, increasing the film composition keeping the film thickness constant as for as two-dip to three-dip films are concerned. Increasing the film thickness from three-dip to four-dip again did not pay any dividend and the sensitivity dropped down substantially. Film

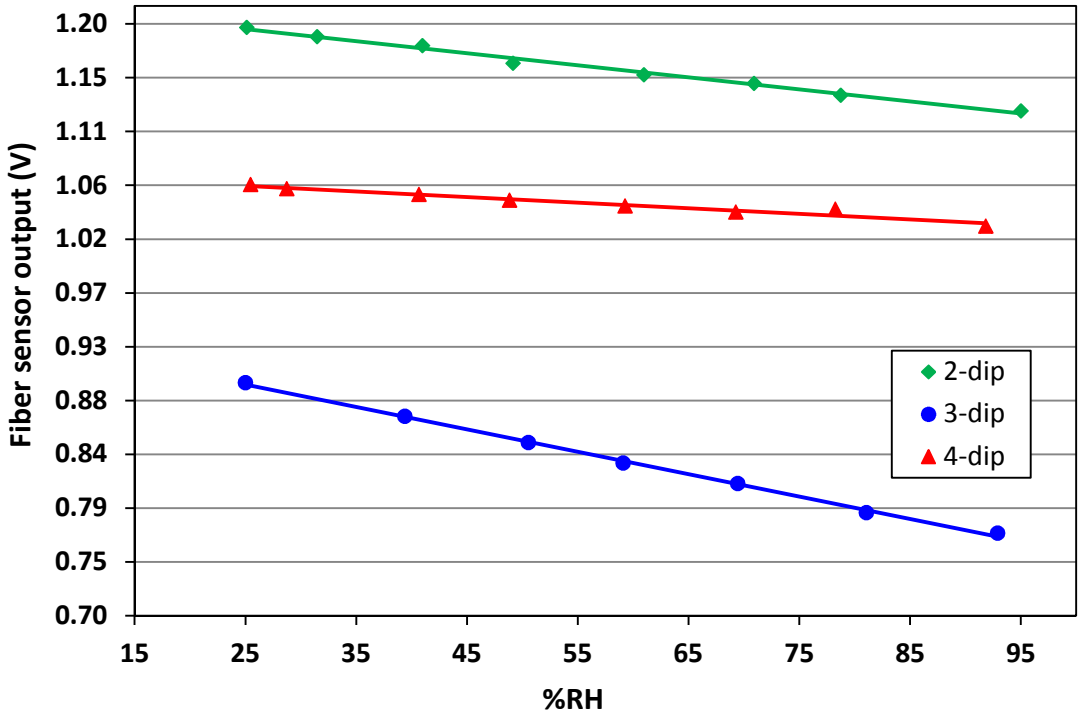

Figure 4.5: *Experimentally observed sensor responses of 2-dip, 3-dip and 4-dip probes with 12%(v/v) nanoparticle concentration in sol.*

composition was further changed to a higher nanoparticle concentration (12%(v/v) nanoparticle concentration in sol) and the corresponding sensor's responses are plotted in Fig. 4.5. Sensor corresponding to three-dip coating again exhibits the best sensitivity as compared to two-dip and four-dip coated ones. However, increasing nanoparticle concentration in sol from 9%(v/v) to 12%(v/v) substantially deteriorated the sensitivity for sensors with all the three film thicknesses. For example, the sensitivity for three-dip coated sensor with this film composition is observed to be 1.87mV/%RH, which is 14.5 times less than the sensitivity observed for 9%(v/v) composition of three-dip coated sensor. This shows even the existence of an optimum film composition along with the optimum film thickness for the present sensor. To understand this, Fig. 4.6 shows a comparison of the sensor responses of 3-dip coated probes of each chemical composition of sol-gel film sensing cladding. As can be

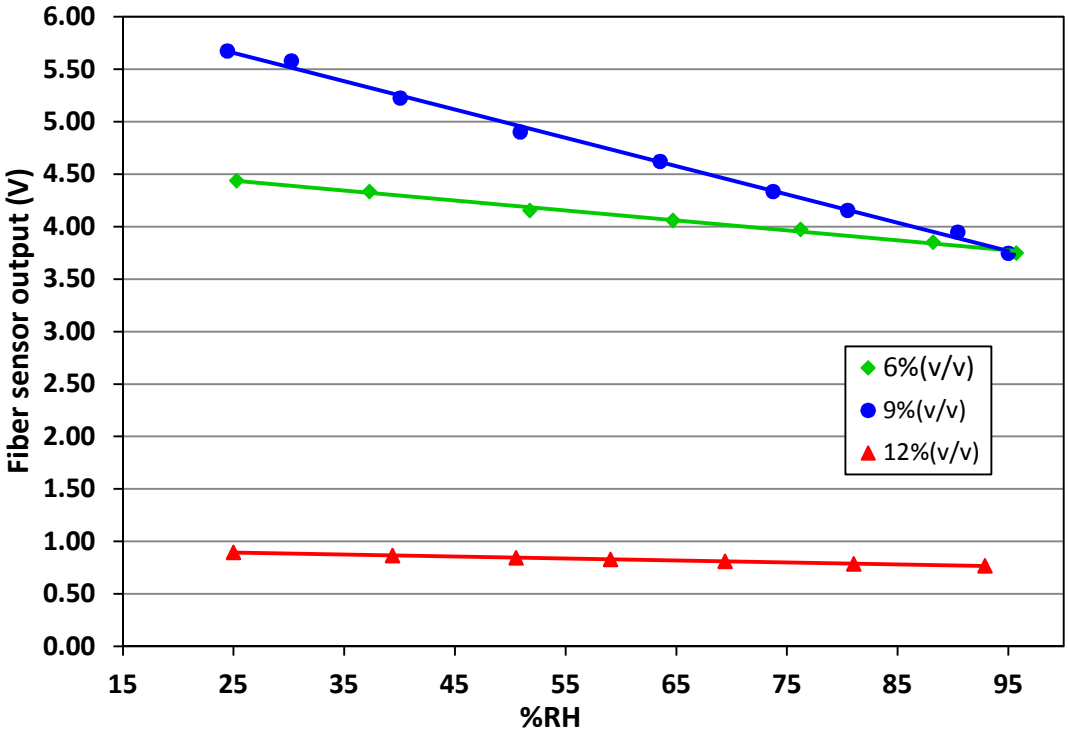

Figure 4.6*: Sensor response comparison of 3-dip coated probes with 6, 9 and 12%(v/v) nanoparticle concentration in sol.*

observed from the figure, increase in nanoparticle concentration from 6%(v/v) to 9%(v/v) (1.5 times) results an increase of the sensitivity from 9.5mV/%RH to 27.1mV/%RH (2.85 times) without affecting the throughout-linear dynamic range. To carefully estimate it, experiments were then extended to 8 and 10%(v/v) TiO_2 nanoparticle colloidal solution concentration in the sol. Comparison of all the responses showed that it's the three-dip coated 9%(v/v) TiO_2 nanoparticle colloidal solution concentration in the sol, which exhibits the best overall sensitivity. Following reasons can be attributed to the observation of optimum film thickness and the composition. For two-dip coating, the film thickness was much less than that of the penetration depth of the evanescent wave [30]. Correspondingly, less number of immobilized nanoparticles was in the sol-gel matrix to interact with the evanescent wave. With the increase in the humidity, water molecules that are diffused into the pores of the film could interact with a limited number of nanoparticles only, resulting in a limited absorption of the optical power carried by the evanescent field in the sensing region. Thus, a low sensitivity was observed. The thickness of the sensing film corresponding to the three-dip coated probe increases sufficiently but remains within the penetration depth and hence, higher than that for the two-dip film. With higher nanoparticles within the sensing film to interact with the optical power and with a maximum exploitation of the optical power available in the evanescent field, optimum optical absorption was observed in this case. This led to the higher sensitivity as compared to the two-dip coated probe. Thickness of the sensing film corresponding to the 4-dip coated probe was more than that of the evanescent wave. Thus, less number of water molecules could diffuse into the volume of the film spanned by the evanescent wave to interact with the corresponding optical power in the wave. This reduced the sensitivity substantially. Further, the effect of changing the film composition with a higher nanoparticle concentration in sol-gel nanostructured sensing film on the centrally decladded straight and uniform fiber is expected to be two-fold. First, increased

amount of nanoparticle makes each dip-coated film having a higher film thickness. Second, high volume fraction of nanoparticles in the sensing nanostructured cladding obstructs the proper diffusion of water molecules into the sensing film upon increasing the humidity, and hence, the optical modulation of the evanescent wave energy. It's the thickness of three-dip coated probe for 9%(v/v) TiO_2 nanoparticle colloidal solution concentration in the sol, which is of the order of the penetration depth. This led to the maximum evanescent interaction, and hence, the maximum sensitivity.

Table 4.1: Response comparison of the developed sensor with other reported sensors.

Authors	Sensing element	Linear dynamic range (%RH)	Sensitivity
Gaston et al. [74]	Side polished SMF	70-90	0.5 dB/%RH
Herrero et al. [75]	Side polished SMF	0-15	0.5 nm/%RH
Tan et al. [89]	LPG	90-99	1.2 dB/%RH
Liu et al. [91]	LPG	38.9-100	0.2 nm/%RH
Yeo et al. [96]	FBG	23-97	5.6 pm/%RH
Huang et al. [97]	FBG	11-98	0.266 mV/%RH
Vijayan et al. [83]	U-shape plastic fiber	80-92	3.406 mV/%RH
Tay et al. [76]	U-shape plastic fiber	65-85	74.85 mV/%RH
Sensor developed in Chapter 3	Nanoporous straight and uniform sol-gel fiber core	5-95	0.93mV/%RH
Developed sensor	Straight and Uniform PCS fiber	24-95	27.1 mV/%RH

Next, sensitivity characteristics of the developed are compared with the other sensors reported employing various schemes in the literature. Table-4.1 lists the sensitivity characteristics of these sensors for comparison. As can be observed from the table, side-polished single mode fiber based sensors are limited by very small dynamic range. Further,

best dynamic range for the LPG based sensor is observed in [91]. Apart from the work reported in this thesis, an overall largest linear dynamic range (11-98%RH) is reported in FBG based sensor of [97] whereas an overall largest sensitivity (74.85mV/%RH) is reported in U-shaped plastic fiber based sensor of [76]. In comparison, the linear dynamic range of developed sensor is slightly lower than the one reported in [97], however, the sensitivity of the reported sensor is ~102 times higher than [97]. With the simplest sensing element (straight and uniform fiber probe), it's easy to fabricate and avoids the need to costly and sophisticated source and detection device. Further, comparing the response of the developed sensor with [76], the linear dynamic range of the developed sensor is much improved over [76]. As far as the sensitivity is concerned, it's worth mentioning that [76] is based on U-shape probe and according to [110], sensitivity increases approximately seventy times for the U-shaped optical fiber probe in comparison to the corresponding straight and uniform optical fiber probe. This means, the expected sensitivity would be of the order of 1897mV/%RH if the straight and uniform optical fiber probe of the developed sensor is replaced with a U-shaped probe of the same optical fiber. This is much higher than the one reported in [76]. Further, the observed sensitivity of the present TiO_2 nanoparticle based sensor is even much higher (~29 times) than the sensitivity observed in exhaustive and guiding mode attenuation through ZnO nanoparticle doped nanoporous sol-gel fiber core as sensing element. Hence, employing exhaustive guided mode attenuation mechanism through TiO_2 nanoparticle doped nanoporous sol-gel fiber core as a sensing element is expected to give a very high sensitivity. Even assuming the same, i.e., ~9 times sensitivity enhancement switching from evanescent wave absorption scheme to guided mode attenuation scheme, one can expect a sensitivity of 243.9mV/%RH! A future scope of reported work in the thesis.

Finally, dynamic performance and the repeatability characteristics of the optimized sensing probe were investigated as detailed in Chapter 2. Observed time response is depicted in Fig.

4.7. As can be observed from the figure, the relative intensity (fiber sensor output) almost instantly and smoothly changes during the forward (5%RH to 90%RH) cycle of humidity change. During reverse (90%RH to 5%RH) cycle of the humidity change it varies in a slower rate compared to the forward cycle. An average response time of 0.01 second was observed for humidification whereas an average response time of 0.06 second for the desiccation. Ideally, the response time of the sensor should have been identical irrespective of the humidification or desiccation processes. A possible reason could be the fact that we could

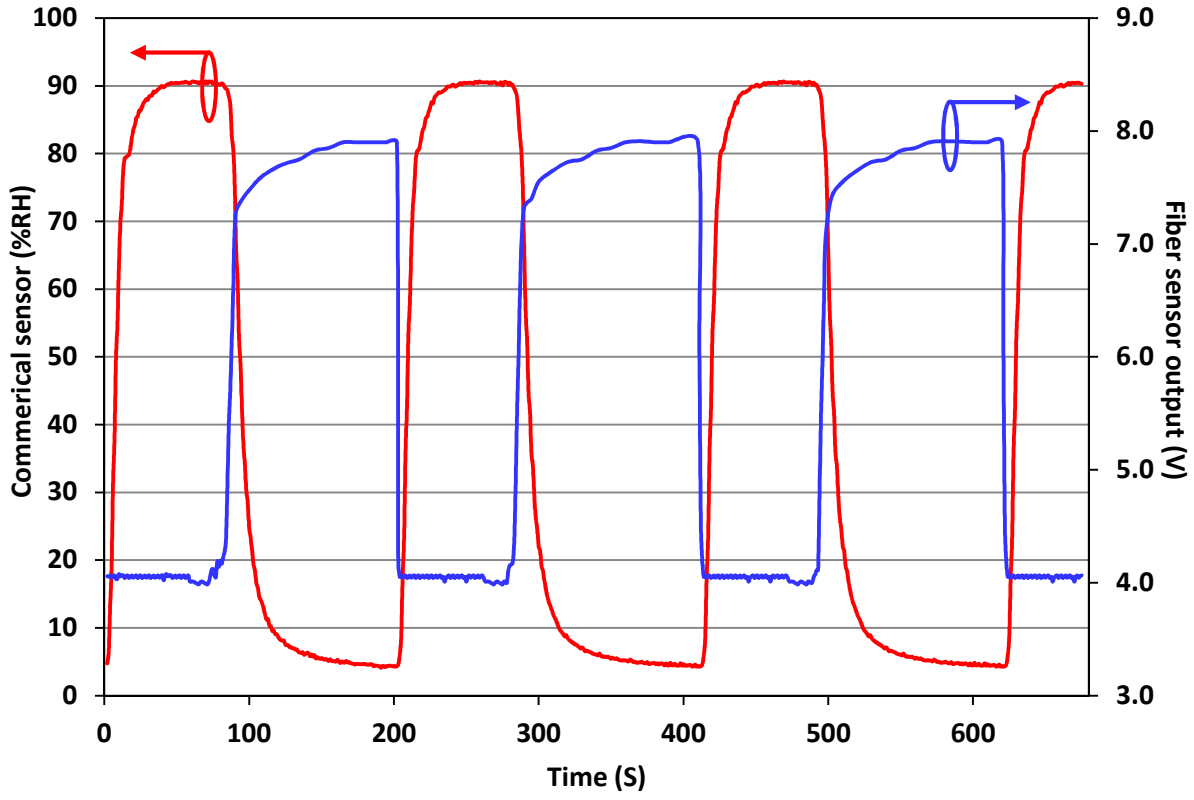

Figure 4.7: *Time response behavior and the repeatability test for the optimized fiber optic humidity sensor against cyclic humidity perturbations.*

not make a step-down variation during the reverse cycle of the humidity change. In any case, the observed response times of the fiber sensor for the forward as well as the reverse humidity cycles were much lower than the response times of the commercial sensor.

This establishes the fact that the developed fiber sensor is much faster than the commercial sensor. Result in Fig. 4.7 also establishes that the developed sensor is highly reversible and repeatable. Furthermore, a maximum fiber output variation is once again observed to be of the order of 10^{-4} only during the repeatability and reversibility test over an interval of few days. This shows a great reliability and repeatability of the developed sensor.

4.4 Conclusion

This chapter described the development of optical fiber RH sensor using different sensing agent, TiO_2 nanoparticle, and employing evanescent wave intensity modulation scheme. In-house developed TiO_2 nanoparticles of controlled particle size were immobilized into a nanostructured sol-gel matrix of appropriate thickness that was deposited onto a centrally decladded plastic-clad silica optical fiber. A comprehensive experimental investigation is carried out in order to optimize the sensor performance by suitably controlling various potential experimental/sensor parameters of interest that can influence the sensor's response. Best response for the sensor is observed against an optimum thickness and composition of nanostructured sensing film corresponding to the three-dip coating of 9%(v/v) nanoparticle concentration in the sol respectively. A much improved sensitivity of 27.1mV/%RH is observed along with the throughout-linear sensor response over a dynamic range as wide as 24% to 95%RH with an average response time of 0.01 second for humidification and 0.06 second for the desiccation.

Chapter 5

Localized Surface Plasmon Resonance based U-shaped Optical Fiber Humidity Sensor

5.1 Introduction

Last three chapters described the experimental investigations for developing optical fiber RH sensors based on intensity modulation scheme employing evanescent wave absorption as well as exhaustive attenuation of entire guided mode. To investigate further optimization possibilities and to make a comparative study, localized surface plasmon resonance (LSPR) scheme is employed to develop an optical fiber RH sensor in the work reported in this chapter. Localized surface plasmons are charge density oscillations, which occurs due to the collective oscillations of free electron cloud in metal nanoparticles [49]. Localized surface plasmon can be excited by light when the frequency of the incident light matches with the oscillation frequency of the conduction electrons and is called the resonance frequency. This resonance frequency strongly depends on the refractive index of the medium surrounding the metal nanoparticles. Nanoparticles of noble metals such as gold and silver exhibit strong absorption band in the UV-visible region due to LSPR. The absorption peak shows a red-shift upon increasing the refractive index of the medium surrounding the nanoparticles [49-50]. This property is used in the present work for developing LSPR based optical fiber RH sensor. A metal nanoparticle as well as metal-dielectric nanoparticles film onto the bare core of optical fiber is deposited. A U-shape probe geometry, rather than the straight and uniform geometry, was used to ease out the realization of nanoparticle film on the fiber surface for

sensor development. A linear dynamic range of 6-90%RH is observed with a sensitivity of 0.0213nm/%RH for gold nanoparticle assisted LSPR optical fiber sensor; whereas for metal-dielectric nanoparticles (gold-TiO_2) assisted LSPR optical fiber RH sensor, the linear dynamic range is observed to be 12-80%RH with a sensitivity of 0.0177nm/%RH. For (silver-TiO_2) nanoparticles assisted LSPR optical fiber RH sensor, the linear dynamic range is observed to be 29-95%RH with sensitivity of 0.0412nm/%RH.

5.2 Principle

5.2.1 Localized surface plasmon resonance in metal nanoparticles

The schematic representation of plasmon oscillation in metal nanoparticles is shown in Fig.5.1. The electric field of the incoming light wave induces a polarization of the (free) conduction electrons with respect to the much heavier ionic core of a spherical nanoparticle [49,111]. The positive charges in the particle are assumed to be immobile and the negative charges, i.e., the conduction electrons, move under the influence of external fields. Therefore, a displacement of the negative charges from the positive ones occurs when the metallic nanoparticle is placed in an electric field, i.e., there results a net charge difference at the nanoparticle boundaries. This, in turn, gives rise to a linear restoring force to the system. As a consequence, plasmon oscillates locally around the nanoparticle, with a frequency termed as localized surface plasmon resonance. The resonance frequency is the characteristic of the metal of which, the nanoparticle is made of. LSPR is sensitive to the changes in the dielectric local environment of nanoparticle [50]. The extinction of a metal nanoparticle is given as [50]

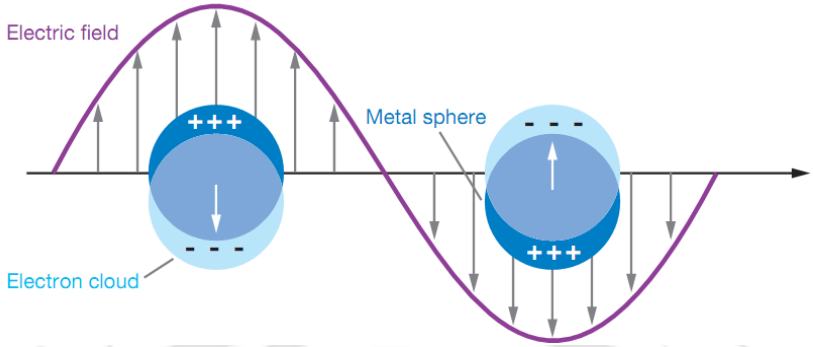

Figure 5.1: *Schematic diagram of plasmon oscillation in metal nanoparticles* [49].

$$E(\lambda,R)=\frac{24\pi R\,\varepsilon_d^{3/2}}{\lambda}\left[\frac{\varepsilon_i(\lambda,R)}{(\varepsilon_r(\lambda,R)+2\varepsilon_d)^2+\varepsilon_i(\lambda,R)^2}\right] \quad (5.1)$$

where λ is the wavelength of the incident light, R is the radius of metal nanoparticle, ε_r and ε_i are the real and imaginary parts of the metal nanoparticle dielectric functions, respectively and ε_d is the dielectric constant of the medium surrounding nanoparticle. E (λ) will be maximum when $\varepsilon_r = -2\varepsilon_d$. This occurs at a particular wavelength called resonance wavelength. The dependence of resonance wavelength on refractive index of the surrounding medium has been used in LSPR based optical as well as optical fiber sensor [51-53]. In an optical fiber LSPR sensor, decladded portion of the fiber is coated by metal nanoparticle film. The evanescent field of the guided ray interacts with metal nanoparticles, resulting in wavelength dependent absorption.

5.3 Experimental

5.3.1 Preparation of U-shaped probe

PCS fiber having same specifications used in Chapter 4 was used to develop the sensing probe. The total length of the fiber used was around 40 cm. Fiber ends were prepared properly to get optically-flat end faces perpendicular to the axis of the fiber which provides the efficient coupling of light from source to fiber and fiber to the detector. About 5 cm of the cladding was carefully removed from the central portion of the fiber. After that it was sonicated in soap solution (Merk) and then in de-ionized water. Finally, it was cleaned with acetone. Realization of nanoparticle film onto a straight probe is quite challenging. Hence, the decladded portion of the fiber was carefully bent into a U-shape by exposing it to a propane flame. In addition, bending of sensing probe causes decrease in angle of incidence of the propagating ray in the sensing region [103]. This results in an increase of the penetration depth of the evanescent field, and hence increases the sensitivity of the LSPR sensor. The experiments were performed only on the probes having uniform core diameter in entire U-shape region and the bend close to U-shape.

5.3.2 Preparation of gold nanoparticles coated sensing probe

To make the sensing probe, first colloidal gold nanoparticles were synthesized. For this, 1 mM Tetrachloroauric acid ($AuHCl_4$) and 38.8 mM Sodium citrate ($Na_3C_6H_5O_7$) solution were prepared [112]. 22 mL of $AuHCl_4$ was pored into a conical flask and it was allowed to boil. To this boiling solution 2 mL of $Na_3C_6H_5O_7$ was added and the boiling was continued for about 10 min. Sodium citrate reduces Au ions to nanoparticles of Au metal. The formation of gold nanoparticles can be observed from the colour change of solution since small gold nanoparticles are red. The U-shaped region of the sensing probe was kept in

chromic acid for 12 hours. After that it was sonicated in de-ionized water. Then the probe was dried in the oven for 30 min at 100^{o}C. Next, the U-shaped probe was dipped in 5% (v/v) ethanol solution of 3-amino-propyltrimethoxysilane (APTMS) for 3 hours. This was done to obtain amine-functionalized glass surface for the attachment of gold nanoparticles in aqueous media [113]. After soaking in APTMS solution, the sensing probe was rinsed with ethanol and dried in the oven for 1 hour at 100^{o}C. The U-shaped probe coated by APTMS was then dipped in gold nanoparticle solution for 2 hours to realize nanoparticle film on the fiber surface. The probe was then removed from gold nanoparticle solution and rinsed with de-ionized water. Finally it was dried in the oven 30 min at 100^{o}C. SEM image of the gold nanoparticles coated fiber surface is shown in Fig. 5.2.

In the next step, the gold nanoparticle film coated probe was further coated by TiO_2 nanoparticles immobilized sol-gel film. For this, sol solution containing TiO_2 nanoparticles having same composition of optimized probe as reported in Chapter-4 was prepared. Metal

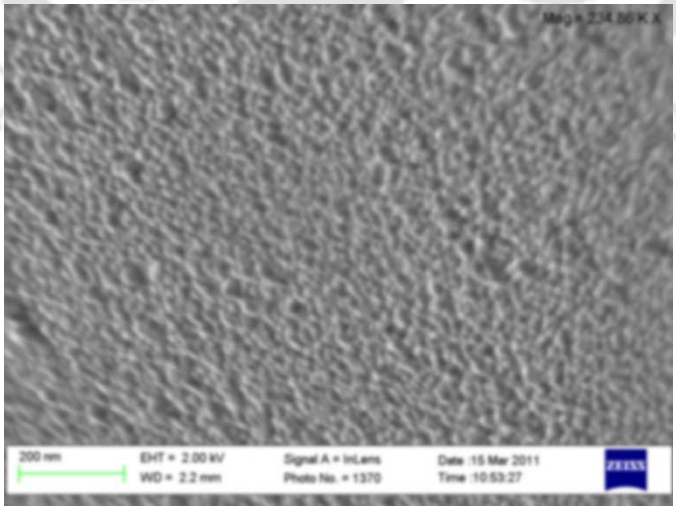

Figure 5.2: *SEM image of gold nanoparticles coated fiber surface.*

nanoparticle layer coated U-shaped probe was dip coated with TiO_2 nanoparticles immobilized sol-gel film. The developed sensing probe was dried at 160ºC in order to remove ethanol and water, from the pores of the sol-gel film.

5.3.2 Preparation of silver nanoparticles coated sensing probe

The U-shaped region of the sensing probe was kept in chromic acid for 12 hours. After that it was sonicated in de-ionized water. Then the probe was dried in the oven for 30 min at 100^{o}C. Silver nanoparticle film was realized onto the fiber core through silver mirror reaction. This was done by the reduction of Tollen's reagent with glucose through following reactions:

$$2\ AgNO_3 + 2\ NaOH \rightarrow Ag_2O + 2\ NaNO_3 + H_2O$$

$$Ag_2O + 4\ NH_3 + 2\ NaNO_3 + H_2O \rightarrow 2\ [Ag(NH_3)_2]\ NO_3 + 2\ NaOH$$

where $[Ag(NH_3)_2]^+$ is called the Tollen's reagent. The reduction of Tollen's reagent with glucose (RCHO) takes as follows

$$RCHO + 2\ [Ag(NH_3)_2]^+ + 2OH^- \rightarrow RCOOH + 2Ag + 4NH_3 + H_2O$$

Tollen's reagent was prepared by first mixing 60 µL of 1M NaOH with 6mL of silver nitrate solution (50mM) to form a dark-brown solution [114]. Ammonia solution was added to this mixture drop by drop to form a transparent solution. The Tollen's reagent was kept in an ice bath for 15 minutes so that the temperature of solution comes down to nearly 0^{o}C. After that, U-shaped region of the fiber was dipped in Tollen's reagent. The fiber was placed in the Tollen's reagent in such a way that it was nearly equidistant from the walls of the beaker. To this, 1.5 mL of 0.5M glucose solution was added in drops under careful stirring. The reduction of Tollen's reagent with glucose is triggered by thermal energy. Since the

temperature of the solution was low it was possible to mix glucose with Tollen's reagent uniformly before the chemical reaction started. Finally, temperature of the hot plate (of magnetic stirrer) was raised to 50^{o}C to start the chemical reaction at a constant rate and the process was continued for 15 min. This has led to the deposition of silver nanoparticle film onto the fiber core. SEM image of the silver nanoparticles coated fiber surface is shown in Fig. 5.3. Next, the sensing probe is further coated by TiO_2 nanoparticles immobilized sol-gel film as it was done for pervious probe. This additional layer protects silver nanoparticle film from direct exposure of water molecules.

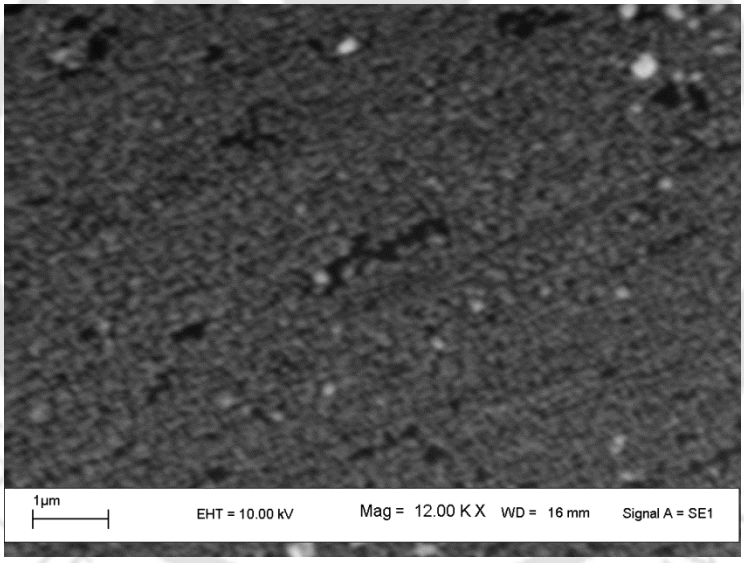

Figure 5.3: *SEM image of silver nanoparticles coated fiber surface.*

5.3.3 Sensing probe characterization

For proper characterization of the LSPR humidity sensing probe, it was fixed inside the humidity chamber in such a way that the U-shaped region was in the middle of the chamber.

The schematic diagram of experimental setup for sensor characterization is shown in Fig.5.4. Light from a Broad Band Source (Mikropack HL-2000-FHSA) was coupled to one end of the sensing probe and the other end was coupled to a spectrometer (Ocean Optics-HR4000). In order to identify the actual fiber sensor output at a particular humidity, we had slowly varied the humidity inside the chamber in steps by keeping constant value of humidity for sufficient time. Fiber sensor output spectra corresponding to different vales of humidity were recorded using the spectrometer.

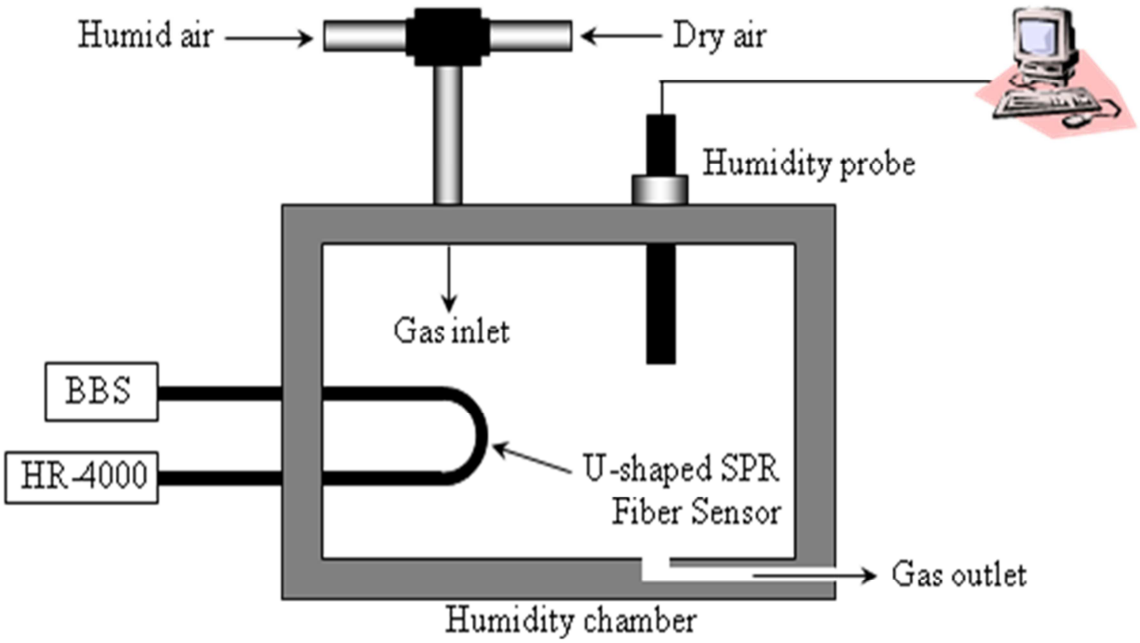

Figure 5.4: *Schematic diagram of experimental setup for optical fiber humidity sensor characterization.*

5.4 Results and Discussion

The sensor is based on localized surface plasmon resonance in metal nanoparticles. Here the evanescent wave associated with the guided modes of the fiber excites plasmons in

nanoparticles. This leads the reduction of the energy corresponding to resonance wavelength, in the transmitted (output) light. The slight change in the sensing region is mapped with a corresponding change in the resonance condition. Thus the shift in the resonance condition depicts the change in the surrounding humidity. In the first step, sensing probe with only gold nanoparticle film was characterized. To carry out the experiment and to study the sensor response, optical fiber sensor was coupled to Broad Band Source with one arm and to the spectrometer with the other arm of U-shape. In order to identify the actual fiber sensor output at a particular humidity, humidity was varied step-wise and very slowly within the chamber in order to retain the constant value for a good recordable time. Instantaneous value of humidity in the chamber was monitored through the commercial sensor and the data acquisition card. This was done by recording the commercial sensor's output as a function of time with a resolution of 1 second. Fiber sensor output spectra corresponding to different values of applied humidity were recorded using the spectrometer during the stabilized portion

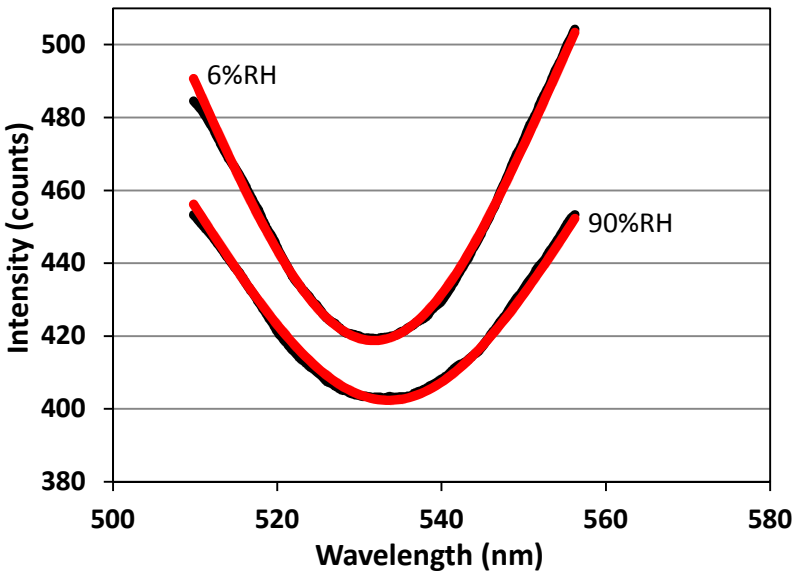

Figure 5.5: *Experimentally observed resonance spectra of gold nanoparticle assisted LSPR based humidity sensor corresponding to two different humidity values (6 and 90%RH).*

(on the time scale) of the response characteristics of the commercial sensors. Fig.5.5 shows the experimentally observed resonance spectra (black curve) corresponding to a lower value of humidity (6%RH) and higher value of humidity (90%RH) for sensing probe with gold nanoparticle film. These spectra were further fitted by Lorentz function (red curve), as described in [115], to identify the peak absorption wavelength. The peak absorption wavelength corresponding to a particular value of humidity was taken as the central wavelength of Lorentz function fitting to its spectrum. Extracted peak absorption wavelengths corresponding to the applied humidity values were then plotted against the humidity values.

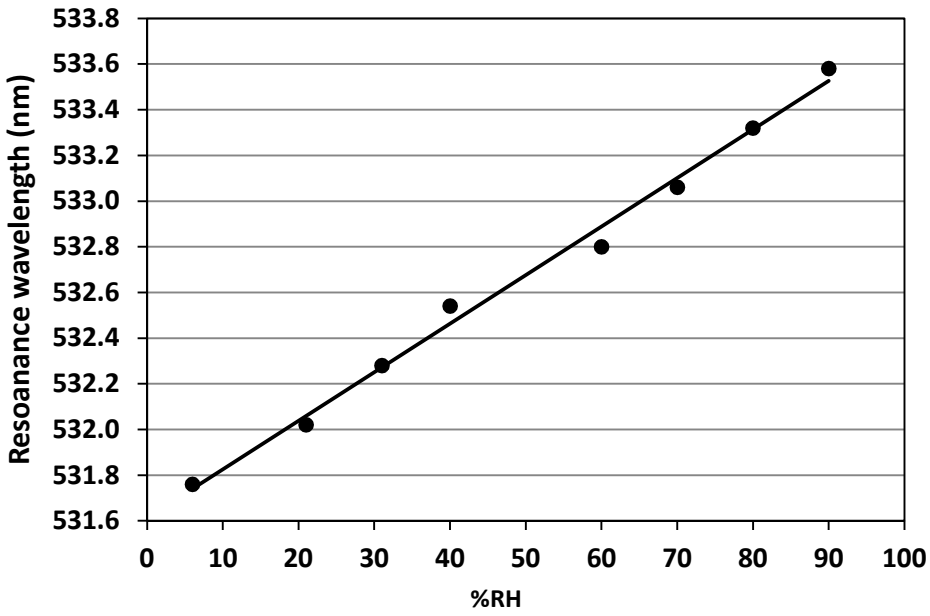

Figure 5.6: *Experimentally observed sensor response of gold nanoparticle film coated LSPR humidity sensor.*

The observed sensor response is depicted in Fig. 5.6. As can be observed from the figure, peak absorption wavelength shifts towards higher wavelength upon increasing the humidity. This is due to the fact that LSPR resonance condition is strongly depends on the refractive

index of the medium surrounding the metal nanoparticles. The increase in humidity causes the increase in effective R.I. of the medium surrounding the nanoparticle film due to the presence of more water molecules. This results the observed red shift of peak absorption wavelength. Importantly, a linear response over a wide dynamic range of 6-90%RH is observed with linear sensitivity of 0.0213nm/%RH for this LSPR sensor.

In the next step, metal nanoparticle layer coated sensing probe was further coated by dielectric (TiO_2) nanoparticle immobilized sol-gel thin film having same composition of optimized probe in Chapter 4. The reason for additional dielectric coating was an expected better stability of metal nanopariticle film onto the bare fiber core and to expectedly and possibly have better environmental changes through analyte molecules entrapped within nanoporous thin sol-gel glass matrix. Experimentally observed resonance spectra corresponding to a lower value of humidity (12%RH) and higher value of humidity (80%RH) are shown in Fig.5.7. As was observed for pure gold nanoparticle film based sensor, here also

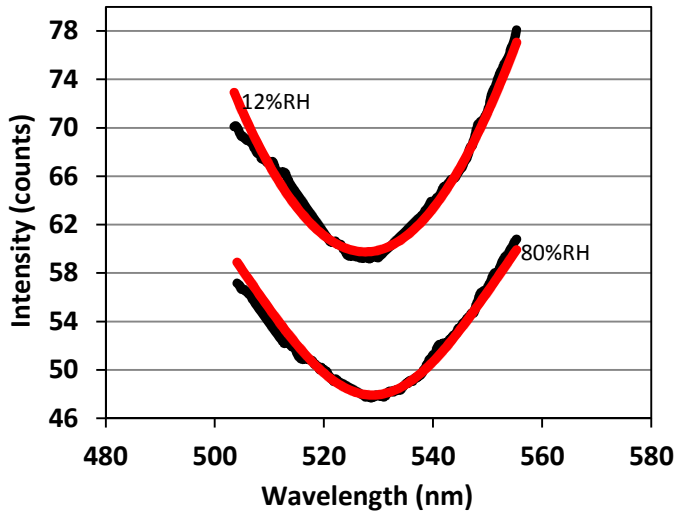

Figure 5.7: *Experimentally observed resonance spectra of gold-dielectric (TiO_2) nanoparticle assisted LSPR based humidity sensor corresponding to two different humidity values (12 and 80%RH).*

the resonance wavelength shows a red shift upon increasing humidity. This is due to the fact that TiO_2 nanoparticles have high adsorption of water molecules. As a result, more water molecule diffuse into the pores of the sol-gel film upon increasing humidity. This led to the increase in effective R.I. of the medium surrounding the metal nanoparticles which results observed red shift of peak absorption wavelength. Fig. 5.8 shows the experimentally observed sensor response to different humidity environments. Here also the resonance

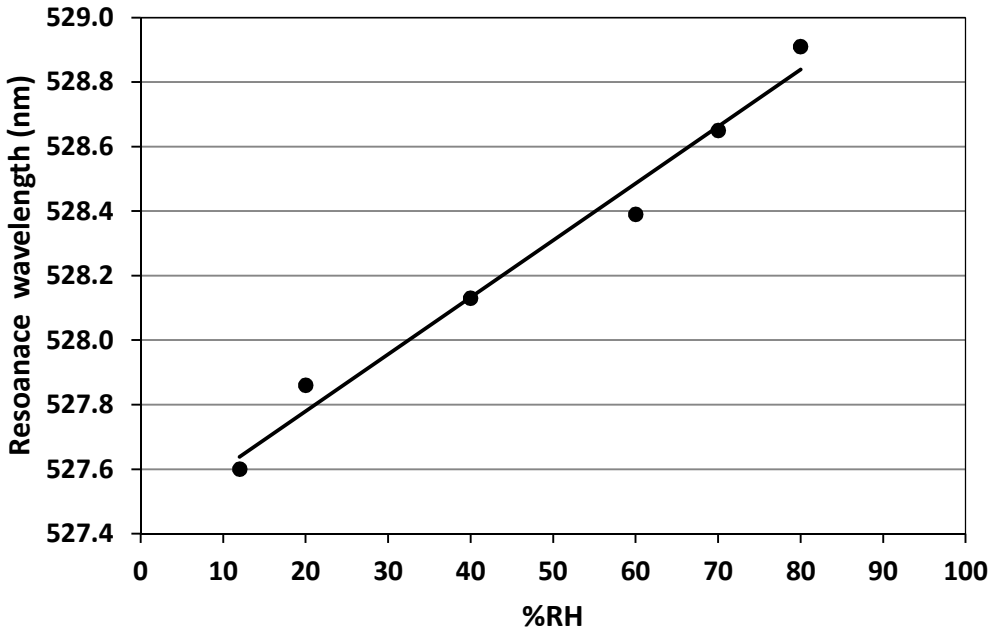

Figure 5.8: *Experimentally observed sensor response of gold-dielectric (TiO_2) nanoparticles assisted LSPR humidity sensor.*

wavelength corresponding to a particular value of humidity was taken as the central wavelength of Lorentz function fitting to its spectrum. As can be observed from the figure, the introduction of reagent immobilized thin nanoporous sol-gel glass matrix in order to possibly entrap water molecules more effectively with a thought of having a better environmental change did not work that way; the linear dynamic range of the sensor is from

12 to 80%RH and sensitivity got reduced to 0.0177nm/%RH (lowered by a factor of 1.2) as compared to the 6 to 90%RH dynamic range and 0.0213nm/%RH sensitivity for a pure gold nanoparticle assisted LSPR sensor. Thus, the incorporation of dielectric nanoparticle film, over gold nanoparticle film, degraded sensor performance.

In the next step, silver-dielectric (TiO_2) nanoparticles assisted LSPR based RH sensor was characterized. Fig. 5.9 shows the experimentally observed resonance spectra corresponding to a lower value of humidity (29%RH) and higher value of humidity (90%RH). As we observed for previous probes here also resonance wavelength shows a red shift upon increasing humidity.

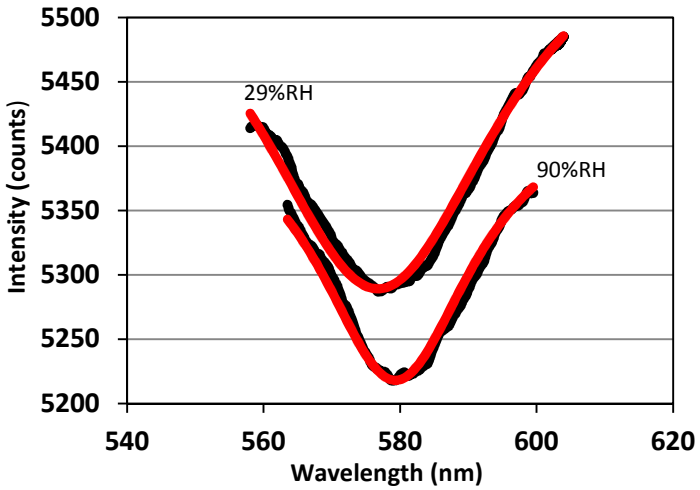

Figure 5.9: *Experimentally observed resonance spectra of silver-dielectric (TiO_2) nanoparticles assisted LSPR based humidity sensor corresponding to two different humidity values (29 and 90%RH).*

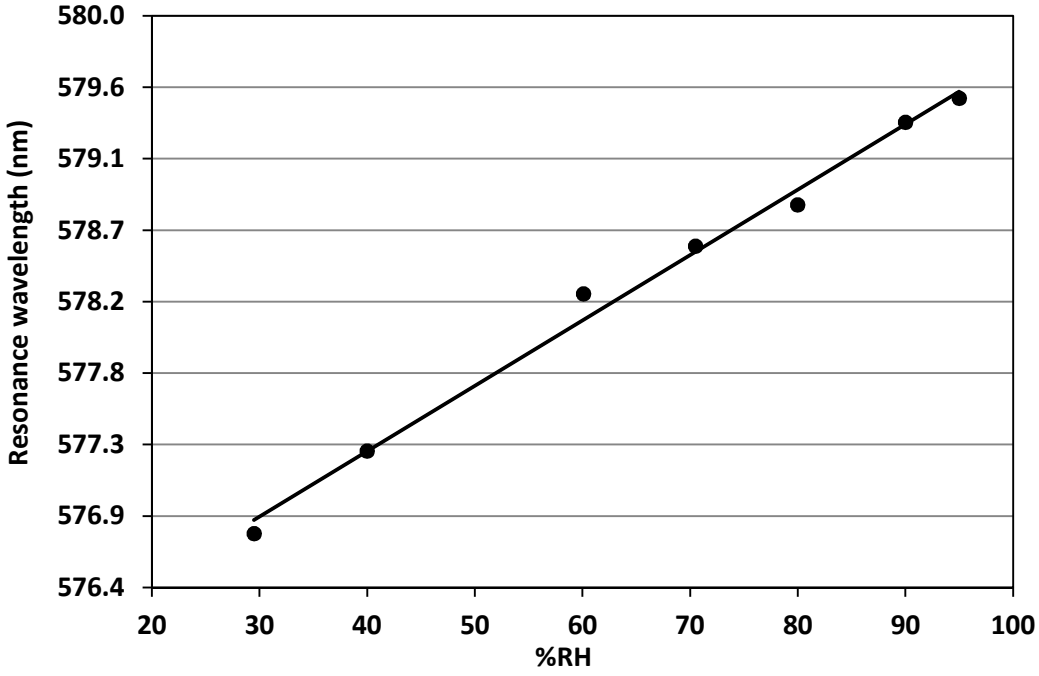

Figure 5.10: *Experimentally observed sensor response of silver-dielectric (TiO_2) nanoparticles assisted LSPR based humidity sensor.*

The experimentally observed sensor response is shown in Fig. 5.10. As can be observed from the figure, the sensor responds linearly over a dynamic range of 29-95%RH with a sensitivity of 0.0412nm/%RH. The observed linear dynamic range is slightly lower than the sensor based on gold nanoparticle film. Nevertheless, the sensitivity is 1.92 times higher than the sensitivity observed for gold nanoparticle assisted RH optical fiber sensor.

Next, response characteristics of the developed sensors are compared with the other RH sensors reported in the literature employing wavelength interrogation schemes. Table 5.1 lists the response characteristics of these sensors for comparison. As can be observed from the table, over all highest sensitivity is reported with side-polished sensing element. However, its

Table 5.1: Response comparison of the developed sensor with other reported sensors.

Authors	Sensing element	Linear dynamic range (%RH)	Sensitivity (nm/%RH)
Herrero et al. [75]	Side polished SMF	0-15	0.5
Liu et al. [91]	LPG	38.9-100	0.2
Yeo et al. [96]	FBG	23-97	0.0056
Gold nanoparticle film based (*developed*)	U-shape PCS fiber	6-90	0.0213
Gold/dielectric nanoparticles film based (*developed*)	U-shape PCS fiber	12-80	0.0177
Silver/dielectric nanoparticles film based (*developed*)	U-shape PCS fiber	29-95	0.041

linear dynamic range is limited to 0-15%RH only. LPG based sensor [91] has better linear dynamic range compared to [75]. Over all largest linear dynamic is reported in FBG based RH sensor [96]. In comparison, linear dynamic range of gold nanoparticle assisted LSPR based sensor is observed to be better than all other RH sensors employing wavelength interrogation scheme (Table 5.1). Sensitivity of this probe is improved by factor 3.8 compared to [96]. For sensor based on silver nanoparticle film, the observed linear dynamic range is slightly lower than the largest reported in the literature. However, its sensitivity is 7.32 times higher than the one reported in [96]. In addition, developed sensor is cheaper, easily fabricate-able and employs much simple and less costly source/detector as compared to other reported sensors.

Finally, repeatability and reliability tests were carried out to rigorously analyze the sensor performance. For this, experiments were repeated at an interval of 4 days. A total of 3 such repeat experiments on three different days were carried out in a span of 11 days. LSPR based fiber sensor response for three different applied humidity values (40, 80 and 90%RH) were

analyzed. Response curve towards the applied humidity were observed to be almost constant over a span of 11 days. This shows a good reliability and repeatability of the reported sensor.

5.5 Conclusion

This chapter described the development of optical fiber RH sensor based LSPR scheme. The sensor was developed by realizing metal nanoparticle film as well as metal-dielectric nanoparticle films onto the bare core (U-shaped region) of PCS fiber. A comparative experimental study is carried out with nanoparticle film of gold and silver. From the analysis of experimental data, it is observed that for the gold nanoparticle assisted LSPR based optical fiber sensor, the linear dynamic range is observed to be 6-90%RH with sensitivity of 0.0213nm/%RH. For silver-dielectric nanoparticle assisted LSPR based optical fiber sensor, the observed linear dynamic (29-95%RH) is lower than the gold nanoparticle film based sensor. However, its sensitivity is observed to be 1.92 times higher than the gold nanoparticle assisted LSPR based optical fiber sensor. As the sensing principle is based on wavelength interrogation scheme, developed sensor is free from the intensity fluctuation of light source. In addition, developed sensor is simpler compared to other optical fiber RH sensors employing wavelength interrogation scheme.

Chapter 6

Conclusion of Thesis

In the present thesis, a comprehensive experimental study is carried out to achieve linear response over a widest possible dynamic range with an optimum sensitivity through a simple optical fiber sensor configuration. Three schemes, namely, evanescent-wave (EW) absorption, in a straight and uniform PCS multimode fiber, employing ZnO as well as TiO_2 nanoparticles immobilized nanostructured sol-gel sensing fiber cladding, direct and exhaustive attenuation of guided mode through a ZnO nanoparticles immobilized microstructured nanoporous sol-gel fiber core, and localized surface plasmon resonance (LSPR) employing in-house scaled metal (gold) as well as metal-dielectric (silver-TiO_2) nanoparticles have been used. Response of all the proposed sensors was optimized against all possible influential compositional parameters such as chemical composition, reaction parameters, thickness etc. Response characteristics of the proposed sensors were compared with the commercial sensor used for the experiment and other optical fiber RH sensors reported in the literature. A maximum linear dynamic range of 4-96%RH is observed for the sensor employing evanescent wave absorption scheme with ZnO nanoparticles immobilized sol-gel silica sensing fiber cladding. The observed linear dynamic range is larger than the highest (11-98%RH, based on FBG) reported in the literature. Thus, a widest possible linear dynamic range is achieved, nevertheless, the sensitivity needed to be further increased. In order to realize this objective, a sensing configuration allowing exhaustive attenuation of entire guided mode was employed using ZnO nanoparticles (that corresponds to the widest

linear dynamic range) immobilized sol-gel microstructured fiber. Almost identical linear dynamic range (5-95%RH) is observed with a manifold (~9 times) increase in the sensitivity as compared to ZnO nanoparticle employed EW fiber sensor and over 3.5 times increase in the sensitivity as compared to the sensor with largest linear dynamic range reported in the literature. The maximum linear dynamic range decreased to 24-95%RH when the ZnO nanoparticles in sol-gel sensing cladding were replaced with TiO_2 nanoparticles. Nevertheless, the optimized sensitivity improved much in comparison with ZnO nanoparticles immobilized sol-gel sensing cladding RH sensor. The observed linear dynamic range of TiO_2 nanoparticle based sensor is slightly lower than the largest reported in the literature; however, its sensitivity is ~102 times higher as compared to the sensor with largest linear dynamic range reported in the literature. It is worth mentioning that performance of the sensor can be further improved by synthesizing the same nanostructured sensing film on a U-shaped geometry of a pre-researched optimized bending radius made of the same optical fiber or employing exhaustive guided mode attenuation mechanism through TiO_2 nanoparticle doped nanoporous sol-gel fiber core. In the last sensing scheme (metal as well as metal-dielectric nanoparticles assisted LSPR), a linear dynamic range of 6-90%RH is observed for sensing probe with gold nanoparticle film. The observed linear dynamic range is better than the highest reported (23-97%RH, based on FBG) in the literature employing wavelength interrogation scheme. Importantly, sensitivity of this probe is 3.8 times higher as compared to the sensor with highest linear dynamic range. For sensor based on silver-TiO_2 nanoparticle film, the linear dynamic range decreased to 29-95%RH; nevertheless, sensitivity is improved ~2 times compared to the sensing probe with gold nanoparticle film. The response characteristics of all developed sensors are observed to be very fast, reversible, and repeatable. Hence, the developed sensors are of great practical importance and use.

References

1. B. P. Pal, “Fundamentals of fiber optics in telecommunication and sensor systems,” (*New Age Inc.*, 2003).
2. X. Y. Fang and M. S. Cao, “Theoretical analysis of 2D laser angle sensor and several design parameters,” *Opt. Laser Technol*., **34**, pp. 225 (2002).
3. X. Ge, Y. Kostov and G. Rao, “High-stability non-invasive autoclavable naked optical CO_2 sensor,” *Biosens. Bioelectron.,* **18**, pp.857 (2003).
4. S. K. Lee and I. Okura, “Porphyrin-doped sol-gel glass as a probe for oxygen,” *Anal. Chim. Acta*, **342**, pp.181 (1997).
5. H. J. Nam, T. Sasaki, and N. Koshizaki, “Optical CO gas sensor using a cobalt oxide thin film prepared by pulsed laser deposition under various argon pressures,” *J. Phys. Chem. B*, **110**, pp. 23081 (2006).
6. J. W. Aylott, D. J. Richardson and D. A. Russell, “Optical biosensing of gaseous nitric oxide using spin-coated sol-gel thin films,” *Chem. Mater.*, **9**, pp.2261 (1997).
7. P. Fedtke, M. Wienecke, M. C. Bunescu, M. Pietrzak, K. Deistung and E. Borchardt, “Hydrogen sensor based on optical and electrical switching,” *Sens. Actuators B,* **100**, pp. 151 (2004).
8. Z. Jin, Y. Su and Y. Duan, “Development of a polyaniline-based optical ammonia sensor,” *Sens. Actuators B,* **72**, pp.75 (2001).
9. E. Higurashi, R. Sawada, and T. Ito, “Monolithically integrated optical displacement sensor based on triangulation and optical beam deflection,” *Appl. Opt.*, **38**, pp.1746 (1999).
10. H. Y. Fu, H. Y. Tam, L. Y. Shao, X. Dong, P. K. A. Wi, C. Lu and S. K. Khijwania, “Novel pressure sensor using a polarization-maintaining photonic crystal fiber based Sagnac interferometer,” *Appl. Opt.*, **47**, pp. 2835 (2008).

11. F. Chiadini, A. Paolillo, and A. Scaglione, "A reflectometric optical fiber temperature sensor," *IEEE J. Sens.*, **3**, pp. 80 (2003).

12. T. Lü and S. Yang, "Extrinsic Fabry-Perot cavity optical fiber liquid-level sensor," *Appl. Opt.*, **46**, pp. 3682 (2007).

13. J. Villatoro and D. M. Hernandez, "Low-cost optical fiber refractive-index sensor based on core diameter mismatch," *J. Lightwave Technol.*, **24**, pp. 1409 (2006).

14. B. Gu, M. Yin, A. P. Zhang, J. Qian, and S. He, "Low-cost high-performance fiber-optic pH sensor based on thin-core fiber modal interferometer," *Opt. Express*, **17**, pp. 22302 (2009).

15. J. Jensen, P. Hoiby, G. Emiliyanov, O. Bang, L. Pedersen, and A. Bjarklev, "Selective detection of antibodies in microstructured polymer optical fibers," *Opt. Express*, **13**, pp.5883 (2005).

16. M. Belal, Z. Song, Y. Jung, G. Brambilla and T. P. Newson, "Optical fiber microwire current sensor," *Opt. Lett.*, **35**, pp. 3045 (2010).

17. K. Bohnert, M. Ingold and J. Kostovic, "Fiber-optic voltage sensor for SF_6 gas-insulated high-voltage switch gear," *Appl. Opt.*, **38**, pp.1926 (1999).

18. A. M. Boronakhin, A. A. Velikosel'tsev, A. N. Tkachenko, A. A. Yankovskiĭ, and D. B. Pukhov, "Fiber-optic rotation sensors for seismic measurements," *J. Opt. Technol.*, **77**, pp. 447 (2010).

19. W. Shen, X. Wu, H. Meng, G. Zhang, and X. Huang, "Long distance fiber-optic displacement sensor based on fiber collimator," *Rev. Sci. Instrum.*, **81**, pp.123104 (2010).

20. A. Malki, P. Lecoy, J. Marty, C. Renouf and P. Ferdinand, "Optical fiber accelerometer based on a silicon micromachined cantilever," *Appl. Opt.*, **34**, pp.8014 (1995).

21. Y. Li, X. Wang, and X. Bao, "Sensitive acoustic vibration sensor using single-mode fiber tapers," *Appl. Opt*., **50**, pp.1873 (2011).

22. R. Gibson, R. Selfridge and S. Schultz, "Electric field sensor array from cavity resonance between optical D-fiber and multiple slab waveguides," *Appl. Opt.*, **48**, pp. 3695 (2009).

23. L. Sun, S. Jiang and J. R. Marciante, "All-fiber optical magnetic-field sensor based on Faraday rotation in highly terbium-doped fiber," *Opt. Express*, **18**, pp. 5407 (2010).

24. D. H. Kim, "A fiber-optic tiltmeter system based on the moire-fringe effect," *Meas. Sci. Technol.*, **20**, pp.025203 (2009).

25. H. Y. Fu, S. K. Khijwania, H. Y. Tam, P. K. A. Wai and C. Lu, "A novel fiber optic polarimetric torsion sensor based on polarization-maintaining photonic crystal fiber", *Appl. Opt.*, **49**, pp.5954 (2010).

26. M. Schmidt, N. Fürstenau, W. Bock and W. Urbanczyk, "Fiber-optic polarimetric strain sensor with three-wavelength digital phase demodulation," *Opt. Lett.*, **25**, pp.1334 (2000).

27. S. K. Khijwania, ''Optical fiber evanescent wave absorption sensor: effect of fiber parameters and probe geometry,'' (*PhD Thesis, Indian Institute of Technology, Delhi, India*, 1999).

28. T. S. Francis and S. Yin, "Fiber Optic Sensors," (*Marcel Dekker Inc.*, 2002).

29. K. T. V. Grattan and B. T. Meggitt, "Optical fiber sensor technology," (*Chapman and Hall*, 1995).

30. S. K. Khijwania, K. L. Srinivasan and J. P. Singh, "Performance optimized optical fiber sensor for humidity measurement," *Opt. Eng.* **44**, pp. 34401 (2005).

31. N. K. Sharma and B. D. Gupta, "Fabrication and characterization of pH sensor based on side polished single mode optical fiber," *Opt. Commun.*, **216**, pp. 299 (2003).

32. H. S. Haddock, P. M. Shankar and R. Mutharasan, "Fabrication of biconical tapered optical fibers using hydrofluoric acid," *Mater. Sci. Eng. B*, **97**, pp.87 (2003).

33. H. Tai, H. Tanaka and T. Yoshino, "Fiber-optic evanescent-wave methane-gas sensor using optical absorption for the 3.392-µm line of a He-Ne laser," *Opt Lett.*, **12**, pp. 437 (1987).

34. S. Sekimoto, H. Nakagawa, S. Okazaki, K. Fukuda, S. Asakura, T. Shigemori and S. Takahashi, "A fiber-optic evanescent-wave hydrogen gas sensor using palladium-supported tungsten oxide," *Sens. Actuators B*, **66**, pp. 142 (2000).

35. K. O. Hill and G. Meltz, "Fiber Bragg Grating Technology Fundamentals and Overview," *J. Lightwave Technol.*, **15**, pp. 1263 (1997).

36. A. D. Kersey, M. A. Davis, H. J. Patrick, M. LeBlanc, K. P. Koo, C. G. Askins, M. A. Putnam, and E. J. Friebele, "Fiber Grating Sensors," *J. Lightwave Technol.*, **15**, pp. 1442 (1997).

37. Y. J. Rao, "In-fibre Bragg grating sensors," *Meas. Sci. Technol.*, **8**, pp. 355 (1997).

38. N. Takahashi, K. Yoshimura, S. Takahashi, and K. Imamura, "Development of an optical fiber hydrophone with fiber Bragg grating," *Ultrasonics*, **38**, pp. 581 (2000).

39. T. A. Berkoff and A. D. Kersey, "Experimental demonstration of a fiber Bragg grating accelerometer," *IEEE Photon. Technol. Lett.*, **8**, pp. 1677 (1996).

40. M. G. Xu, H. Geiger, and J. P. Dakm, "Fiber grating pressure sensor with enhanced sensitivity using a glass-bubble housing," *Electron.Lett.*, **32**, pp. 128 (1996).

41. H. Y. Au, S. K. Khijwania, H. Y. Fu, W. H. Chung and H. Y. Tam, "Temperature insensitive fiber Bragg grating based tilt sensor with large dynamic range", *J. Lightwave Technol.*, **29**, pp. 1714 (2011).

42. X. G. Tian and X. M. Tao, "Torsion measurement using fiber Bragg grating sensors," *Exp. Mech.*, **41**, pp. 248 (2001).

43. J. Lim, Q. P. Yang, B. E. Jones and P. R. Jackson, “DP flow sensor using optical fiber Bragg grating,” *Sens. Actuators A*, **92**, pp.102 (2001).

44. S. W. James and R. P. Tatam, “Optical fiber long-period grating sensors: characteristics and application,” *Meas. Sci. Technol.*, **14**, pp. R49 (2003).

45. S. Korposh, S. W. Lee, S. W. James and R. P. Tatam, “Refractive index sensitivity of fibre-optic long period gratings coated with SiO_2 nanoparticle mesoporous thin films,” *Meas. Sci. Technol*., **22,** pp. 075208 (2011).

46. Y. P. Wang, L. Xiao, D. N. Wang and W. Jin, “Highly sensitive long-period fiber-grating strain sensor with low temperature sensitivity,” *Opt. Lett*., **31**, pp. 3414 (2006).

47. S. Khaliq, S. W. James and R. P. Tatam, “Enhanced sensitivity fibre optic long period grating temperature sensor,” *Meas. Sci. Technol.*, **13**, pp. 792 (2002).

48. X. K. Kalantar-zadeh and B. Fry, “Nanotechnology-enabled sensors,” (*Springer*, 2008).

49. K. A. Willets and R. P. Van Duyne, “Localized surface plasmon resonance spectroscopy and sensing,” *Annu. Rev. Chem.*, **58**, pp.267 (2007).

50. S. K. Srivastava, R. K. Verma and B. D. Gupta, “Theoretical modelling of a localized surface plasmon resonance based intensity modulated fiber optic refractive index sensor," Appl. Opt., 48, pp.3796 (2009).

51. T. Okamoto and I. Yamaguchi, “Local plasmon sensor with gold colloid monolayers deposited upon glass substrates,” *Opt. Lett.*, **25**, pp.372 (2000).

52. V. V. R. Sai, T. Kundu and S. Mukherji, “Novel U-bent fiber optic probe for localized surface plasmon resonance based biosensor,” *Biosens. Bioelectron.*, **24**, pp.2804 (2009).

53. H. Lee, H. Kim, J. Park, D. H. Jeong and S. Lee, “Effects of surface density and size of gold nanoparticles in a fiber-optic localized surface plasmon resonance sensor and its application to peptide detection,” *Meas. Sci. Technol.*, **21**, pp.085805 (2010).

54. P. B. Tarsa, D. M. Brzozowski, P. Rabinowitz and K. K. Lehmann, "Cavity ring down strain gauge," *Opt. Lett.*, **29**, pp.1339 (2004).

55. Y. Jiang, D. Yang, D. Tang and J. Zhao, "Sensitivity enhancement of fiber loop cavity ring-down pressure sensor," *Appl. Opt.*, **48**, pp. 6082 (2009).

56. S. C. Mukhopadhyay, "New developments in sensing technology for structural health monitoring," (*Springer*, 2011).

57. J. M. López-Higuera, L. R. Cobo, A. Q. Incera, and A. Cobo, "Fiber optic sensors in structural health monitoring," *J. Lightwave Technol.*, **29**, pp. 587 (2011).

58. A. Norris**,** M. Saafi and P. Romine**,** "Temperature and moisture monitoring in concrete structures using embedded nanotechnology/microelectromechanical systems (MEMS) sensors," *Constr. Build. Mater.*, **22**, pp.111 (2008).

59. Z. Chen and C. Lu, "Humidity sensors: A review of materials and mechanisms," *Sens. Lett.*, **3**, pp. 274 (2005).

60. T. L. Yeo, T. Sun and K. T. V. Grattan, "Fiber–optic sensor technologies for humidity and moisture measurement," *Sens. Actuators A*, **144**, pp.280 (2008).

61. Z. M. Rittersma, "Recent achievements in miniaturised humidity sensors-a review of transduction techniques", *Sens. Actuators A*, **96**, pp.196 (2002).

62. U. Kang and K. D. Wise, "A high-speed capacitive humidity sensor with on-chip thermal reset," *IEEE Trans. Electron. Devices*, **47**, pp.702 (2000).

63. A. P. Russell and K. S. Flectcher, "Optical sensor for determination of moisture," *Anal. Chim. Acta*, **170**, pp. 209 (1985).

64. D. S. Ballantine and H. Wohltjen, "Optical waveguide humidity detector,'' *Anal. Chem.*, **58**, pp.2883 (1986).

65. Q. Zhou, M. R. Shahriari, D. Kritz and G. H. Sigel, "Porous fiber-optic sensor for high-sensitivity humidity measurement," *Anal. Chem.*, **60**, pp.2317 (1988).

66. F. Mitschke, “Fiber-optic sensor for humidity”, *Opt. Lett.*, **14**, pp.967 (1989).

67. T. E. Brook, M. N. Taib and R. Narayanaswamy, “Extending the range of a fibre-optic relative-humidity sensor,” *Sens. Actuators B*, **38-39**, pp.272 (1997).

68. S. Otsuki, K. Adachi, and T. Taguchi, “A novel fiber-optic gas-sensing configuration using extremely curved optical fibers and an attempt for optical humidity detection,” *Sens. Actuators B*, **53**, pp.91 (1998).

69. D. C. Bownass, J. S. Barton and J. D. C. Jones, “Detection of high humidity by optical fiber sensing at telecommunications wavelengths,” *Opt. Commun.*, **146**, pp.90 (1998).

70. C. Bariain, I. R. Matıas, F. J. Arregui and M. Lopez-Amo, “Optical fiber humidity sensor based on a tapered fiber coated with agarose gel,” *Sens. Actuators B*, **69**, pp.127 (2000).

71. B. D. Gupta and Ratnanjali, “A novel probe for fiber optic humidity sensor,” *Sens. Actuators B*, **80**, pp.132 (2001).

72. F. J. Arregui, I. R. Matías, K. L. Cooper and R. O. Claus, “Simultaneous measurement of humidity and temperature by combining a reflective intensity-based optical fiber sensor and a Fiber Bragg Grating,” *IEEE J. Sens.*, **2**, pp.482 (2002).

73. S. Muto, O. Suzuki, T. Amano and M. Morisawa, “A plastic optical fiber sensor real-time humidity monitoring”, *Meas. Sci. Technol.*, **14**, pp. 746 (2003).

74. A. Gaston, I. Lozano, F. Perez, F. Auza, and J. Sevilla, “Evanescent wave optical-fiber sensing (temperature, relative humidity, and pH sensors),” *IEEE J. Sens.*, **3**, pp.806 (2003).

75. A. A. Herrero, H. Guerrero and D. Levy, “High-sensitivity sensor of low relative humidity based on overlay on side-polished fibers,” *IEEE J. Sens.*, **4**, pp.52 (2004).

76. C. M. Tay, K. M. Tan, S. C. Tjin, C. C. Chan and H. Rahardjo, “Humidity sensing using plastic optical fiber”, *Micro. Opt. Technol. Lett.*, **43**, pp.387 (2004).

77. S. K. Shukla, G. K. Parashar, A. P. Mishra, P. Misra, B. C. Yadav, R. K. Shukla, L. M. Bali and G. C. Dubey, "Nano-like magnesium oxide films and its significance in optical fiber humidity sensor," *Sens. Actuators B*, **98**, pp.5 (2004).

78. S. K. Khijwania, K. L. Srinivasan and J. P. Singh, "An evanescent-wave optical fiber relative humidity sensor with enhanced sensitivity," *Sens. Actuators B*, **104**, pp.217 (2005).

79. I. R. Matias, F. J. Arregui, J. M. Corres, and J. Bravo, "Evanescent field fiber-optic sensors for humidity monitoring based on nanocoatings," *IEEE J. Sens.*, **7**, pp.89 (2007).

80. J. M. Corres, F. J. Arregui and I. R. Matias, "Sensitivity optimization of tapered optical fiber humidity sensors by means of tuning the thickness of nanostructured sensitive coatings," *Sens. Actuators B*, **122**, pp.442 (2007).

81. J. M. Corres, I. R. Matias, M. Hernaez, J. Bravo and F. J. Arregui, "Optical fiber humidity sensors using nanostructured coatings of SiO_2 nanoparticles," *IEEE J. Sens.*, **8**, pp.281 (2008).

82. L. Zhang, F. Gu, J. Lou, X. Yin and L. Tong, "Fast detection of humidity with a subwavelength-diameter fiber taper coated with gelatin film," *Opt. Express.*, **16**, pp.13349 (2008).

83. A. Vijayan, M. Fuke, R. Hawaldar, M. Kulkarni, D. Amalnerkar and R. C. Aiyer, "Optical fibre based humidity sensor using Co-polyaniline clad," *Sens. Actuators B*, **129**, pp.106 (2008).

84. K. L. Sreenivasan, S. K. Khijwania, T. Philip and J. P. Singh, "Humidity estimation using neural network and optical fiber sensor," *Micro. Opt. Technol. Lett.*, **51**, pp.641 (2009).

85. S. Akita, H. Sasaki, K. Watanabe and A. Seki, "A humidity sensor based on a hetero-core optical fiber," *Sens. Actuators B,* **147**, pp.385 (2010).

86. Q. Wu, Y. Semenova, J. Mathew, P. Wang, and G. Farrell, "Humidity sensor based on a single- mode hetero-core fiber structure," *Opt. Lett.*, **36**, pp.1752 (2011).

87. M. Hernáez, C. R. Zamarreño, I. R. Matías and F. J. Arregui, "Optical fiber humidity sensor based on surface plasmon resonance in the infra-red region," *J. Phys.: Conf. Ser. (IOP)*, **178**, pp.012019 (2009).

88. C. R. Zamarre, M. Hernaez, I. D. Villar, I. R. Matias and F. J. Arregui, "Tunable humidity sensor based on ITO-coated optical fiber," *Sens. Actuators B*, **146**, pp.411 (2010).

89. K. M. Tan, C. M. Tay, S. C. Tjin, C. C. Chan and H. Rahardjo, "High relative humidity measurements using gelatin coated long-period grating sensors," *Sens. Actuators B*, **110**, pp.335 (2005).

90. M. Konstantaki, S. Pissadakis, S. Pispas, N. Madamopoulos and N. A. Vainos, "Optical fiber long-period grating humidity sensor with poly (ethyleneoxide)/cobalt chloride coating," *Appl. Opt.*, **45**, pp.4567 (2006).

91. Y. Liu, L. Wang, M. Zhang, D. Tu, X. Mao and Y. Liao, "Long-period grating relative Humidity sensor with hydrogel coating," *IEEE Photon. Technol. Lett.*, **19**, pp.880 (2007).

92. T. Venugopalan, T. L. Yeo, T. Sun and K. T. V. Grattan, "LPG-based PVA coated sensor for relative humidity measurement," *IEEE J. Sens.*, **8**, pp.1093 (2008).

93. D. Viegas, J. Goicoechea, J. M. Corres, J. L. Santos, L. A. Ferreira1, F. M. Araujo and I. R. Matias, "A fibre optic humidity sensor based on a long-period fibre grating coated with a thin film of SiO_2 nanospheres," *Meas. Sci. Technol.* **20**, pp.34002 (2009).

94. D. Viegas, J. Goicoechea, J. L. Santos, F. M. Araújo, L. A. Ferreira, F. J. Arregui and I. R. Matias, "Sensitivity improvement of a humidity sensor based on silica nanospheres on a long-period fiber grating," *Sensors*, **9**, pp.519 (2009).

95. Y. Miao, B. Liu, H. Zhang, Y. Li, H. Zhou, H. Sun, W. Zhang and Q. Zhao, "Relative humidity sensor based on tilted fiber Bragg grating with polyvinyl alcohol coating," *IEEE Photon. Technol. Lett.*, **21**, pp.441 (2009).

96. T. L. Yeo, T. Sun, K. T. V. Grattan, D. Parry, R. Lade and B. D. Powell, "Characterization of a polymer-coated fiber Bragg grating sensor for relative humidity sensing," *Sens. Actuators B*, **110**, pp.148 (2005).

97. X. F. Huang, D. R. Sheng, K. F. Cen and H. Zhou, "Low-cost relative humidity sensor based on thermoplastic polymide-coated fiber Bragg grating," *Sens. Actuators B*, **127**, pp.518 (2007).

98. J. Lin and C. W. Brown, "Sol–gel glass as a matrix for chemical and biochemical sensing," *Trends Anal. Chem.*, **16**, pp. 200 (1997).

99. A. K. Mcevoy, C. Mcdonagh and B. D. Maccraith, "Optimisation of sol-gel-derived silica films for optical oxygen sensing," *J. Sol-Gel Sci. Technol*., **8**, pp.1121 (1997).

100. B. D. Mac Craith, G. O. Keeffe, C. McDonagh and A. K. McEvoy, "LED-based fiber optic oxygen sensing using sol-gel coating," *Elect. Lett.*, **30**, pp.888 (1994).

101. S. A. Grant and R. S. Glass, "A sol-gel based fiber optic sensor for local blood pH measurements," *Sens. Actuators B*, **45**, pp.35 (1997).

102. J. H. Jiwan and J. Soumillion, "A halogen anion sensor based on the hydrophobic entrapment of a fluorescence probe in sol-gel thin films," *J. Non-Cryst. Solids.*, **220**, pp.316 (1997).

103. S. K. Khijwania and B. D. Gupta, "Fiber optic evanescent field absorption sensor: Effect of fiber parameters and geometry of the prob," *Opt. Quantum Electron*., **31**, pp.625 (1999).

104. S. K. Khijwania and B. D. Gupta, "Effect of fiber parameters on the sensitivity of the fiber-optic evanescent field absorption sensor based on tapered probe," *Proc. SPIE*, **3666**, pp.578 (1998).

105. J. Jaglarz, P. Karasinski, and E. Skoczek, "Optical properties of silica antireflective films formed in sol-gel processes", *Phys. Status Solidi C*, **8**, pp.2645 (2011).

106. C. J. Brinker, G. C. Frye, A. J. Hurd, and C. S. Ashley, "Fundamentals of Sol Gel dip coatings", *This Solid Films*, **201**, 97-108 (1991). f

107. S. K. Khijwania and B. D. Gupta, "Fiber optic evanescent field absorption sensor with high sensitivity and linear dynamic range," *Opt. Commun.*, **152**, pp.259 (1998).

108. J. J. Frioiat, A. Jelli, G. Poncelet and J. Andre, "Thermodynamic properties of adsorbed water molecules and electrical conduction in montmorillonites and silicas," *J. Phys. Chem.*, **69**, pp. 2185 (1965).

109. J. H. Anderson and G. A. Parks, "Electrical conductivity of silica gel in the presence of adsorbed water," *J. Phys. Chem.*, **72**, pp.3662 (1968).

110. S. K. Khijwania and B. D. Gupta, "Fiber optic evanescent field absorption sensor with high sensitivity and linear dynamic range," *Opt. Commun.*, **152**, pp.259 (1998).

111. S. K. Ghosh and T. Pal, "Interparticle coupling effect on the surface plasmon resonance of gold nanoparticles: from theory to applications," *Chem. Rev*., **107**, pp.4797 (2007).

112. A. D. McFarland, C. L. Haynes, C. A. Mirkin, R. P. Van Duyne and H. A. Godwin, "Color my nanoworld," *J. Chem. Educ.*, **81**, pp.544A (2004).

113. O. Seitz, M. M. Chehimi, E. C. Deliry, S. Truong, N. Felidj, C. Perruchot, S. J. Greaves and J. F. Watts, "Preparation and characterisation of gold nanoparticle assemblies on silanised glass plates," *Colloids Surf., A*, **218**, pp.225 (2003).

114. M. L. Cheng and J. Yang "Influences of composition on electroless deposition of silver nanoparticles on glass substrates for surface-enhanced Raman scattering measurements," *Appl. Spectrosc.*, **62**, pp.1384 (2008).

115. R. Slavík, J. Homola, J. Čtyroký, and E. Brynda, "Novel spectral fiber optic sensor based on surface plasmon resonance," *Sens. Actuators B*, **74**, pp.106 (2001).